ACS Biomaterials SCIENCE & ENGINEERING

pubs.acs.org/journal/abseba

Review

Recent Progress in Graphene- and Related Carbon-Nanomaterial-based Electrochemical Biosensors for Early Disease Detection

Heba Mohamed Fahmy,*,○ Esraa Samy Abu Serea,*,○ Reem Essam Salah-Eldin, Sara Ayman Al-Hafiry, Miar Khaled Ali, Ahmed Esmail Shalan,* and Senentxu Lanceros-Méndez*

Cite This: *ACS Biomater. Sci. Eng.* 2022, 8, 964–1000

Read Online

ACCESS | Metrics & More | Article Recommendations

ABSTRACT: Graphene- and carbon-based nanomaterials are key materials to develop advanced biosensors for the sensitive detection of many biomarkers owing to their unique properties. Biosensors have attracted increasing interest because they allow efficacious, sensitive, selective, rapid, and low-cost diagnosis. Biosensors are analytical devices based on receptors for the process of detection and transducers for response measuring. Biosensors can be based on electrochemical, piezoelectric, thermal, and optical transduction mechanisms. Early virus identification provides critical information about potentially effective and selective therapies, extends the therapeutic window, and thereby reduces morbidity. The sensitivity and selectivity of graphene can be amended via functionalizing it or conjoining it with further materials. Amendment of the optical and electrical features of the hybrid structure by introducing appropriate functional groups or counterparts is especially appealing for quick and easy-to-use virus detection. Various techniques for the electrochemical detection of viruses depending on antigen−antibody interactions or DNA hybridization are discussed in this work, and the reasons behind using graphene and related carbon nanomaterials for the fabrication are presented and discussed. We review the existing state-of-the-art directions of graphene-based classifications for detecting DNA, protein, and hormone biomarkers and summarize the use of the different biosensors to detect several diseases, like cancer, Alzheimer's disease, and diabetes, to sense numerous viruses, including SARS-CoV-2, human immunodeficiency virus, rotavirus, Zika virus, and hepatitis B virus, and to detect the recent pandemic virus COVID-19. The general concepts, mechanisms of action, benefits, and disadvantages of advanced virus biosensors are discussed to afford beneficial evidence of the creation and manufacture of innovative virus biosensors. We emphasize that graphene-based nanomaterials are ideal candidates for electrochemical biosensor engineering due to their special and tunable physicochemical properties.

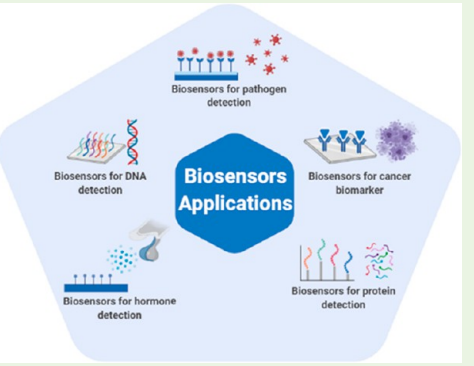

KEYWORDS: *graphene, carbon nanomaterials, biosensors, disease detection, protein, viruses*

INTRODUCTION

Common diseases threaten the lives of many people in the world. Pandemic outbreaks, such as the one we are experiencing nowadays related to COVID-19, strongly visualize this reality. Most of these diseases are leading to death at a young age, and the number of patients and deaths related to diabetes, cancers, and Alzheimer's disease (AD) is increasing year by year. Diabetes mellitus is a metabolic disorder that leads to increasing levels of glucose in the blood. High levels of glucose are associated with heart disease, blindness, and kidney failure. Therefore, early detection of glucose concentration is a very important issue.[1,2] In addition, cancer is considered to be the most common and widespread disease worldwide as usually results from different genetic factors or is caused by environmental factors. Cancer is an abnormal growth of cells and causes the formation of masses of cells, which are characterized as a tumor and can then spread from the original site of injury to the rest of the cells and organs in the body. Unfortunately, in this case, it is difficult cure.[3] Therefore, the early diagnosis of cancer in its early stage can decrease the risk of a fatal outcome. AD is a neurodegenerative disorder that appears in the dementia form and often affects people aged 65 or older. Its clinical diagnosis is not good compared with other diseases, and there is no suitable treatment. It has been found to have affected more than 37 million people worldwide, which is largely due to the aging of the population and the lack of medicines for those cases. Moreover, it is a global crisis because of its high cost, which could reach around 600 billion dollars.[3]

Received: May 28, 2021
Accepted: February 10, 2022
Published: March 1, 2022

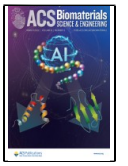

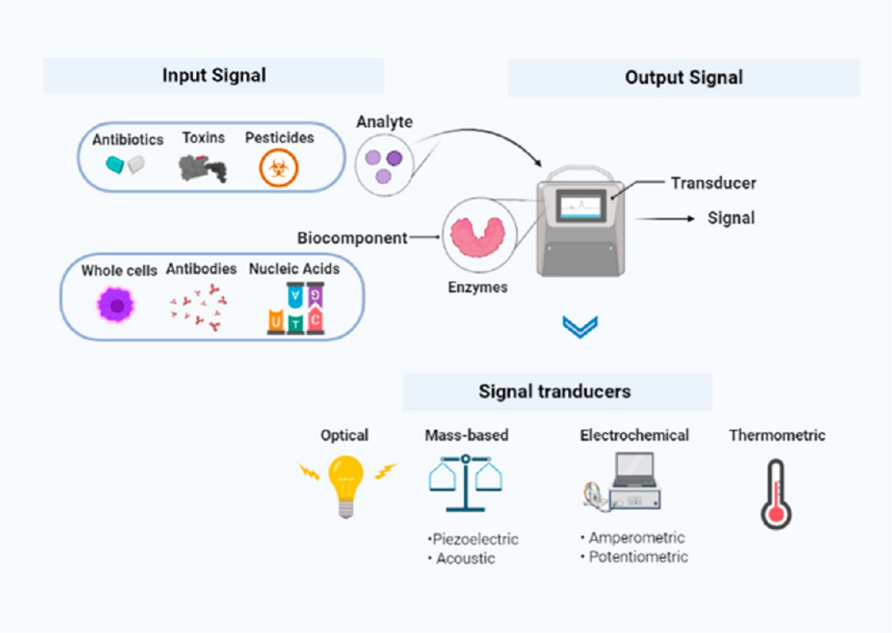

Figure 1. Representation of biosensors depending on signal transducer mechanisms.

The conventional techniques for monitoring and diagnosing diabetes, such as commercial glucose analyzers, are based on finger pricking, which has defect inaccuracy and neglects changes in glucose concentration at differences in time between taking samples, for example, at night during sleeping. For cancer, the cross-sectional computed tomography (CT) scan is expensive, and centrifugation, fluorescence, chromatography, and magnetic-activation processes reduce the quality or the diagnosis because it depends on personal judgment. Efforts have been carried out to detect these diseases early to overcome the problems of the conventional methods. Biosensors are an attractive and interesting alterative because they are effective, sensitive, selective, rapid, and low-cost diagnosis tools. The biosensor is an analytical device that is based on receptors for the process of detection and transducers for measuring the response. Biosensors depend on different transduction mechanisms like electrochemical, piezoelectric, thermal, and optical mechanisms. Biosensors can be used for the recognition of enzymes, genes, proteins, and antibodies (Figure 1). Biosensors can be used for different applications including DNA detection, pathogen detection, hormone detection, protein detection, and cancer biomarkers (Figure 2). Carbon is an attractive material for use in sensors as both 1-D carbon nanotubes (CNTs) and 2-D graphene.[4−10]

Sensors that convert biological reactions, such as enzyme−substrate reactions and antigen−antibody interactions, into electrical signals are referred to as electrochemical biosensors.[4] An electrode is a critical component of an electrochemical biosensor because it serves as a firm substrate for biomolecule immobilization and electron mobility.[5−7] Furthermore, selecting the right functional material aimed at the electrode is an important step in achieving excellent biosensor performance. Various electrochemistry-driven biosensing approaches for inexpensive and small analytical devices aimed at on-site analysis have recently been introduced. However, designing an appropriate on-site biosensor that meets the needed sensitivity while maintaining excellent reproducibility is still a challenge. For high-performance electrochemical analysis, the use of well-designed nanomaterials as a supportive condition aimed at signal amplification has gained traction.[7] Nanomaterials have a huge surface area that allows for greater filling aptitude and reactant mass transport, which are directed to a synergistic effect for signal strengthening.[8−10]

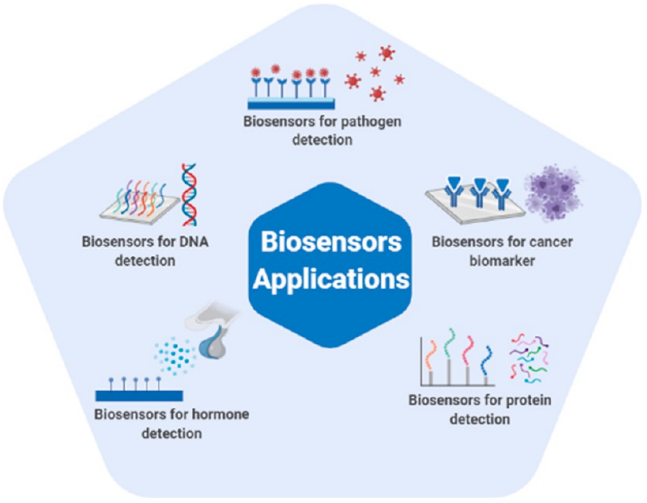

Figure 2. Different biomedical applications of biosensors including DNA detection, pathogen detection, hormone detection, protein detection, and cancer biomarkers.

The detection of a biological interaction on the electrode surface is the basis for all electrochemical biosensors. The biorecognition element and its accessibility/reactivity determine the sensor's sensitivity, stability, reusability, specificity, and cost. Given the functional mechanism of electrochemical biosensors, proper electrode surface modification is critical to their effectiveness. Surface alterations aid not only in the appropriate immobilization of bioreceptors but also in noise reduction and increased sensitivity. More importantly, surface functionalization reduces nonspecific binding of the analyte or other components on the surface, which is undesirable. Furthermore, the structure of biomolecules on the surface

https://doi.org/10.1021/acsbiomaterials.1c00710
ACS Biomater. Sci. Eng. 2022, 8, 964−1000

displays an imperative effect on determining a biosensor's sensitivity and selectivity. To put it another way, the biosensor performance is heavily influenced by the materials utilized to modify the surfaces and the surface chemistry or functionalization approach employed to immobilize the bioreceptors. Silicon, glass, gold, CNTs, conducting polymers, graphene, and other electrode surfaces are utilized for the immobilization of biomolecules in electrochemical biosensors.[9]

Surface modification of electrodes has a crucial influence on the efficiency and application of electrochemical biosensors. The materials employed for surface modifications should be biocompatible and stable to guarantee the stable immobilization of bioreceptors. Self-assembled monolayers (SAMs), conductive polymers, and other nanomaterials are commonly employed for surface modification. Nanomaterials, with their large surface area, high electron-transfer rate, and superior biocompatibility, play an essential role in the development of electrochemical biosensors. The bioreceptor's use and nature should guide the selection of the best immobilization strategy. An antibody should be immobilized on the surface in the "end-on" orientation in an affinity-based sensor to enable it to bind the antigen. Similarly, the upright or nearly upright orientation of DNA is critical for efficient target hybridization. If the covalent link does not alter the reactivity, then covalent binding via active ester chemistry is one of the most suitable and stable techniques of immobilization. The emphasis point in defining the efficacy of the electrochemical biosensor is the assortment of a suitable surface modification strategy and the immobilization of the bioreceptor.[8−10]

Graphene, CNTs, crystalline diamond, and diamond-like carbon are considered as carbon nanomaterials with extraordinary electrochemical features that have led to their prevalent utilization. In addition, the promise of new carbon-derived nanostructures in sensing applications is undeniable because they exhibit features not found in bulk materials. As a result, they can work under harsh conditions with greater sensitivity and selectivity and over a wider temperature ranger in addition to dynamic ranges. For electrochemical detection, a variety of materials have been utilized as electrode materials, together with platinum, gold, and various kinds of carbon.[5−8] Carbon polymorphs, for instance, graphene, CNTs, and diamond, have been engaged as electrode materials aimed at electrochemical sensing in recent years.[10] The exceptional features of carbon nanomaterials, for instance, their huge surface-to-volume ratio, high conductivity, and electron mobility at ambient temperature, have targeted toward several improvements in electrochemical sensors.[4−8] Graphene, on the contrary, has a limited quantity and is hydrophobic, which limits its application in biosensors.[8] Graphene oxide (GO) and reduced graphene oxide (rGO) solved the problem by enhancing the hydrophilicity of the graphene layer, which resulted in outstanding electrical conductivity and ease of surface modification for biomolecule immobilization, respectively.[12]

On the subject of GO's excellent physicochemical characteristics, its utilization in novel optical biosensing systems has been studied.[13] Although it is possible to use GO as a long-range photoluminescence quenching agent, it can also be treated in suspension and easily complexed with biological molecules. GO photoluminescence can also be seen with donor/acceptor molecules exposed on a planar surface, as we demonstrated.[13] Even though nothing was known about the impact of GO characteristics on biosensing performance 6 years ago, it is now recognized that they can be adjusted based on the oxidation degree, lateral size, and layer count. Biosensors based on genetically engineered organisms are able to operate as colloidal suspensions. As a matter of fact, recent studies have shown novel ways to integrate GO-based biosensors into solids without the necessity of colloidal suspensions, which makes possible their use in new devices. In addition to photoluminescent signals, the bulk of GO-based optical biosensing approaches use photoluminescence. However, new developments in label-free optical biosensing approaches using GO have also been made. These findings are presented in a progress report on this interesting topic, highlighting both its difficulties and its potential.

In addition, CNTs have outperformed materials widely applied as electrode interfaces that have high conductivity and chemical stability according to the literature. Because of their enhanced sensitivity and improved signal-to-noise ratio, electrochemical transducers that use CNTs as substrates boost the performance of amperometric enzyme electrodes, immunosensors, and nucleic-acid-sensing instruments. CNT-modified electrode interfaces are extremely tempting for use aimed at a range of amperometric oxidase- and dehydrogenase-based biosensors due to the increased electrochemical reactivity of species like nicotinamide adenine dinucleotide (NADH) and hydrogen peroxide.[9−11] Transducers made of CNTs have been shown to improve biocatalytic reactions while also serving as a platform aimed at multiple enzyme tags. CNTs behave like molecular wires when aligned as "forests", allowing for smoother the insolubility of electron transfer between the underlying electrode and the enzyme's redox center. CNTs have been applied in a diversity of applications, including sensors, actuators, and energy storage, due to their specific properties.[8−12] In addition, CNTs and graphene show several features such as electrical, structural, chemical, and mechanical properties that are appropriate for the progress of biosensors. These include electrical conductivity and tremendous electrocatalytic activity, good stability, a large surface area, and flexible mechanical features.[11,12]

Single-walled carbon nanotubes (SWCNTs) have recently become popular in biosensors to improve their electrical characteristics. SWCNTs reveal outstanding electrical and mechanical features.[14] SWCNTs in electrochemical biosensors have gained researchers' curiosity because of their physicochemical properties.[15] Their large surface area could help to enhance the quantity of immobilized enzymes, expand the reaction regions between the enzyme and the substrate, improve the electrical conductivity, and boost the biosensor signal response.[16] However, the insolubility of SWCNTs may hinder their biological uses. Certain nanocomposites with high biocompatibility were utilized to overcome the stable insolubility in aqueous solutions.[17−19] Multifunctional SWCNTs serve as a platform for developing innovative biosensor systems that incorporate immobilized biomolecules in conjunction with enzymes and redox mediators. Holzinger et al. investigated a variety of SWCNT functionalizations to develop a polyvalent sensing electrode.[20]

It is well known that SWCNTs are highly desirable nanomaterials aimed at an extensive assortment of applications because of their mechanical, chemical, and optical features. SWCNTs manufactured in bulk exhibit a wide range of chiral species and properties (e.g., electronic structures). A highly filtered and segregated process is required to fully utilize SWCNTs.[21] The limited surface area of the biosensor makes it

https://doi.org/10.1021/acsbiomaterials.1c00710
ACS Biomater. Sci. Eng. 2022, 8, 964−1000

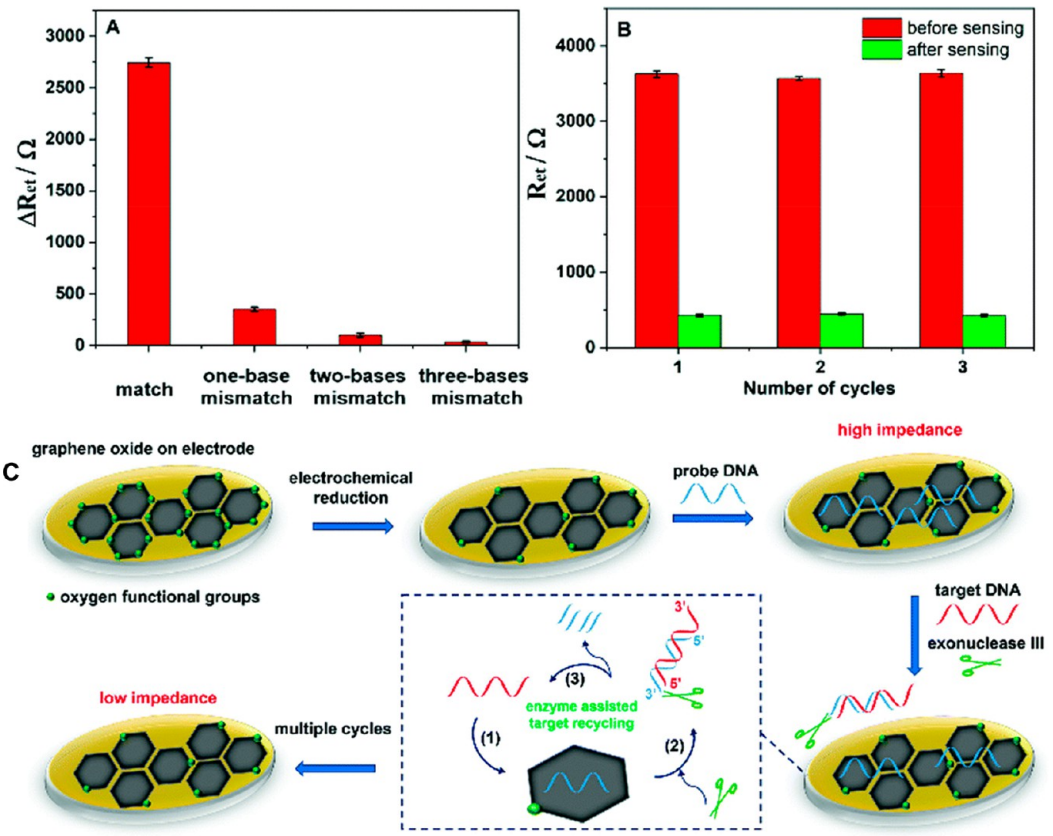

Figure 3. (A) Shift in impedance caused by sensing mismatched DNA bases. (B) Reproducibility as a function of cycle count. (C) Diagram of the DNA impedimetric biosensor's assembly and recognition via enzyme-assisted target recycling. In panel C, electrochemically reduced graphene oxide (ERGO), which is readily accessible, may be a useful medium for signal amplification in DNA hybridization EIS measurements. With the use of enzyme-assisted target recycling, efficient interfacial tuning can be obtained, including high impedance caused by ssDNA samples directly adsorbed on graphene materials and low impedance caused by the continuous desorption of target−sample DNA hybrids in addition to the subsequent digestion of the sample. Just a few DNA targets can lead to the enzymatic digestion of many DNA samples. Because of the brilliant electrical conductivity of rGO, electron-transfer resistance is drastically decreased after DNA samples are limited. Reproduced with permission from ref 36. Copyright 2019 The Royal Society of Chemistry.

difficult to engage with large biorecognition agents like mammalian cells, to manage sensor production, and to undergo chemical modification.[22] This is especially true when using bodily fluid samples that contain several proteins and lipids.[23] For example, the nonspecific binding impact directly affects the analytical performance of the biosensor, and hence more advanced sensors are necessary.[22]

Multiwalled carbon nanotubes (MWCNTs) are made up of numerous layers of concentric single-walled graphene cylinders held together by van der Waals forces.[24] MWCNTs have a sidewall structure like graphite.[25] The solid substrate is chemically altered for antibody immobilization.[26] A suitable functioning MWCNT surface is necessary due to the structural degradation of MWCNTs during functionalization, including decapping at the ends and slicing and breaking the length. The oxygen functional groups of functionalized MWCNTs and the $-NH_2$ groups of the antibody form covalent bonds.[27] According to Zheng and Zheng, hydrophobic−hydrophobic forces immobilize the nonpolar amino acid chain of gelatin to the side wall of MWCNT, resulting in a stable dispersion.[27] Increasing the quantity of MWCNTs in the MWCNT/gelatin dispersion improves its strength.[28−30] Using MWCNTs in nanoparticles (NPs) can increase the analytical performance. Li et al. developed an ultrasensitive electrochemical biosensor using AuNP hybrid MWCNTs-SO_3H as an electrode material.[30] Xu et al. created an amperometric glucose biosensor using glucose oxidase and dendrimer-encapsulated Pt NPs on MWCNTs.[31] A low limit of detection (LOD), wide linearity, high precision, and better functioning constancy were achieved because of the enzyme electrode's unique 3-D shape. CNTs have a number of disadvantages. One of which is that their production progression is not completely organized. The difficulty of aggregation and the lack of homogeneity are crucial.[32,33] CNTs are also often insoluble, which makes them difficult to use in practical applications. Strong stacking and van der Waals forces cause MWCNTs in aqueous solution to develop irreversible aggregation, limiting their utility.[34] MWCNT surfaces are chemically treated with sulfonic acid groups, hydroxyl groups, and carboxyl groups to improve the film dispersity and uniformity on electrode surfaces.[35]

ADVANTAGES AND DRAWBACKS OF GRAPHENE AND ITS RELATED MATERIALS AIMED AT ELECTROCHEMICAL BIOSENSOR APPLICATIONS

There has been a rise in interest in the growth of electrochemical biosensors with enhanced performance because of their wide range of applications, from medical diagnostics and healthcare to environmental monitoring and industrial manufacturing. The high sensitivity, selectivity, repeatability, and stability are among the major problems in

https://doi.org/10.1021/acsbiomaterials.1c00710
ACS Biomater. Sci. Eng. 2022, 8, 964−1000

developing biosensors. Sensor surface stability and interference from other analytes must be kept to a minimum as well. The use of graphene and similar materials in biosensor applications has a few advantages and disadvantages. We can briefly summarize the advantage of graphene materials to be the high electrical and thermal conductivities and the high control of functionalization and the disadvantages to be the hydrophobicity, high cost, difficult workability, and small production. The water dispensability, polar functionalization, low cost, and easy workability are strong advantages for GO, whereas the lower electrical and thermal conductivity, surface random functionalization, and poor control on postpreparation functionalization are disadvantages. The high electrical and thermal conductivities, good control on functionalization, and lower cost than neat graphene are the advantages of rGO, and the hydrophobicity, difficult workability, and properties related to the production methodology used are disadvantages.

This work provides a survey with respect to biosensors depending on graphene and CNTs and their suitability aimed at the detection and early diagnoses of common diseases such as diabetes, cancers (in particular, lung cancer, which is among the principal causes of death), and AD. Moreover, the ability of graphene and CNTs to detect DNA, proteins, hormones, enzymes, and viruses is presented.

DNA Detection. Cao et al. proposed a new electrochemical impedimetric nanobiosensor depending on electrochemically active rGO deposited on a gold working electrode to detect the HIV-1 virus gene. The nanobiosensor used the exonuclease III enzyme to improve the electrochemical indication measured at the detection time based on its affinity to break double-stranded DNA (dsDNA) molecules rather than single-stranded DNA (ssDNA). ssDNA was noncovalently directly immobilized on the rGO surface without using any linker molecules to detect the target DNA. On the contrary, target DNA was added to the cell matrix with known changed concentrations to test the functionality of the nanobiosensor, revealing an LOD of 10 aM (10×10^{-18} M). Moreover, the sensitivity of the nanobiosensor without reducing GO was also evaluated. The result shows that the GO reduction plays a relevant role in the signal amplification along with exonuclease III, as the LOD of GO electrode was 50 fM, which is significantly larger than that of the rGO electrode. According to Cao et al, the nanobiosensor was fully reproducible just by adding new DNA probes. Figure 3A indicates the high selectivity of the nanobiosensor, and Figure 3B reveals its reproducibility.[36] Furthermore, the assembly of the DNA impedimetric biosensor and its recognition via the enzyme supported objective recycling, as shown in Figure 3C.

Cao et al. proposed a simple, responsive, and repeatable label-free DNA impedimetric sensor device. The readily accessible electrochemically reduced graphene oxide (ERGO) is supposedly a useful medium for amplification of signals in DNA hybridization electrochemical impedance spectroscopy (EIS) measurements when combined with exonuclease III. Using enzyme-assisted target recycling, extraordinary impedance generated through ssDNA probes unswervingly adsorbed on top of graphene materials can be converted to squat impedance produced by the persistent desorption of target−probe DNA hybrids and the subsequent probe digestion. Because of rGO's excellent electrical conductivity, the electron-transfer resistance is significantly reduced after the DNA probes are withdrawn. By combining enzymatic and electrical amplification, expanded variations in impedimetric signals should be able to detect DNA targets more accurately. It should also be noted that both DNA targets and probes are label-free, and the sensor can be reproduced merely by switching the DNA probes.[36]

Li et al. established a label-free graphene-based nanobiosensor to distinguish the gene of human immunodeficiency virus 1 (HIV1) using its complementary ssDNA probe immobilized above the surface of the detecting rGO/graphene electrode. The nanobiosensor was fabricated via bonding ERGO noncovalently to the surface of glassy graphene electrodes. In addition, the proposed nanobiosensor electrode rGO/graphene was compared with bare rGO, bare graphene, and GO/graphene electrodes, showing its sensitivity advantage. This advanced sensitivity was used to detect the amount of target DNA, reaching an LOD of 1.58×10^{-1} pM and a linear range (1 μM to 10 pM). The fabrication method has advantages based on its low cost and label-free recognition and due to the fact that no signal amplification or ssDNA immobilizing steps are needed. In addition, fluorescence emission analysis was used to study the functionality of the nanobiosensor in detecting the target DNA. The study showed that ssDNA was strongly noncovalently bonded to the GO surface. After the addition of the target DNA, it took 30 min for it to completely bond with the ssDNA due to the strong forces between ssDNA and GO, which, over time, were weakened by the new bond between the dsDNA. A noncomplementary DNA sequence was applied to show a good selectivity for the target DNA arrangement to study the selectivity of the nanobiosensor. However, the stability of the nanobiosensor still needs improvements due to the breakdown of ssDNA molecules. Furthermore, the sensitivity of the suggested nanobiosensor still needs improvement compared with nanobiosensors with metal nanomaterial and covalently bonded graphene/DNA sensors.[37]

Cai et al. assembled a graphene-based nanobiosensor on a field-effect transistor (FET) chip for DNA detection using a peptide nucleic acid (PNA) probe. Chemically reduced GO was added to the sensor chip; then, 1-pyrenebutanoic acid succinimidyl ester (PBSE) was introduced above the rGO surface to link PNA molecules to the nanobiosensor. DNA detection and quantization were predicted through PNA−DNA hybridization with no labeling and a 100 fM LOD. Using PNA as a detection probe enhanced the sensitivity of the nanobiosensor chip because of the absence of electric repulsion between the negative charges of the deoxyribose phosphate basis of the DNA molecule and the neutral backbone of the PNA molecule. Moreover, the nanobiosensor differentiated between the target DNA and a DNA molecule with one different base beside a noncomplementary DNA molecule. In addition, the proposed nanobiosensor has interesting advantages, such as reduced background noise, signals of high resolution, and relatively low-cost fabrication methods. However, the reproducibility of the nanobiosensor still needs improvement, as shown in the experiments where the signal decreased to 96.67% of the first signal in the second detection experiment and to 83.33% in the third detection experiment.[38]

Dong et al. assembled a nanobiosensor based on rGO that deposited electrochemically on glassy carbon electrodes (GCEs) for DNA detection. Gold nanoparticles (AuNPs) labeled with ssDNA probes and carbon nanospheres functionalized with horseradish peroxidase (HRP) were applied for signal amplification. In addition, ssDNA probes labeled with a thiol group were used to link the AuNPs to rGO surfaces.

https://doi.org/10.1021/acsbiomaterials.1c00710
ACS Biomater. Sci. Eng. 2022, 8, 964−1000

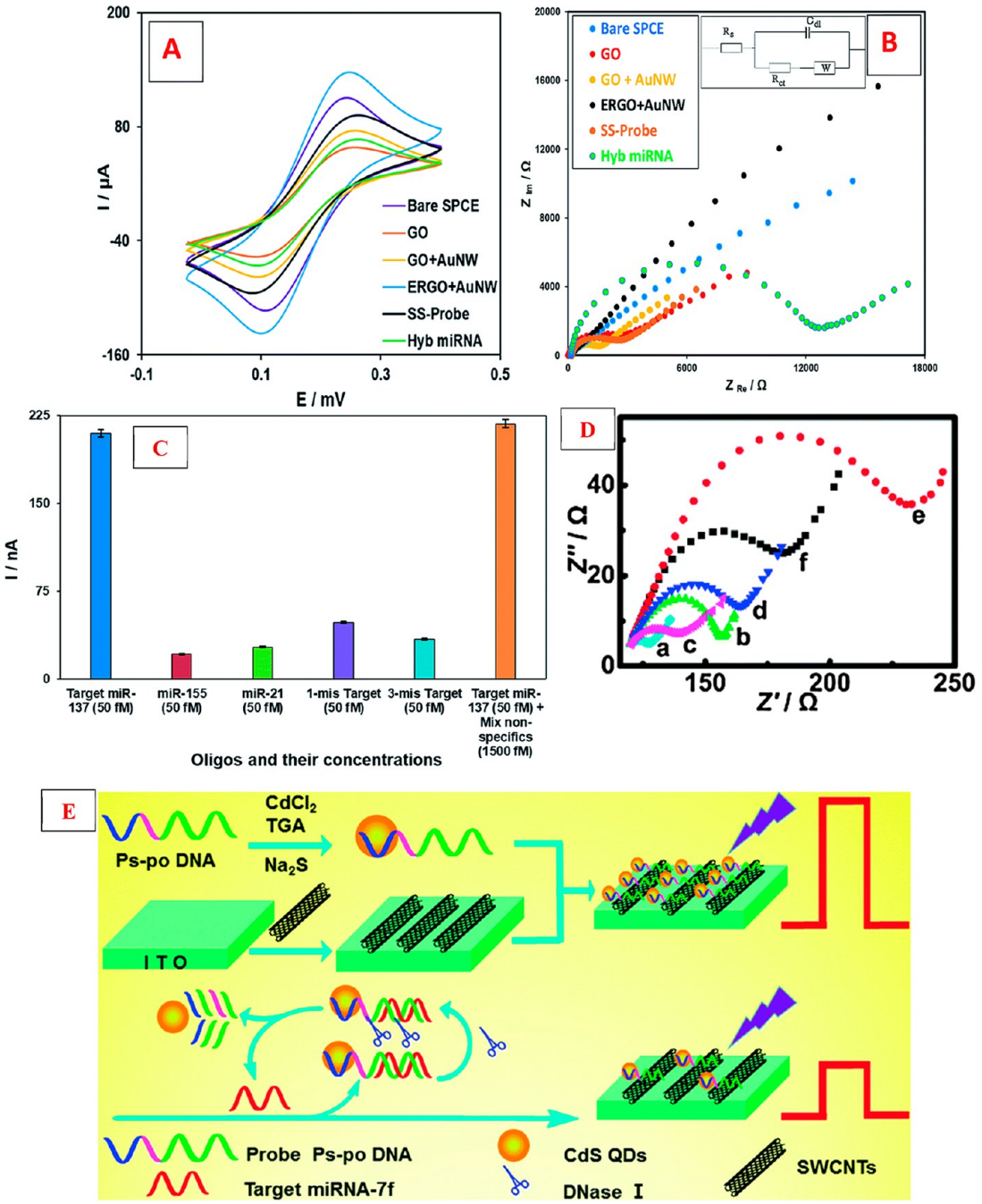

Figure 4. Electrochemical signaling by (A) CV and (B) EIS investigation in $[Fe(CN)_6]^{3/4}$ solution through the nanobiosensor operation. (C) Specificity and selectivity of the nanobiosensor based on experiments repeated four times, illustrated in the bar chart. Panels A–C are reproduced with permission from ref 42. Copyright 2017 The Royal Society of Chemistry. (D) Photoelectrochemical signaling by EIS analysis. (E) Diagram of the photoelectrochemical biosensor aimed at microRNA recognition. In addition, the method is dependent on the development of oligonucleotides with two distinct domains: one that phosphorothioates (ps-) DNA (ps: sulfur-containing variants of the phosphodiester backbone) and the other that phosphates (po-) DNA. When faced with nucleotides, Cd^{2+} has a 3000-fold preference for sulfur over oxygen binding, despite the fact that po-DNA can interact with CdS. As a result, Cd^{2+} would prefer to intermingle with ps-DNA, and the structure of DNA–CdS QDs would be established. Panels D and E are reproduced with permission from ref 43. Copyright 2014 The Royal Society of Chemistry.

Furthermore, the biotinyl group was used for target labeling. The results show very high sensitivity with 5 aM LOD and a linear domain from 1×10^{-17} to 1×10^{-13} M. Furthermore, the nanobiosensor differentiated the target DNA from two other DNAs, the first with one-base mismatching and the other with three-base mismatching. The proposed nanobiosensor holds great potential in the biomedical field for its high sensitivity and selectivity; however, its fabrication and sensing method is costly and complicated.[39]

Alzheimer's Disease Detection. AD is a serious neurodegenerative disease that affects more than 17 million people around the world, mainly aged over 65 years old. AD is associated with memory and cognitive loss, which leads to disability on a daily basis. With the huge burden this disease causes socially and economically, it is necessary to find a

https://doi.org/10.1021/acsbiomaterials.1c00710
ACS Biomater. Sci. Eng. 2022, 8, 964–1000

diagnostic method to detect this illness in its early stages.[40] Recently, several biosensors/nanobiosensors have proven to be useful for the estimation of diverse AD biomarkers by means of approaches other than electrochemical methods.[41]

Azimazadeh et al. applied ERGO as an electrochemical biosensor and miR-137 as a biomarker to detect AD.[42] Furthermore, a screen-printed carbon electrode (SPCE) was adjusted by the addition of GO and gold nanowires (Au NWs) to improve the selectivity of the nanobiosensor. The GO was reduced electrochemically to ERGO to increase its electrical conductivity. Subsequently, ssDNA thiolated probes (ssDNA probes) were added to the nanobiosensor to bind to mi-R137 and form a double-stranded miRNA−DNA probe through the detection process. Doxorubicin (Dox) is a powerful anticancer drug with a wide range of effects. Its use is unfortunately linked to the development of dose-dependent, cumulative, permanent, and long-term cardiotoxic side effects. Genetic and epigenetic fingerprints in each patient can influence the frequency and severity of Dox cardiotoxicity. Dox can also have an effect on epigenetic control. Dox affects mitochondrial metabolism, and epigenetic modifications are based on mitochondrial metabolites that serve as cofactors or substrates for several epigenetic enzymes, according to research. As a result, Dox-mediated changes in the cardiac mitochondrial metabolism may have an impact on the epigenetic landscape and may help us to understand why Dox cardiotoxicity persists long after drug administration. Dox was used in the experiment as an electrochemical label to improve the selectivity of the nanobiosensor due to its low reduction potential, which allows the nanobiosensor to differentiate between the target miRNA and other molecules. Furthermore, the Dox intercalation mechanism is its interaction with double-stranded oligonucleotides, allowing double-stranded miR-137 and ssDNA probes to be differentiated from other nonspecific single-stranded oligonucleotides (miR-155, miR-21, and one-base and three-base mismatch oligos).[42,43]

Through the electrode modification, the cyclic voltammetry (CV) curves are varied at both oxidation and reduction, as shown in (Figure 4A). Furthermore, the Nyquist plots (Figure 4B) show that the SPCE electrode has a low charge-transfer resistance (R_{ct}) (1860 U) and thus a higher electrical conductivity. The CV and EIS plots show appropriate outcomes throughout the change of the nanobiosensor electrode, as the EIS study reveals the increase in R_{ct} by the presence of SS-probes (2449 U) and the target miRNA (11813 U).

Consequently, the nanobiosensor (Figure 4C) showed high selectivity toward the target miRNA (miR-137) in the presence of other highly concentrated oligos and miRNA (miR-21 and miR-155).

MicroRNAs (miRNAs) are small noncoding RNAs that use an antisense mechanism to repress target mRNAs.[42,43] Furthermore, Nyquist plots of the EIS analysis (Figure 4D) showed the efficiency of the nanobiosensor fabrication. The electron-transfer resistance (R_{et}) increased because of the addition of an ssDNA probe, which connected to SWCNTs-COOH by a π interaction. In addition, the fabricated nanobiosensor can be used to recognize other miRNAs by using a suitable ssDNA probe.[43,44]

Cao et al. indicated that DNA−CdS quantum dot (QD)-sensitized SWCNTs-COOH were used to create a flexible photoelectrochemical biosensing platform. A convenient, sensitive, and precise biosensor for the direct detection of miRNAs was intended using cyclic enzymatic amplification, resulting in a novel approach for miRNA analysis.[43] The SWCNTs were added to an indium tin oxide (ITO) electrode to distinguish the target miRNA alongside the DNA−CdS QDs for detection enhancement (Figure 4E). As a result, the presynthesized method was replaced in this study by a one-step suitable preparation pathway of DNA-labeled QDs. When faced with nucleotides, Cd^{2+} has a 3000-fold partiality for sulfur over oxygen binding, despite the fact that phosphate (po)-DNA can interact with CdS. As a result, Cd^{2+} would prefer to interrelate with phosphorothioate (ps)-DNA, and the structure of DNA−CdS QDs would be established, as displayed in Figure 4E.

Using miRNA-7f as a guide, a novel signal-off photoelectrochemical biosensor was created, which caused an enormous number of CdS QDs to break away from SWCNTs-COOH after hybridizing with DNA probes, lowering the photocurrent (Figure 4E). This research established a new, sensitive, and selective method aimed at the straight exposure of miRNAs using low-potential visible-light irradiation, which could be used in other biological assays.

Hormone Detection. Baluta et al. assembled electrochemical nanobiosensors depending on graphene quantum dots (GQDs) to detect the adrenaline hormone with an 83 nM LOD and a linear response ranging between 1 and 120 × 10^{-6} M.[45] The laccase enzyme was linked by glutaraldehyde on a GCE adjusted with GQDs. This nanobiosensor has advantages based on its simple fabrication and cost-effectiveness. Furthermore, it shows great stability when stored at 4 °C because it maintains its activity for more than 3 months. Moreover, the nanobiosensors showed good selectivity for adrenaline among many other coexisting molecules, including ascorbic acid (AA), uric acid (UA), cysteine, tryptophan, and glutathione.[45]

Sun et al. anticipated an electrochemical CNT-based nanobiosensor for the simultaneous sensing of dopamine (DA) and serotonin. GCE was modified with CNTs; then, nickel(II) oxide (NiO) and poly(3,4-ethylene dioxythiophene) (PEDOT) were added. Differentiation between DA and serotonin was possible in the presence of CNTs. In addition, NiO and PEDOT were used in the structure of the nanobiosensor to enhance its sensitivity toward biological molecules. The experiments reported an LOD of 0.026 μM and a linear domain of 0.03 to 20 μM for DA and an LOD of 0.063 and a linear domain of 0.3−35 μM for serotonin. Moreover, the nanobiosensor preserved 95.3% of its signal for serotonin detection and 91.3% of its signal for DA detection after 37 days.[46]

Apetrei et al. proposed a label-free nanobiosensor with a very simple fabrication strategy for the detection of DA and adrenaline from the catecholamine family. In addition, the working electrode was assembled via the installation of graphene on a carbon electrode. Tyrosinase was used for signal amplification and was linked to the electrode by glutaraldehyde. The nanobiosensor showed acceptable sensitivity with a 2.42 × 10^{-1} μM LOD and a 0.2−25 μM linear range for DA and a 6.56 × 10^{-1} μM LOD and 1−27.5 μM linear range for adrenaline. The nanobiosensor conducted almost 10 detection tests with a signal drop of <5% to evaluate the reproducibility. However, the nanobiosensor stability was not sufficient for long-term use, as it restored only 67% of the original signal after storage for 3 days at 4 °C.[47]

https://doi.org/10.1021/acsbiomaterials.1c00710
ACS Biomater. Sci. Eng. 2022, 8, 964−1000

Kim et al. created a noninvasive label-free immunosensor depending on rGO for cortisol sensing through the cortisol monoclonal antibody (c-Mab). In addition, rGO was added to an ITO electrode; then, c-Mab was covalently attached to its surface by an ethyl(dimethylaminopropyl) carbodiimide/*N*-hydroxysuccinimide (EDC/NHS) linker. Furthermore, ethanolamine was also added to the nanobiosensor electrode to minimize nontarget molecule attachment. A real sample of human saliva with a low LOD of 27.6 pM was used to test the nanobiosensor's accuracy. The functionality of the nanobiosensor was evaluated in slices of rat adrenal gland solution rich with molecules with comparable structures to that of cortisol. In addition, the fabricated nanobiosensor revealed a good selectivity toward cortisol in the solution, which can be explained by the c-Mab affinity toward cortisol and the noise reduction caused by ethanolamine. No details, however, were mentioned about the reproducibility or stability of the nanobiosensor.[48]

Raymundo-Pereira et al. technologically advanced a low-cost carbon-based nanobiosensor to detect estriol hormone in water. The working electrode was a porous-structured thin film of carbon black nanoballs (CNBs) and silver nanoparticles (AgNPs) deposited on a GCE. CNBs were prepared from carbon black powder, then hybridized with AgNPs. The use of metal nanomaterial in the electrode, such as AgNPs in this case, prevents the gathering of estriol electro-oxidation on the electrode surface. In addition, the nanobiosensor exhibited good sensitivity and a relatively low LOD of 0.16 μmol L^{-1}; however, it showed a narrow linear domain from 0.2 to 3.0 μmol L^{-1}. Moreover, the stability was evaluated, indicating adequate reproducibility, as just a 5.5% relative standard deviation was reported after 50 pulses of differential pulse voltammetry (DPV).[49]

Cincotto et al. invented an electrochemical enzyme nanobiosensor depending on GO reduced chemically by $NaBH_4$ and hybridized with antimony pentoxide (Sb_2O_5) attached to the rGO oxygen functional groups to detect estriol hormone in water and urine. Furthermore, the rGO/Sb_2O_5 hybrid was added to a GCE to compose the working electrode. Sb_2O_5 has advantages in electrochemical sensing due to its surface deformity and acidic characteristics. Furthermore, glutaraldehyde was used to link laccase enzymes covalently to the electrode surface based on its oxidizing properties, which act on estriol as a phenol-containing molecule. A low LOD of 11 nM was reported alongside an extensive linear region from 25 nM to 1.03 μM. Additionally, a fast signal response of almost 4 s was recorded. Moreover, concentrations (10 and 100 times the estriol concentration) of eight different nontarget molecules (hydroquinone, catechol, DA, progesterone, BPA, 17beta-estradiol, ethinyl estradiol, and vitamin C) that may cause background noise were used to test the selectivity of the nanobiosensor. These nontarget molecules caused no apparent detection signal at 10 times the concentration of estriol; however, signals equivalent to the estriol signals were recorded for 17beta-estradiol and ethinyl estradiol at 100 times the concentration of estriol, which can be explained by the comparable structures of these molecules. The stability of the nanobiosensor was estimated via storing it for 2 months at −4 °C, and 84 and 52% of its functionality was restored after 1 and 2 months, respectively. Equally important, the nanobiosensor detected the target hormone in a real urine sample and retrieved nearly 100% of the added concentration.[50]

Protein and Cancer (Protein) Biomarkers. Eissa et al. applied a graphene-based immunosensor to estimate the β-lactoglobulin protein that is present in milk products. The immunosensor displayed a suitable selectivity and sensitivity for antigen−antibody formation. The graphene screen-printed electrode (SPE) was adjusted with 4-nitrophenyl diazonium cations; then, the nitro groups were electrochemically reduced to amine groups, forming an organic sheet over the graphene SPE. Glutaraldehyde was used to stimulate the amine groups, which immobilized the antibodies of β-lactoglobulin on the graphene SPE. After immunosensor fabrication, the voltammetric analysis was used to study the functioning of the nanobiosensor. With the progressive addition of β-lactoglobulin, the measured current declined sequentially in a linear perspective. This result shows the efficiency of the immunosensor fabrication, where the current decline indicates the successful attachment of the β-lactoglobulin protein to the antibodies on the graphene SPE surface. Moreover, the sensitivity of the immunosensor was tested to reveal an estimation limit of 0.85 pg·mL^{-1} and a linear range of 0.001−100 ng·mL^{-1}. In addition, the selectivity of the anticipated immunosensor was observed by using four proteins other than the target protein (casein, ovalbumin, bovine serum albumin (BSA), and egg lysozyme), and it showed negative results. Furthermore, the immunosensor was tested with a real sample of milk-containing snacks and sweets, and it showed quite similar results to those previously mentioned. In conclusion, this study proposes an immunosensor with good sensitivity with a 0.85 pg·mL^{-1} LOD and a wide linear range (0.001−100 ng·mL^{-1}) with no label or amplification and good selectivity of the target protein. These good characteristics can be attributable to the high stability of the organic sheet on the graphene SPE surface and the large number of immobilized β-lactoglobulin antibodies.[51]

Feng et al. used an electrochemical-label-free graphene-based nanobiosensor aimed at the estimation of the cyclin A_2 protein. The nanobiosensor was fabricated by adding a layer of chemically converted graphene to *meso*-tetra(4-carboxyphenyl) porphyrin (TCPP) on a GCE. The addition of TCPP improved the chemical stability of the electrode and facilitated the attachment of higher amounts of P_0 peptide by providing extra carboxylic groups. The attachment probe used in the proposed nanobiosensor was hexapeptide P_0, which showed a high tendency to connect specifically to the target protein cyclin A_2. Furthermore, Tween 20 (polyoxyethylene sorbitol ester) was used in the experiment as a biocompatible surfactant to elude the attachment of nonspecific molecules to the electrode and thus to minimize the effect of background noise on the nanobiosensor. After the fabrication of the nanobiosensor, the electron-transfer resistance reached a value of 143.8 Ω, and it increased significantly to 348.7 Ω after the addition of cyclin A_2, which indicated the attachment of the target protein to the surface of the electrode. In addition, with the addition of more cyclin A_2, the resistance grew even more, showing a linear relation between the concentration of cyclin A_2 and the electrical resistance. The EIS analysis showed a good LOD of 0.32 pM for protein sensing. Additionally, the electrical resistance increased slightly after the introduction of nonspecific proteins (BSA, human serum albumin (HSA), and lysozyme) to the nanobiosensor, indicating a good selectivity for the target protein. Moreover, the nanobiosensor response to the addition of starved cell extract can be ignored. This selectivity can be explained by the tendency of P_0 to specifically

https://doi.org/10.1021/acsbiomaterials.1c00710
ACS Biomater. Sci. Eng. 2022, 8, 964−1000

attach to cyclin A_2 and the ability of Tween 20 to minimize nonspecific molecule attachment.[52]

Yagati et al. used a graphene-based label-free nanobiosensor to perceive C-reactive protein noninvasively in human serum at room temperature with high specificity at low frequencies. An array of eight microelectrodes of ITO were adjusted with an ERGO/AuNP hybrid, which improved the conductivity of the electrode. Furthermore, the electrical conductivities of ITO/AuNP and ITO/ERGO electrodes were tested separately, with the ITO/ERGO/AuNP electrodes showing the best electrical conductivity among all electrodes. The nanobiosensor was then adjusted with anti-C-reactive protein antibodies to recognize C-reactive protein antigens during the detection process. The BSA protein was also compiled with the nanobiosensor to reduce the background noise responses and to enhance the discrimination against the targeted protein. Afterward, the functionality of the nanobiosensor was evaluated in human serum samples. The samples were organized through the addition of known dissimilar quantities of the target protein in diluted serum. In addition, the results showed good specificity at low frequencies and without any amplification with an estimation limit of almost 0.08 ng mL^{-1} and a linear domain of 1−1000 ng mL^{-1}. Moreover, the nanobiosensor preserved its functionality after 1 week of storage at 4 °C and pH 7.4. This result indicates that the proposed nanobiosensor is good at maintaining the biomaterial on its surface, which can be explained by the presence of AuNPs on it. AuNPs avert the amassing of graphene films, which aids in maintaining the antibodies of the target protein and prevents their release from the surface over time. Moreover, this promising nanobiosensor can be applied to detect other different proteins and antigens by using the appropriate antibodies.[53]

Cancer biomarkers are small molecules in the blood and tissue of humans, and their abnormal concentration can point out the presence of certain cancers.[54] Consequently, the exposure of tumor markers is very significant in cancer diagnoses, especially at the beginning level of cancer. Many proteins represent biomarkers for the detection and diagnosis of cancer.[55] The common protein biomarkers are carcinoembryonic antigen (CEA), α-fetoprotein (AFP), cancer antigen 15-3 (CA15-3), cancer antigen 125 (CA125), and prostate-specific antigen (PSA).[56] As shown in Table 1, CEA can be linked to lung, breast, ovarian, and colon cancers.[57] The AFP concentration in healthy human serum is <25 ng/mL, and increases in the concentration of AFP can indicate liver, testicular, and nasopharyngeal cancers.[58] A CA15-3 concentration of >100 U/mL is the most associated biomarker of breast cancer.[59] CA125 or MUC16 can be used to estimate ovarian cancer, and a higher concentration of CA125 (>5 U/mL) is associated with ovarian cancer.[60] PSA is a biomarker applied to diagnose prostate cancer.[61] Thus it is highly relevant to detect biomarkers sensitively in low concentrations. Therefore, various biosensors are applied for the exposure of protein biomarkers, such as electrochemical detection methods, optical detection methods, and mass-based detection techniques.[62] Graphene and CNTs are attractive nanomaterials for modification in biosensors to detect biomarkers.

Table 1. Different Biomarkers Used for Cancer Detection

cancer biomarker	type of cancer detection	ref
carcinoembryonic antigen (CEA)	lung, breast, ovarian, and colon	57
α-fetoprotein (AFP)	liver, testicular, and nasopharyngeal	58
cancer antigen 15-3 (CA15-3)	breast	59
cancer antigen 125 (CA125)	ovarian	60
prostate-specific antigen (PSA)	prostate	61

To recognize the CEA cancer biomarker, Singh et al. described a low-cost and lightweight biosensor. The fabricated biosensor consists of a graphene film developed on copper (Cu) via chemical vapor deposition (CVD). In addition, PBSE was applied as a linker to immobilize the CEA antibody, and BSA was used to cover unspecific centers. After the addition of CEA, the charge-transfer resistance (R_{ct}) standards were increased because of the formation of CEA and anti-CEA complexes that blocked the transfer of electrons. Therefore, the BSA/anti-CEA/PBSE/graphene/Cu electrode can be used in CEA detection with a sensitivity value of 563.4 Ω ng^{-1} mL cm^{-2}, an LOD value of 0.23 ng mL^{-1}, and a linear response range value of 1.0−25.0 ng mL^{-1} (normal value of ∼5.0 ng mL^{-1}). Anti-CEA/BSA/PBSE/graphene/Cu electrodes can thus be used as prospective biosensors for the early stage of cancer because of their elevated sensitivity, selectivity, stability, and reliability that aim at the detection of CEA via EIS measurements.[63]

For the responsive exposure of AFP, Yang et al. technologically advanced a label-free electrochemical immunosensor relying on AuNPs-poly(3,4-ethylenedioxythiophene) (PEDOT)/Prussian blue (PB)-rGO. Furthermore, the AuNPs-PEDOT 3D nanostructure had a large surface area, which enabled the AFP antibody to be effectively captured. AFP antigen was also immobilized on anti-AFP/AuNPs-PEDOT/PB-rGO/GCE, resulting in a reduction in the sensor's peak present. As a result, AFP was distinguished through the sensor. With a linear range of 0.01−50 ng mL^{-1} and a low LOD of 3.3 pg mL^{-1}, the AuNPs-PEDOT/PB-rGO nanocomposite displays efficient electrochemical operation, strong conductivity, and excellent stability. When compared with the traditional enzyme-linked immunosorbent assay (ELISA) approach for detecting AFP in human serum, this biosensor produces adequate results.[64]

Some efforts have been made to detect CEA and AFP instantaneously. Jia et al. incorporated rGO/AuNPs into thionine (Thi) and PB on an ITO electrode for the simultaneous detection of CEA and AFP (Figure 5A).[65] In addition, rGO/AuNPs/Thi was applied toward the immobilization of anti-CEA and rGO/AuNPs/PB for the immobilization of anti-AFP. The sensor is based on the reaction between antibodies and their antigens, the detection targeted for a reduction trend in the peak current of Thi and PB (Figure 5B). The multiplexed biosensor exhibits linear working ranges of 0.01−300 ng mL^{-1}, and the LODs are 0.650 pg mL^{-1} for CEA and 0.885 pg mL^{-1} for AFP.[65] Furthermore, Chen et al. studied a low-cost electrochemical immunosensor in sandwich format aimed at the synchronized detection of CEA and AFP. This biosensor depends on a sensing platform of chitosan-AuNPs (CHIT-AuNPs) and multiple signal labels depending on carboxylated GO sheets added to toluidine blue (TB)/anti-CEA ($Ab_{1,1}$) for CEA detection and PB/anti-AFP ($Ab_{1,2}$) for AFP detection. This sensor revealed a linear range of 0.5−60 ng mL^{-1} and LODs of 0.1 ng mL^{-1} for CEA and 0.05 ng mL^{-1} for AFP.[66]

Researchers used rGO/Thi/AuNPs and rGO/PB/AuNPs nanocomposites to assess the CEA and AFP levels to realize

https://doi.org/10.1021/acsbiomaterials.1c00710
ACS Biomater. Sci. Eng. 2022, 8, 964−1000

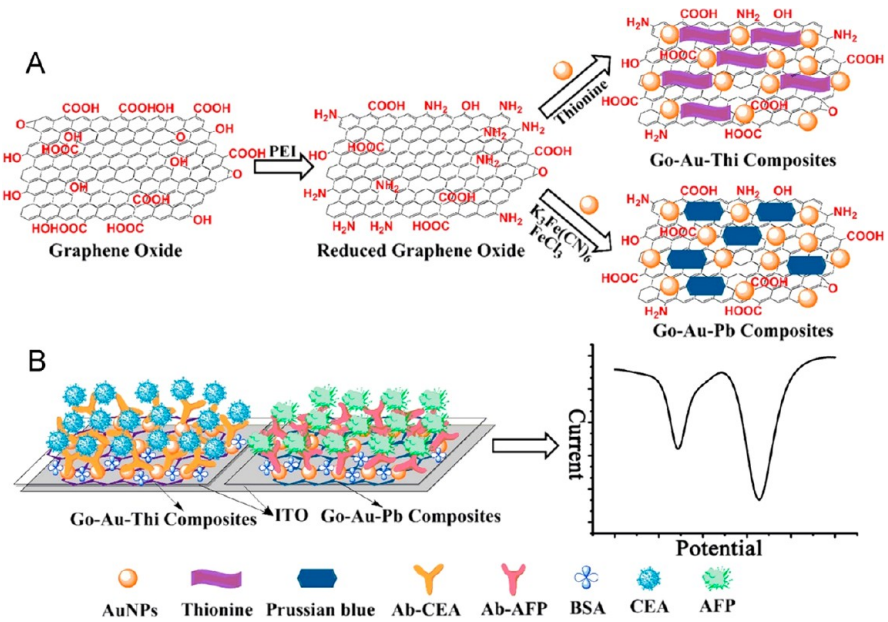

Figure 5. (A) Thi molecules were noncovalently appended to the rGO surface via $\pi-\pi$ stacking interrelations, whereas PB nanoparticles were cultivated upon this rGO surface via an in situ reduction method to demonstrate the nanocomposite solidification process of rGO/Thi/AuNPs and rGO/PB/AuNPs. Because of the interaction between the amine groups of rGO and the AuNPs, AuNPs were immobilized on rGO/Thi and rGO/PB nanocomposites. (B) Schematic representation of the electrochemical immunoassay procedure. Interactions between antibody amine groups and AuNPs immobilized anti-CEA and anti-AFP through into relevant aspects coated with rGO/Thi/AuNPs and rGO/PB/AuNPs, respectively. AuNPs' distinct features create an ideal microenvironment for antibody immobilization while preserving biological proteins. A single square-wave voltammetry (SWV) test was observed after the cells were independently subcultured to various doses of CEA and AFP. Because of the increased steric hindrance caused by the formation of antibody−antigen immunocomplexes on the ITO surface, the peak currents of Thi and PB, which were directly proportional to the concentrations of the corresponding antigens, were reduced. The CEA and AFP levels in blood sample could be assumed to be constant upon this relationship. Reproduced with permission from ref 65. Copyright © 2013 Elsevier.

the electrochemical immunoassay protocol.[66] Figure 5A demonstrates the noncovalent attachment of Thi molecules to the rGO surface via $\pi-\pi$ stacking interactions, whereas PB NPs were grown on the rGO surface via an in situ reduction technique. AuNPs were immobilized on rGO/Thi and rGO/PB nanocomposites by the interaction between the amine groups of rGO and the AuNPs. Anti-CEA and anti-AFP were immobilized to analogous extents and coated with rGO/Thi/AuNPs and rGO/PB/AuNPs, respectively, as shown in Figure 5B, through the relationships of the amine groups of antibodies with the AuNPs. After the cells were incubated separately with various quantities of CEA and AFP, a single square-wave voltammetry (SWV) test was performed. The peak currents of Thi and PB, which were unswervingly relative to the concentrations of conforming antigens, were reduced as a result of increased steric hindrance caused by the formation of antibody−antigen immunocomplexes on the ITO surface. On the basis of the relationship, the levels of CEA and AFP in serum samples could be measured.

Khoshroo et al. established a label-free electrochemical sensor aimed at recognition of CA15-3 cancer biomarkers depending on CoS_2-GR and AuNPs composites with graphite SPEs. In this research, an electrochemical sensing platform for electrochemical immunosensors was built using CoS_2-GR and AuNP composites (CoS_2-GR-AuNPs). AuNPs serve as an immobilization site for antibody binding in the proposed immunosensor. In addition to a vast surface area, the CoS_2-GR nanocomposite possesses remarkable electrocatalytic action for catechol oxidation, which helps boost the amount of immobilized CA15-3 antibody. In addition, CoS_2-GR-AuNPs (CA15-3)-modified graphite-SPEs were employed to produce an enzyme-free and label-free electrochemical immunosensor to detect the protein biomarker CA15-3. The CoS_2-GR composite was used due to its high electrocatalytic activity of catechol oxidation and the ability to increase the immobilization effect of the CA15-3 antibody through its wide surface area. They also added AuNPs as the sites of immobilization to bind antibodies. The CA15-3 antigen could be detected from the electrocatalytic activity of CoS_2-GR-AuNPs/SPE for catechol oxidation, where they found a decrease in the peak current when the interaction between the antigen and the antibody occurred (Figure 6). This issue is due to the development of an insulating layer from the anti-CA15-3 and CA15-3 antigen complexes that prevents electron transfer and catechol oxidation. The biosensor shows a varied linear range of 0.1−150 U mL^{-1} and a low LOD of 0.03 U mL^{-1}. CoS_2-GR-AuNPs can be used for clinical application in human serum. The immunosensor performed well in regards to its accuracy, stability, and specificity, and it was effectively used to detect CA15-3 in serum models.[67]

Fan et al. developed a paper-based electrochemical immunosensor aimed at the discovery of CA125. Furthermore, the biosensor depends on rGO/Thi/AuNPs nanocomposites and has been developed through screen-printing on low-cost pure cellulose paper. CA125 antibody was put out of action by the working electrode to specify the sensor for the recognition of the CA125 antigen. The formation of anti-CA125 and CA125 antigen, which takes a maximum of 20 min, leads to an insulating layer for electron transfer to the electrode surface, targeting a reduction in the peak current of Thi. Therefore, this biosensor can detect the CA125 antigen. This electrochemical sensor exhibited excellent replicability, stability, and confidence

https://doi.org/10.1021/acsbiomaterials.1c00710
ACS Biomater. Sci. Eng. 2022, 8, 964−1000

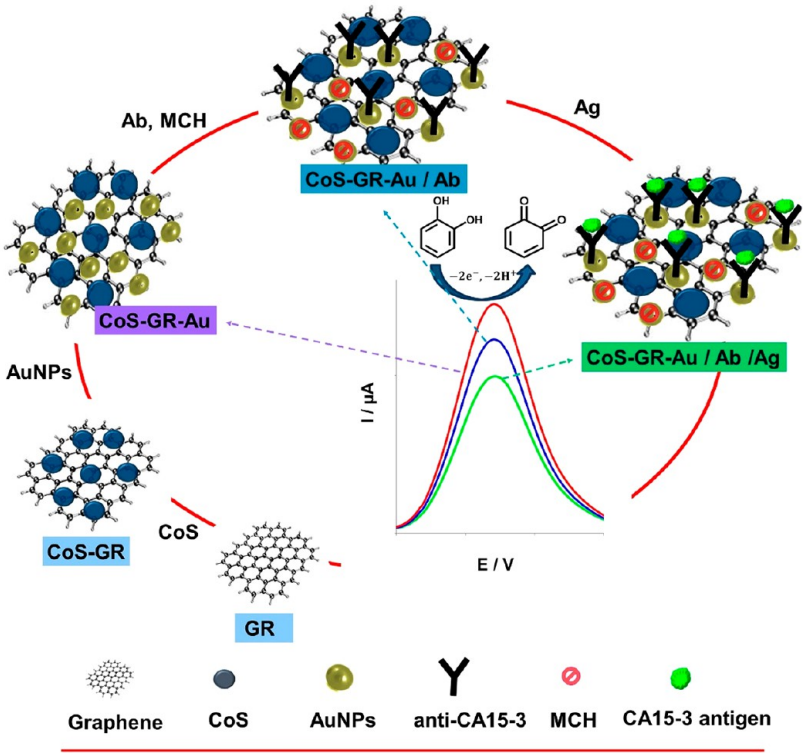

Figure 6. Fabrication procedure of the CoS_2-GR-AuNPs immunosensor. An electrochemical sensing platform aimed at electrochemical immunosensors was built via CoS_2-GR and AuNPs composites (CoS_2-GR-AuNPs). AuNPs serve as an immobilization site for antibody binding in the proposed immunosensor. In addition to a vast surface area, the CoS_2-GR nanocomposite possesses remarkable electrocatalytic action for catechol oxidation, which helps raise the aggregation of immobilized CA15-3 antibody. Graphite screen-printed electrodes adapted with CoS_2-GR-AuNPs (CA15-3) were used to produce an enzyme-free and label-free electrochemical immunosensor to detect the CA15-3 protein biomarker. Because of the electrocatalytic activity of the CoS_2-GR nanocomposite in catechol oxidation as a sample, the CA15-3 antigen was characterized through amended screen-printed electrodes after binding to the electrode surface through interaction with the CA15-3 antibody. Additionally, the immunosensor was designed to have a linear range of 0.1−150 U mL^{-1} and an LOD of 0.03 U mL^{-1}. In addition, the immunosensor performed well in terms of the accuracy, stability, and specificity, and it was efficaciously used to detect CA15-3 in serum models. Reproduced with permission from ref 67. Copyright 2017 Elsevier.

with a linear range from 0.1 to 200 U mL^{-1} and an LOD of 0.01 U mL^{-1}. rGO/Thi/AuNPs nanocomposites can be used toward the recognition of CA125 in human blood serum.[68]

An exceedingly sensitive electrochemical immunosensor built on MWCNTs and ionic liquid (IL) nanocomposites adapted with GCEs aimed at the uncovering of PSA was established by Salimi et al. In addition, the fabricated sensor depends on the immobilization of PSA-antibody (anti-PSA) onto MWCNTs/IL nanocomposites and the binding of PSA antigen to the active sites of the PSA antibody. The higher concentration of PSA antigen leads to a decrease in the active sites of the antibody. Therefore, the sensor can effectively detect PSA antigen. The DPV peak current of the immunosensor shows a sensitivity of 0.95 mA ng mL^{-1}, an LOD of 20 pg mL^{-1}, and two linear concentration ranges of 0.2 to 1.0 and 1−40 ng mL^{-1}. It was found that the ILs/CNTs immunosensor shows a promising performance in noticing PSA in cancer tissue and human serum samples with accuracy, high sensitivity, and selectivity for the detection of PSA.[69]

It is crucial to discover and characterize cancer biomarkers early to make an accurate diagnosis. Mandal et al. used this knowledge to industrialize a biosensor based on CNT electrodes with interdigitated electrode patterns and integrated polydimethylsiloxane (PDMS) microfluidic channels to estimate the CA-125 cancer biomarker. The biosensor improves detection by lowering the process time, cost, and space requirements. CNTs have a large surface area, which enhances the electron transport and thus increases the sensitivity. Additionally, the CA-125 antibodies improve the biosensor's stability. The study method is primarily based on the design of a surface modification process for increased sensitivity under shear flow rate circumstances using CNTs. The interdigitated electrode transducer was modified with functionalized CNTs to improve the signal. The biosensor was connected to PDMS microfluidic channels to enable a directed self-driven flow. The results reveal that by employing CNT-modified interdigitated electrodes in a capillary flow state, disease-specific antigens (CA-125) may be differentiated in a microvolume of biofluid.[70]

Because of the chemical dealings between both the antibody and the antigen to form the CA-125 antibody and CA-125 antigen complex, the dielectric characteristics and capacitance were altered. This modification defined the biosensor's success for recognizing the CA-125 antigen.[70] Additionally, Mandal et al. demonstrated the feasibility of developing a functioning carboxylic CNT biosensor with an interdigitated electrode pattern and an integrated microfluidic channel. Even at low CA-125 antigen concentrations, the interdigitated electrodes aided the sensing process in a confined space. CNTs exhibited a greater capacitance value due to their remarkable surface-to-volume ratio and increased electron-transfer rate, which had a direct effect on the sensor's sensitivity enhancement. The CA-

https://doi.org/10.1021/acsbiomaterials.1c00710
ACS Biomater. Sci. Eng. 2022, 8, 964−1000

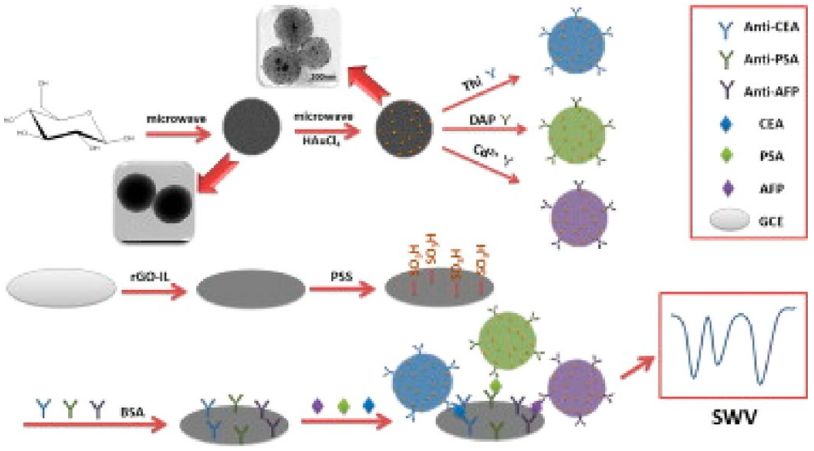

Figure 7. Representation of the electrochemical immunoassay protocol. CGN-Thi-anti-CEA, CGN-DAP-anti-PSA, and CGN-Cd^{2+}-anti-AFP bioconjugates were first prepared to make electrochemical immunoprobes. The reduction of AuNPs and the carbonization of glucose took place in a microwave-assisted reaction. The reactive oxygen groups of CGN immobilized three redox probes: Thi, DAP, and Cd^{2+}. Three electrochemical immunoprobes were obtained after the antibodies were directly immobilized on CGN AuNPs. Reproduced with permission from ref 72. Copyright 2015 Elsevier.

125 antibodies were covalently devoted to the carboxylic CNTs in this study, resulting in enhanced antibody stability, even at high shear flow rates. The tests in this work used carboxylic-functionalized CNTs with a 3% surface coverage. The existence of a higher proportion of carboxylic-functionalized groups on the surface of CNTs may give a location for the attachment of more antibodies, which would affect the stability of the CNTs and their sensitivity. Additionally, the biosensor based on CNT interdigitated electrodes may be a viable tool for the discovery of additional disease biomarkers.

For the recognition of AFP, an innovative sandwich-type electrochemical immunosensor depending on functionalized nanomaterial labels and bienzyme biocatalyzed precipitation was created by Yang and coworkers. They studied the electrochemical immunosensor depending on single-walled carbon nanohorns (SWCNHs) by means of labels and bienzymes (HRP and glucose oxidase). In addition, enzymes acting as biocatalysts accelerated the oxidation of 4-chloro-1-naphthol (4-CN) by H_2O_2, resulting in an insoluble substance on the electrode surface; the mass stacking on the device directed to a dramatic increase in amplitude. With a linear range of 0.001−60 ng mL^{-1} and a low LOD of 0.33 pg mL^{-1} for the detection of AFP, the immunosensor demonstrates high sensitivity, good selectivity, and stability. Moreover, bienzyme/Ab_2/SWCNHs biosensors can be applied in serum testers.[48] In addition, the immunosensor has strong selectivity, stability, and reproducibility. The study concluded the following main points, which are responsible for the dramatic signal amplification: (1) For sandwich-type immunosensors, enzymatically catalyzed precipitates depending on the bienzyme direction greatly improved the signal strength. (2) SWCNHs can serve as suitable carriers with a wide surface area for effective biomolecule immobilization and a large space for insoluble items. (3) Antibodies can be increased by using Au−graphene as an electrode modifier. In clinical tumor biomarker screening, the amplification strategy showed promise. Yang et al. believe that this innovative approach can easily be extended to identify other proteins and that it has clinical application potential.[71]

Xu et al. introduced a sandwich-format electrochemical immunosensor that simultaneously exposed three cancer biomarkers: CEA, PSA, and AFP (Figure 7). Carbon−gold nanocomposite (CGN)-Thi-anti-CEA and CGN-DAP-anti-PSA in addition to CGN-Cd^{2+}-anti-AFP bioconjugates were manufactured first to render electrochemical immunoprobes. In a microwave-assisted reaction, AuNPs were reduced, and glucose was carbonized. Three redox probes were immobilized by CGN's reactive oxygen groups: Thi, DAP, and Cd^{2+}. After the antibodies were immobilized in a straight line on CGN AuNPs, three electrochemical immunoprobes were acquired (Figure 7). Using the casting process, the GCE was directly amended with positively charged IL-rGO for modification. GCE was then immersed in an aqueous polystyrene sulfonate (PSS) solution for a few minutes. Because the isoelectric point of the antibody was a pH of ∼9.0, it was usually positively charged. CEA-, AFP-, and PSA-captured antibodies were immobilized on GCE using this technique. Because of the exceedingly biospecific recognition interactions between the antigens and the corresponding antibodies, a sandwich-type immunoassay was formed after the immunosensor was consecutively incubated with a mixture of antigen solutions and a mixture of 1:1:1 diluted CGN-Thi-anti-CEA, CGN-DAP-anti-PSA, and CGN-Cd^{2+}-anti-AFP bioconjugates. SWV was applied to collect the most recent responses. The concentrations of equivalent antigens were directly compared to the distinct voltammetric peaks of Thi, DAP, and Cd^{2+}. The obtained linear relationship allowed for the quantitative measurement of CEA, AFP, and PSA in serum models.

Consequently, the immunosensor is based on the carbon−gold nanocomposite (CGN) as a probe in addition to Thi-anti-CEA, DAP-anti-PSA, and Cd^{2+}-anti-AFP to detect the three antibodies, CEA, PSA, and AFP, respectively. Because of the profusion of reactive oxygen functional groups on its surface, this nanocomposite demonstrated excellent adsorption aptitude for redox probes, for instance, certain organic dyes and metal ions. Additional binding sites were supplied by the AuNPs on the nanocomposite for the three antibodies, CEA, PSA, and AFP. In addition, the immunosensor is based on the reaction between antibodies and their antigens. Via SWV, three distinct signals can be perceived in a single run. In addition, the current response measurements of Thi, DA, and Cd^{2+} were related to their corresponding antigens, and the SWV peak

https://doi.org/10.1021/acsbiomaterials.1c00710
ACS Biomater. Sci. Eng. 2022, 8, 964−1000

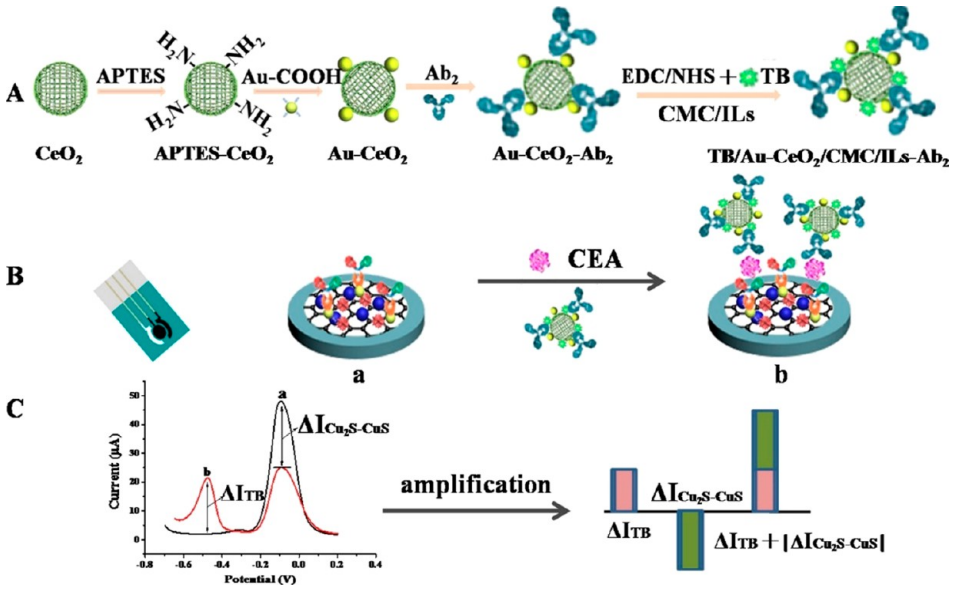

Figure 8. (A) Incubation of CEA labels. The Au-CeO_2 (1 mL, 1.8 mg/mL) solution was treated ultrasonically for 30 min before being combined with a detecting antibody dispersion (1 mL, 10 g/mL) and incubated for 12 h at 4 °C. Blue toluidine (TB, 2 mg) and EDC/NHS (10 mM/2 mM) were then incubated for 12 h at 4 °C. The tetrafluoroborate was mixed with CMC (10 mg) as the ionic liquid (IL, 8 mg) after centrifugation and incubated at 4 °C for 1 h. After centrifugation, the supernatant was washed with PBS (pH 7.4) to eradicate excess TB prior to the colorless supernatant. The mixture from TB/Au-CeO_2/CMC/ILs-Ab_2 was then dissolved in PBS (1 mL, pH 7.4) and held at a temperature of 4 °C. (B) Immunosensor diagram (TB/Au-CeO_2/CMC/Ils). Bare SPCE was amended to create an efficient surface area of the electrode with the distributed Au-Cu_2S-CuS/graphene (4.5 L, 1.2 mg/mL) to produce a directly usable surface. Former layers were incubated in a type of Ab1 (4.5 L, 10 g/mL) and BSA solution (4.5 L, 0% by weight) with unpredictable concentrations of CEA (4.5 L) and TB/Au-CeO_2/CMC/IL. (C) Double-signal enhancement technique. The peak oxidation current of Cu_2S-CuS decreases, whereas the peak oxidation current of TB increases. The response to the quantitative determination signal of the CEA is the shift of double signals "$\Delta I = \Delta I_{TB} + |\Delta I_{Cu_2S\text{-}CuS}|$". ($\Delta I_{TB}$ and $|\Delta I_{Cu_2S\text{-}CuS}|$ are the changes in the oxidation peak currents of TB and Cu_2S-CuS currents, respectively.) The LOD is 0.78 pg/mL, and the linear range is 0.001−100 ng/mL. The ratiometric electrochemical method is a basic technique for detecting tumor markers with accuracy, simplicity, and sensitivity, and it shows promise for the quantitative recognition of other tumor markers in clinical diagnoses. Reproduced with permission from ref 81. Copyright 2017 Elsevier.

currents of Thi, DA, and Cd^{2+} improved with increasing concentration of the corresponding antigens. This sensor revealed good sensitivity and selectivity with a linear range of 0.01−100 ng mL^{-1}, and the LODs were 2.7 pg mL^{-1} for CEA, 4.8 pg mL^{-1} for PSA, and 3.1 pg mL^{-1} for AFP for the detection of CEA, PSA, and AFP simultaneously.[72]

Lung cancer is the leading cause of death for men and the second leading cause of death for women.[73] Furthermore, lung cancer is categorized into two major types: small cell lung cancer (SCLC) and nonsmall cell lung cancer (NSCLC). Additionally, SCLC represents ∼20% of lung malignancy, and NSCLC represents >80% of lung malignancy.[74,75] Therefore, there is much interest in the detection of NCLC and SCLC. Detection of the high concentration of biomarkers related to lung cancer is essential for the monitoring and diagnosis of lung cancer. In addition, NSCLC can be detected through biomarkers such as CEA, cytokeratin fragment antigen 21-1 (CYFRA21-1), EGFR gene, and microRNA (miR-25).[76−78] A neuron-specific enolase (NSE) biomarker is used for the sensitive and specific estimation of SCLC.[79] Biosensors are widely used to determine biomarker levels with high sensitivity aimed at the diagnosis of lung cancer.[80]

Wei et al. used the dual-signaling electrochemical radiometric approach to study an electrochemical biosensor aimed at CEA recognition. This sandwich-type biosensor uses AuNPs with a Cu_2S-CuS/graphene composite (Au-Cu_2S-CuS/graphene) as the matrix material and carboxyl-AuNPs with mesoporous CeO_2 NPs and a TB complex (TB/Au-CeO_2/carboxymethyl cellulose (CMC)/Ils) to detect CEA (Figure 8A,B). Furthermore, the electrochemical behavior of the biosensor indicates the decrease in the Cu_2S-CuS oxidation peak current and the increase in the TB oxidation peak current when the CEA concentration is increased (Figure 8C). In addition, the TB/Au-CeO_2/CMC/ILs-Ab_2 synthesis method is shown in Figure 8A. The Au-CeO_2 solution (1 mL, 1.8 mg/mL) was ultrasonically treated for 30 min before being mixed with a detection antibody dispersion (1 mL, 10 g/mL) and incubated at 4 °C for 12 h. The mixture was then incubated at 4 °C for 12 h with TB (2 mg) and EDC/NHS (10 mM/2 mM). 1-Butyl-pyridine tetrafluoroborate was mixed with CMC (10 mg) as an IL (8 mg) and incubated for 1 h at 4 °C after centrifugation. Figure 8B demonstrates a representative illustration of a sandwich-type electrochemical immunosensor. After being rinsed with phosphate-buffered saline (PBS) (pH 7.4), the completed electrode was preheated for electrochemical experiments. Figure 8C also shows the dual-signaling augmentation methodology used by the electrochemical ratiometric immunosensor. "$\Delta I_{TB} + |\Delta I_{Cu_2S\text{-}CuS}|$" is applied as the response signal to amplify the electrochemical response to quantitatively evaluate the deliberation of CEA. With increasing CEA concentration, the oxidation peak current of Cu_2S-CuS decreases, whereas the oxidation peak current of TB increases. The response signal aimed at the quantitative determination of CEA is the change of dual signals "$\Delta I = \Delta I_{TB} + |\Delta I_{Cu_2S\text{-}CuS}|$". ($\Delta I_{TB}$ and $|\Delta I_{Cu_2S\text{-}CuS}|$ are the alteration principles of the oxidation peak currents of TB and Cu_2S-CuS, respectively.) The linear range is 0.001 to 100 ng/mL,

https://doi.org/10.1021/acsbiomaterials.1c00710
ACS Biomater. Sci. Eng. 2022, 8, 964−1000

with an LOD of 0.78 pg/mL (S/N = 3). Additionally, the ratiometric electrochemical structure is a humble approach aimed at distinguishing tumor indications that is accurate, simple, sensitive, and precise, and it is promising for the quantitative recognition of other tumor markers in clinical diagnosis. Therefore, the quantitative concentration of CEA from the peak current of the oxidation of TB and Cu_2S-CuS can be detected with a linear range of 0.001−100 ng/mL and an LOD of 0.78 pg/mL. Additionally, this electrochemical biosensor shows high performance in clinical application for human blood serum due to its accuracy and selectivity.[81]

Zhu et al. established an electrochemical immunosensor focusing on the sensitive identification of CEA through the antibody and antigen reaction and based on graphene decorated by a AuNP (Au-GN) amended with a GCE and the immobilization of HRP and an HRP-labeled anti-CEA antibody (HRP-anti-CEA) on Au-GN/GCE. The effect of the reaction between HRP-anti-CEA and the CEA antigen was remarkable, where the cathodic peak current response of hydroquinone (HQ) decreased. In addition, the immunosensor was thus able to detect CEA effectively. Additionally, the HRP/HRP-anti-CEA/graphene nanoplatelets (GNPs)-GNs/GCE biosensor exhibits high selectivity and stability with a linear range of 0.10−80 ng mL^{-1} and an LOD of 0.04 ng mL^{-1} for CEA detection. This biosensor has possible use in human serum samples when associated with ELISA measurement.[82]

Zhang et al. assembled a label-free electrochemical immunosensor that consists of a 3-D macroporous reduced graphene oxide/polyaniline (3DM rGO/PANI) film aimed at the recognition of NSE for SCLC. In addition, the 3DM rGO/PANI composite is categorized through an auspicious surface area that expands the immobilization of NSE antibodies. In addition, the immunosensor can prevent the adsorption of other antibodies and specify an NSE antibody by blocking the rest of the active sites by 1 wt % of BSA. The complex of anti-NSE and NSE antigen blocks electron transfer to the electrode; therefore, the peak current of the sensor decreases. Consequently, the sensor succeeds in NSE detection. The current response of PANI decreases with increasing NSE concentration, so, PANI is important to indicate the concentration of NSE. Furthermore, the 3DM rGO/PANI immunosensor shows a linear range (0.5 pg mL^{-1} to 10.0 ng mL^{-1}) and an LOD of 0.1 pg mL^{-1} aimed at NSE detection. In addition, the immunosensor can be useful in serum samples to detect NSE when compared with the electrochemiluminescence (ECL) analyzer.[83]

To detect the specific and important biomarker of NSCLC, Chen et al. established a 3-D electrochemical DNA biosensor for CYFRA21-1 (CYFRA21-1 DNA) detection based on 3D graphene and AgNPs (3D GF/AgNPs). The applied 3D GF/AgNPs DNA biosensor is dependent on the probe ssDNA immobilization of the modified electrode and the hybridization with target DNA, targeting toward a reduction in the peak current of the electrode. This biosensor shows an LOD of 1.0×10^{-14} M and a linear range from 1.0×10^{-14} to 1.0×10^{-7} under optimal conditions, with high sensitivity, good stability, and selectivity for CYFRA21-1 DNA detection. The 3D GF/AgNPs biosensor has excellent performance when applied to lung cancer tissue samples due to its low price, outstanding accuracy, and rapid response time.[84]

Shoja et al. used a two-step electropolymerization of Ni(II)-oxytetracycline-guiding metallopolymer NPs (Ni-OTC NPs) over a pencil graphite electrode (PGE) surface adapted with an rGO/carboxyl-functionalized ordered mesoporous cation to develop an electrochemical genobiosensor aimed at detecting EGFR exon 21 point mutations. rGO and carboxyl-functionalized ordered mesoporous carbon (f-OMC) were deposited above the electrode surface to increase the electrical conductivity and the electrochemical effective surface area. They described a DNA biosensor for the exposure of NSCLC EGFR exon21 (L858R mutation point). The biosensor consists of a PGE adapted with an rGO/carboxyl-functionalized ordered mesoporous carbon (rGO/f-OMC) composite with added metallopolymer Ni-OTC NPs through two-step electropolymerization. A strong amide-bond-immobilized ssDNA apprehension probe with amine groups at the 5′ end served as a recognition element on the rGO/f-OMC/PGE surface. Electropolymerized Ni-OTC metallopolymer NPs were electropolymerized to the rGO/ssDNA-OMC/PGE surface; then, hybridization was carried out using Ni-OTC NPs as a redox label in DPV. The prepared rGO/f-OMC/Ni-OTC NPs/PGE biosensor demonstrated long-term stability (21 days) with a broad linear range (0.1 to 3 μM) and a strong linear response (R^2 = 0.998) with high sensitivity (0.0188 mA/μM) and a low LOD (120 nM) under ideal conditions.[62] This DNA biosensor had a low-cost fabrication process along with good stability and repeatability. Only suitable for use in alkaline solutions, the modified rGO/f-OMC/Ni-OTC NPs/PGE has the ability to be used in the production of other electrochemical DNA biosensors and electrochemical immunosensors.[85]

Jia et al. describes a cheap, optical, and fast immunochromatographic assay system on cotton thread for the detection of CEA by the use of nanocomposite reporter NPs of CNT/GNPs. This biosensor shows a lower cost and higher sensitivity than the ordinary reported probe based on CNTs or GNPs. The performance of the biosensor for the detection of CEA can be perceived via the naked eye, where a deep color appears in the absence of CEA on the test zone, providing a negative test, because only the CNT/GNPs reported probe was in the sample (Figure 9). CEA has been immobilized on a cotton thread for the construction of a test area. The capillary effect caused the CNT/GNP sample solution to flow through the long axis of the cotton thread when loaded on the sampling pad. In addition, in the presence of target CEA, the decreasing combined quantity of CNT/GNPs nanocomposite reporter probes on the test zone was directly read via the naked eye (Figure 9). Meanwhile, a commercially available scanner may be used to perform quantitative detection. As compared with standard AuNPs or CNTs as reporter probes, the method's sensitivity was increased by two to three orders of magnitude. The CNT/GNP-based immunochromatographic assay exhibits good selectivity with a linear range of 5−500 ng/m and an LOD of 2.32 ng/mL CEA (S/N 3) under ideal conditions, which is sensitive for clinical diagnosis.[86] Finally, when compared with previously recorded individual CNT or GNP reporter probes, the CNT/GNPs nanocomposite reporter probe demonstrated significant sensitivity improvements. This proposed method performed well for CEA detection and had a low LOD. These findings suggest that the innovative CNT/GNPs nanocomposite reporter-probe-based immunochromatographic assay on cotton thread is mostly well suited for point-of-care (POC) diagnostics in resource-constrained areas.[86] The research method's ease of use and high sensitivity make it a promising candidate for further protein biomarker

https://doi.org/10.1021/acsbiomaterials.1c00710
ACS Biomater. Sci. Eng. 2022, 8, 964−1000

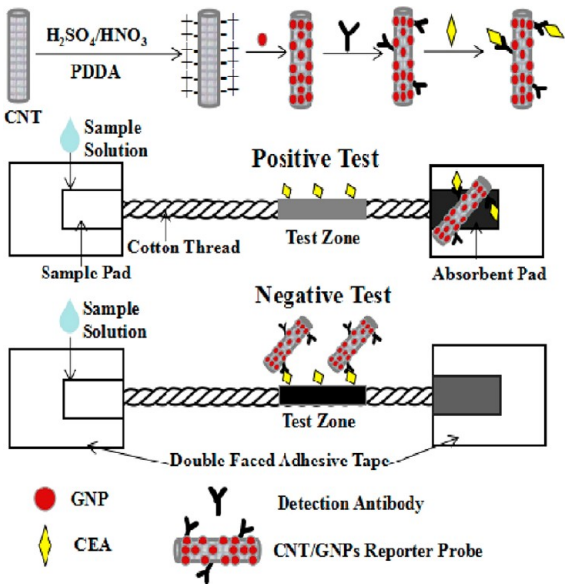

Figure 9. Bonding event between CEA inside the sample solution (unknown concentration) and established CEA (immobilized on the cotton thread test zone) and dAb in the area of the CNT/GNPs nanocomposite is used for the novel nanocomposite test of the CNT/GNPs nanocomposite probe depending on the cotton thread biosensor aimed at CEA exposure. CEA has been immobilized on cotton thread to create a test area. The capillary effect caused the CNT/GNP nanomaterial reporter's CEA solution to move along the long axis of the cotton thread when loaded on the sample pad. The CNT/GNPs nanocomposite accumulates only periodically on the test area as a result of the competition between CEA in the sample solution and that preimmobilized at the test zone. There was a drastic worsening of the color band of the test zone with a reduction in the accumulation of CNT/GNPs. The strength of the color band was inversely comparative to the levels of the analyte. The test zone had a considerably strong color, showing that the biosensor was functioning properly, in the absence of the goal CEA. The sample solution was dropped into the sample pad with the nanocomposite reporter sample of the analytes CEA and CNT/GNPs, and a positive test resulted in the sample solution with the CNT/GNP nanocomposite reporter with an unaccompanied sample. Reproduced with permission from ref 86. Copyright 2017 Elsevier.

studies in clinical diagnosis. The identification of cancer biomarkers will be multiplexed in future research.

Gao et al. designed a new amperometric immunosensor depending on gold nanoclusters. The identical nanomultilayer film was first created by the layer-by-layer (LBL) fabrication of positively charged carbon nanotubes (PDCNTs) enveloped in poly(diallyldimethylammonium chloride) and negatively charged poly(sodium-*p*-styrene-sulfonate) $(PSS/PDCNT)_2$ that provided a large manageable surface area and a biocompatible microenvironment. Gold nanoclusters were electrodeposited on the electrode to immobilize the anti-CEA. The Au/PDCNT/$(PSS/PDCNT)_2$ multilayer-film-modified GCE was used for the sensitive detection of CEA. Gold nanoclusters were electrochemically deposited on the changed electrode in $HAuCl_4$ solution (1.5 mM) between 0.2 and 1.0 V at a scan rate of 50 mV s^{-1} for 15 cycles to obtain the Au/PDCNTs/$(PSS/PDCNTs)_2$/GCE. It was then soaked in anti-CEA solution for an overnight period at 4 °C. Finally, the electrode was incubated in 0.2% BSA for 2 h to prevent nonspecific adsorption through blocking any residual active sites of gold nanoclusters and magnetic carbon nanotubes (MCNTs). This immunosensor depends on the interaction between the antibody and the antigen, which leads to a further increase in the charge-transfer resistance (R_{ct}) by EIS measurement. The Au/PDCNT/$(PSS/PDCNT)_2$ multilayer film exhibited two linear ranges, 0.1 to 2.0 ng mL^{-1} and 2.0–160.0 ng mL^{-1}, with an LOD of 0.06 ng mL^{-1}, enhanced stability, good selectivity, and good reproducibility for CEA detection.[87] In addition, the amperometric immunosensor that was developed had great sensitivity, a low LOD, and good durability. The developed immunosensor showed adequate accuracy when compared with the data acquired from the ELISA.

Asadzadeh-Firouzabadi et al. manufactured an electrochemical genosensor consisting of AgNPs and SWCNTs (AgNP/SWCNT nanohybrids) acting as a mark to detect miRNA (miR-25) associated with lung cancer. The nanogenosensor is based on the hybridization of different miRNA targets to a conjugated AgNPs/SWCNTs nanohybrid at the probe/GA/Cys-AuNPs/GCE surface (Figure 10i). The peak current of the AgNPs/SWCNTs nanohybrid on the modified electrode after hybridization with targets was decreased by 100.0% with a complementary target, 45.8% with a single-base mismatch target, and 8.5% with a noncomplementary target (Figure 10ii). Therefore, the AgNPs/SWCNTs nanohybrid genosensor can discriminate complementary, single-base mismatch, or noncomplementary targets and detect the target concentration from its oxidation signals.[88]

Table 2 summarizes the detection of breast, ovarian, colon, liver, testicular, nasopharyngeal, and prostate cancer biomarkers through graphene- and carbon-based biosensors, and Table 3 summarizes the discovery of lung cancer biomarkers through utilizing both graphene and carbon biosensors.

Diabetes Detection (Enzyme-based). Diabetes is considered a chronic disease and a public health issue around the world.[89] In 2017, the number of adults aged 20–79 with diabetes was 425 million, and it is anticipated to increase to 629 million people by 2045. In the same year, the number of deaths due to diabetes was ~5 million.[90] Diabetes is caused by high blood glucose levels.[91] Diabetes can be categorized into type 1, type 2, and gestational diabetes. Type 1 diabetes is due to the destruction of autoimmune cells, whereas type 2 diabetes is due to a defect in β cells in the pancreas, leading to a deficiency in insulin secretion that is responsible for controlling blood glucose levels. Gestational diabetes results from a high glucose level in pregnancy.[92] Monitoring glucose levels is the best way to detect of diabetes.[93] There have been numerous efforts to detect glucose via electrochemical biosensors. An enzymatic glucose sensor based on enzymes like glucose oxides or glucose dehydrogenase in the electrode has been used to detect glucose.[94] This sensor is used due to its outstanding sensitivity and selectivity, but the obstacles to its use are the high cost, instability, and rapid loss of activity of the enzyme. In addition, the enzyme is affected by factors of the external environment like the temperature, humidity, and pH.[94,95] Therefore, a nonenzymatic sensor is an excellent alternative to detect glucose because of its many advantages, such as its low cost, stability, and robustness.[95−98] CNTs, whether MWCNTs or SWCNTs, can be applied for biosensors. Additionally, SWCNTs have a great surface area, high sensitivity, and excellent electrical activity.[99] MWCNTs show a wide surface area, good stability, and elevated adsorption ability.[100] Therefore, graphene and CNTs have promising performance in biosensors.

https://doi.org/10.1021/acsbiomaterials.1c00710
ACS Biomater. Sci. Eng. 2022, 8, 964−1000

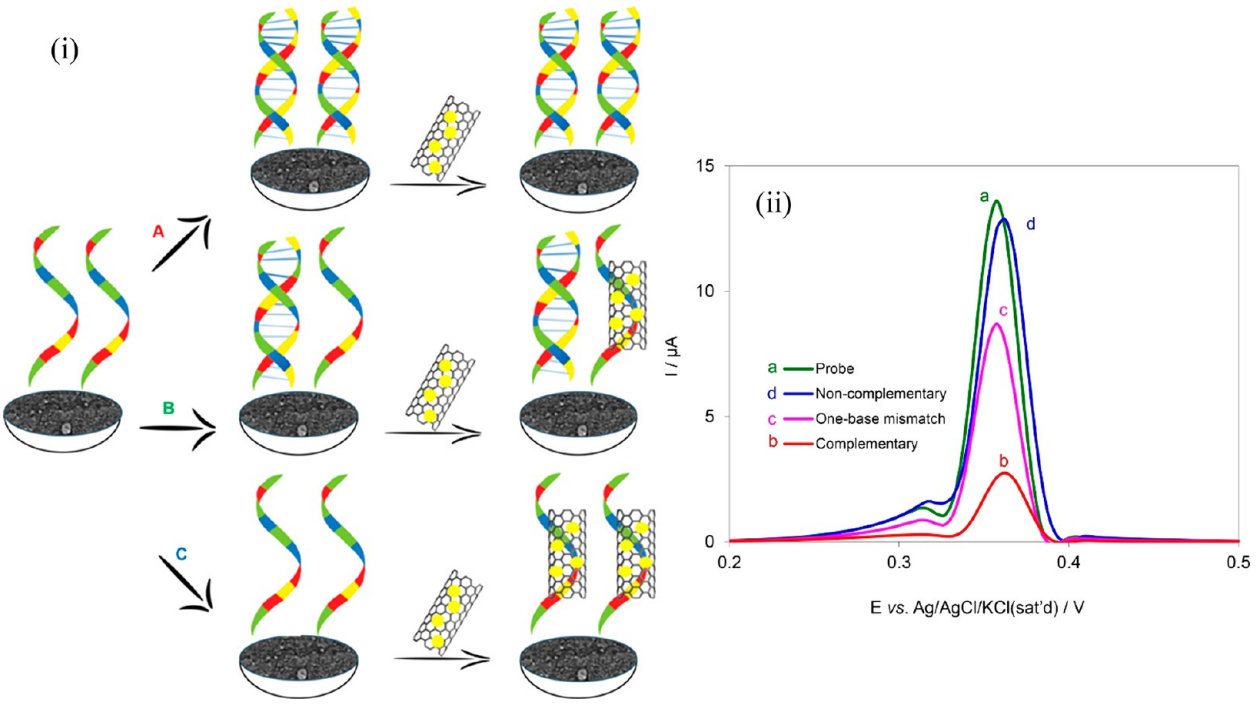

Figure 10. (i) Nanogenosensor performance as a mark based on AgNPs/SWCNTs. The hybridization stage was completed with (A) a complementary target, (B) a single-base mismatch target, and (C) a noncomplementary target. (ii) Distinction pulse voltammograms of the conjugated AgNPs/SWCNTs nanohybrid at the probe/GA/Cys-AuNPs/GCE surface (a) before hybridization with a 1.0×10^{-9} M target solution of (b) a complementary target, (c) a single-base mismatch target, and (d) a noncomplementary target in 0.1 M PBS (pH 7.0). Reproduced with permission from ref 88. Copyright 2018 Elsevier.

Table 2. Summary of Graphene- and Carbon-based Biosensors Aimed at the Detection of Breast, Ovarian, Colon Liver, Testicular, Nasopharyngeal, Breast, Ovarian, and Prostate Cancer Biomarkers

materials	biomarker	electrode	detection limit	linear range	ref.
PBSE/graphene/Cu/BSA	CEA	G/Cu	0.23 ng mL^{-1}	1.0–25.0 ng mL^{-1}	63
AuNPs-PEDOT/PB-rGO	AFP	GCE	3.3 pg mL^{-1}	0.01–50 ng mL^{-1}	64
Thi/rGO/AuNPs	CEA	ITO	0.650 pg mL^{-1}	0.01–300 ng mL^{-1}	65
PB/rGO/AuNPs	AFP	ITO	0.885 pg mL^{-1}	0.01–300 ng mL^{-1}	65
TB/GO-COOH	CEA	GCE	0.1 ng mL^{-1}	0.5–60 ng mL^{-1}	66
PB GO-COOH	AFP	GCE	0.05 ng mL^{-1}	0.5–60 ng mL^{-1}	66
CoS_2-GR-AuNPs	CA 15-3	SPE	0.03 U mL^{-1}	0.1–150 U mL^{-1}	67
rGO/Thi/AuNPs	CA 125	carbon working electrode	0.01 U mL^{-1}	0.1–200 U mL^{-1}	68
ILs/MWCNTs	PSA	GCE	20 pg mL^{-1}	0.2–40 ng mL^{-1}	69
SWCNHs-bienzyme	AFP	GCE	0.33 pg mL^{-1}	0.001–60 ng mL^{-1}	71
CGN-Thi	CEA	GCE	2.7 pg mL^{-1}	0.01–100 ng mL^{-1}	72
CGN-DAP	PSA	GCE	4.8 pg mL^{-1}	0.01–100 ng mL^{-1}	72
CGN-Cd^{2+}	AFP	GCE	3.1 pg mL^{-1}	0.01–100 ng mL^{-1}	72

Table 3. Summary of Graphene and Carbon Biosensors Aimed at Lung Cancer Biomarker Recognition

nanomaterials	biomarker	electrode	detection limit	linear range	ref
Au-Cu_2S-CuS/graphene and TB/Au-CeO_2/CMC/ILs	CEA	SPCE	0.78 pg/mL	0.001–100 ng/mL	81
Au-GN	CEA	GCE	0.04 ng mL^{-1}	0.10–80 ng mL^{-1}	82
3DM rGO/PANI film	NSE	Au	0.1 pg mL^{-1}	0.5 pg mL^{-1} to 10.0 ng mL^{-1}	83
3D GF/AgNPs	CYFRA21-1	nickel foam	1.0×10^{-14} M	1.0×10^{-14} to 1.0×10^{-7}	84
rGO/ssDNA-OMC/Ni-OTC NPs	EGFR exon 21 point mutation	PGE	120 nM	0.1–3 μM	85
CNT/GNPs	CEA		2.32 ng/mL	5–500 ng/m	86
Au/PDCNT/$(PSS/PDCN)_2$multilayer film	CEA	GCE	0.06 ng mL^{-1}	0.1–2.0 ng mL^{-1} 2.0–160.0 ng mL^{-1}	87
AgNPs/SWCNTs nanohybrid	miRNA (miR-25)	GCE	3.13×10^{-13} M	1.0×10^{-12} – 1.0×10^{-10} M 1.0×10^{-10} to 1.0×10^{-8} M	88

https://doi.org/10.1021/acsbiomaterials.1c00710
ACS Biomater. Sci. Eng. 2022, 8, 964–1000

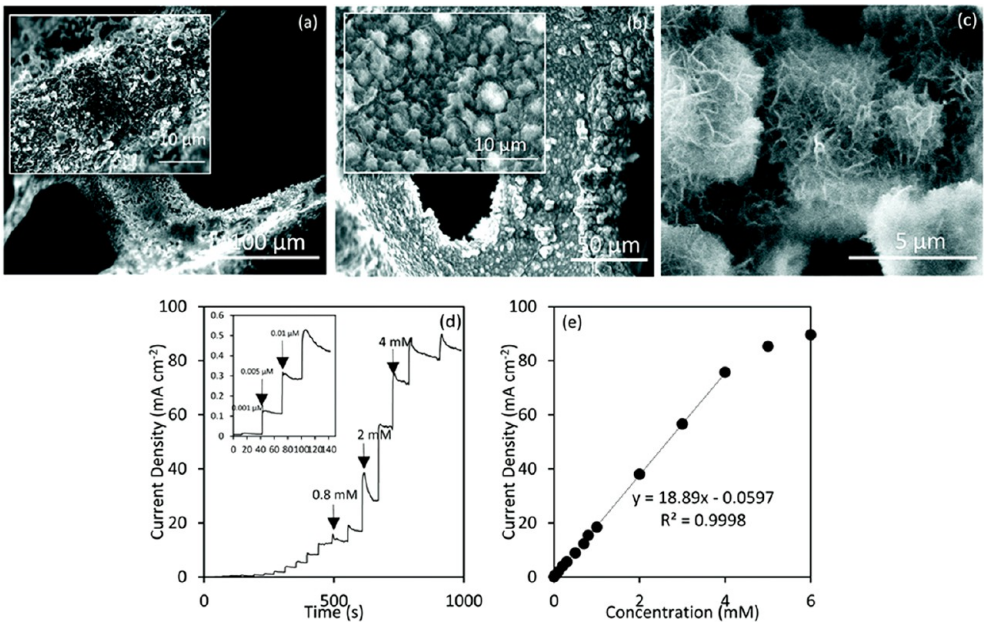

Figure 11. (a) SEM images of rGO on Ni foam at lower magnification. (The inset displays a higher magnification SEM image of rGO@NF.) (b) SEM images of $CoNi_2Se_4$-rGO on Ni foam at lower magnification. (The inset shows a higher magnification SEM image.) (c) SEM images of $CoNi_2Se_4$-rGO@NF presenting a nanoflake-like geometry with a rough electrode surface. (d) Amperometric response of $CoNi_2Se_4$-rGO@NF upon the successive addition of glucose. Inset: Current response with the existence of a low concentration of glucose. (e) Calibration curve for the current response to glucose concentration. Reproduced with permission from ref 101. Copyright 2019 The Royal Society of Chemistry.

Recently, Amin et al. produced a $CoNi_2Se_4$-rGO@NF sensor with a nanoflake-like geometry with an identical and highly 3D catalytic film system for the detection of glucose (Figure 11a–c). The amperometric and calibration curves for the existing response of the sensor were sharply amplified with growing glucose in diverse amounts (Figure 11d,e). This sensor was tested on blood samples to estimate the glucose level, and it showed values that were very similar to those obtained from a commercially available glucometer (ReliOn), indicating the reliability of this sensor and its accuracy and promise for practical use for glucose detection in blood.[101]

By a one-pot hydrothermal treatment, Yan et al. assembled a nonenzymatic glucose sensor depending on copper sulfide nanoflakes and an rGO (rGO/CuSNFs) nanocomposite adapted to a GCE for glucose detection. Using a one-pot hydrothermal treatment that simultaneously reduced GO and formed CuS nanoflakes in situ, an rGO/CuSNF nanocomposite was successfully synthesized in this research. The disposable rGO/CuSNFs nanocomposite was then applied to produce a nonenzymatic electrochemical sensor aimed at the exceedingly sensitive and selective exposure of glucose. In addition, the enzymeless sensor demonstrated noteworthy catalytic activity against glucose oxidation under optimized conditions, with a quick response time of 6 s, a broad linear range of 1 to 2000 μM, a high sensitivity of 53.5 μM $(cm^2\ mM)^{-1}$, and a low LOD of 0.19 μM. Furthermore, glucose models in both human urine and blood serum were successfully distinguished by the present sensor, showing that the nanocomposite rGO/CuSNF is an identical auspicious nonenzymatic glucose-sensing material for real-world samples.

The in situ synthesis of rGO/CuSNFs nanocomposites is depicted in Figure 12a. First, by electrostatic interaction, Cu^{2+} ions were absorbed above the GO nanosheet surface. Cu^{2+} ions then hydrolyzed in the NaOH solution to create nucleated $Cu(OH)_2$. After that, the S^{2-} generated by the decomposition of total amino acids (TAAs) was capable of sulfurating $Cu(OH)_2$ and reducing GO sheets. In addition, graphene worked as a corresponding surfactant in the synthesis process, preventing the formation of CuS nanoflake clusters, while the CuS nanoflakes served as spacers, reducing graphene restacking. Furthermore, the anodic peak current at rGO/CuSNFs/GCE increased after the addition of 0.3 mM of glucose, demonstrating the high performance of the sensor for the oxidation of glucose and its detection (Figure 12b). Increasing the oxidation current with the growth of glucose concentration (Figure 12c) allowed the quantitative sensing of glucose. The electrochemical current response was studied in the presence of Na^+, Ca^{2+}, Al^{3+}, NO_3, Cl^-, SO_4^{2-}, folic acid (FA), DA, oxalic acid (OA), AA, UA, fructose, maltose, and lactose. In addition, it showed good stability, good reproducibility, and high selectivity for glucose (0.5 mM) over AA, DA, FA, OA (0.1 mM), and other carbohydrates. Additionally, the rGO/CuSNFs/GCE sensor gave effective results when applied to human urine and blood serum samples for glucose detection.[102]

Yan et al. were able to design a simple one-pot procedure for producing a rGO/CuSNFs nanocomposite utilizing in situ hydrothermal handling. In addition, during the hydrothermal treatment, GO suppression and the in situ manufacturing of CuS nanoflakes were realized. Additionally, the nanocomposite rGO/CuSNFs in development can effectively speed up electron transport while also extending catalytically active areas despite the high electrochemical efficiency. When evaluated under ideal conditions, the nonenzymatic glucose sensor has a broader linear assortment, low recognition threshold, great reproducibility, extended storage stability, admirable anti-interferential capabilities, and realistic sensing applications. As a result, the rGO/CuSNFs nanocomposite facilitates the enzyme-free glucose sensor development approach.[102]

https://doi.org/10.1021/acsbiomaterials.1c00710
ACS Biomater. Sci. Eng. 2022, 8, 964−1000

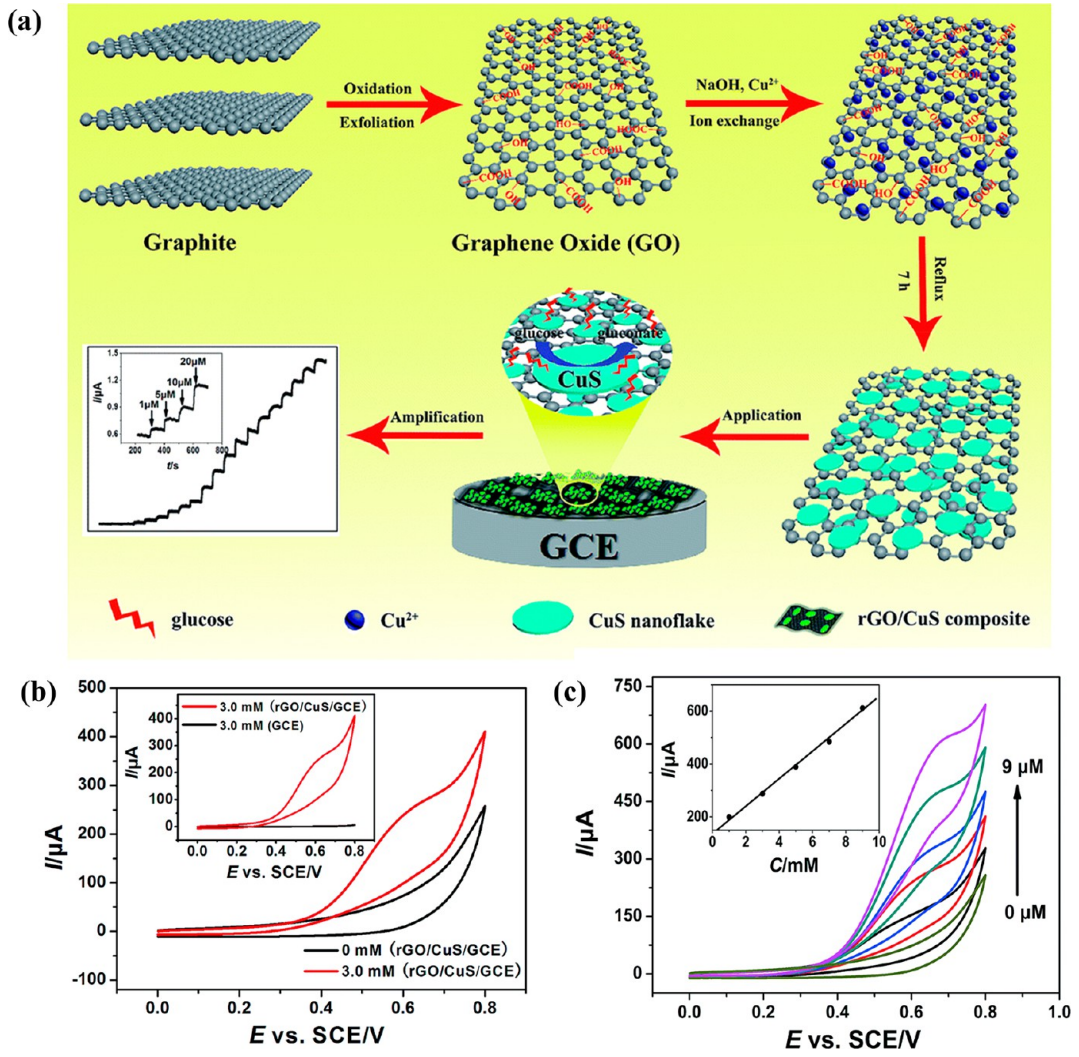

Figure 12. (a) rGO/CuSNFs composite creation and its use in nonenzymatic glucose sensing. First, by an electrostatic interaction, Cu^{2+} ions were engaged above the GO nanosheet surface. Cu^{2+} ions then hydrolyzed in NaOH solution to create nucleated $Cu(OH)_2$. As a final point, the S^{2-} generated by the disintegration of TAA was capable of concurrently sulfurating $Cu(OH)_2$ and reducing the GO sheets. Furthermore, graphene assisted as an equivalent surfactant in the synthesis process, preventing the collection of CuS nanoflakes, while the CuS nanoflakes served as spacers, reducing graphene restacking. (b) CVs of the rGO/CuSNFs/GCE in 0.1 M NaOH solution without and with 3.0 mM glucose. (c) CVs of the rGO/CuSNFs/GCE in 0.1 M NaOH solution with different concentrations of glucose. Reproduced with permission from ref 102. Copyright 2018 The Royal Society of Chemistry.

Rao et al. used hydrothermal treatment and calcination to make a $NiCo_2O_4$/nitrogen-doped rGO/IL ($NiCo_2O_4$@N-rGO/IL) nanocomposite. By means of a GCE, the biosensing features of $NiCo_2O_4$@N-rGO/IL, $NiCo_2O_4$@N-rGO, and $NiCo_2O_4$ against glucose were investigated. In addition, the sensor can be applied to reliably measure glucose in a sample of human blood serum. Figure 13a shows a detailed schematic diagram of the prepared biosensor, which uses $NiCo_2O_4$, nitrogen-doped reduced graphene, and a $NiCo_2O_4$/N-rGO/IL nanocomposite to identify glucose. In addition, Figure 13b displays the TEM images of $NiCo_2O_4$/N-rGO/IL, which shows high electrical conductivity. IL provides electron transfer, and the electrode widens the linear range of $NiCo_2O_4$/N-rGO sensors. Therefore, the metal oxides, GO, and the IL synergistic composition lead to excellent electrocatalytic activity aimed at glucose with a rapid response time. In addition, the $NiCo_2O_4$/N-rGO/IL composite has a sensitivity of almost 3.76 mA mM^{-1} cm^{-2}, with a respectable linear value from 0.001 to 4.555 mM at a potential of +0.5 V in addition to an LOD of 0.18 mM (Figure 13c,d). Its long-term stability and reproducibility make $NiCo_2O_4$/N-rGO/IL sensors promising for real-world use. When compared with a commercial glucose meter, the $NiCo_2O_4$/N-rGO/IL biosensor was applied to assess glucose levels in human blood serum and provided promising performance (Hitachi).[103]

Wang et al. described the one-step synthesis of rGO reinforced platinum−nickel oxide nanoplate arrays (Pt-NiO/rGO) for the detection of glucose (Figure 14A). The SEM appearance of Pt-NiO is demonstrated in Figure 14B. The 3D array structure of Pt-NiO/rGO/GCE improves the electron transfer and increases the attachment of NiO/rGO onto the electrode to boost the specific surface area, targeting a double increase in the oxidation current compared with Pt-NiO/GCE after the addition of glucose. The obtained sensitivity was 832.95 mA cm^2 mM, the LOD was 2.67 mM, and the linear values were between 0.008 and 14.5 mM (Figure 14C). The fabricated sensor had high stability, repeatability, and selectivity for glucose with some chemicals and organic

https://doi.org/10.1021/acsbiomaterials.1c00710
ACS Biomater. Sci. Eng. 2022, 8, 964−1000

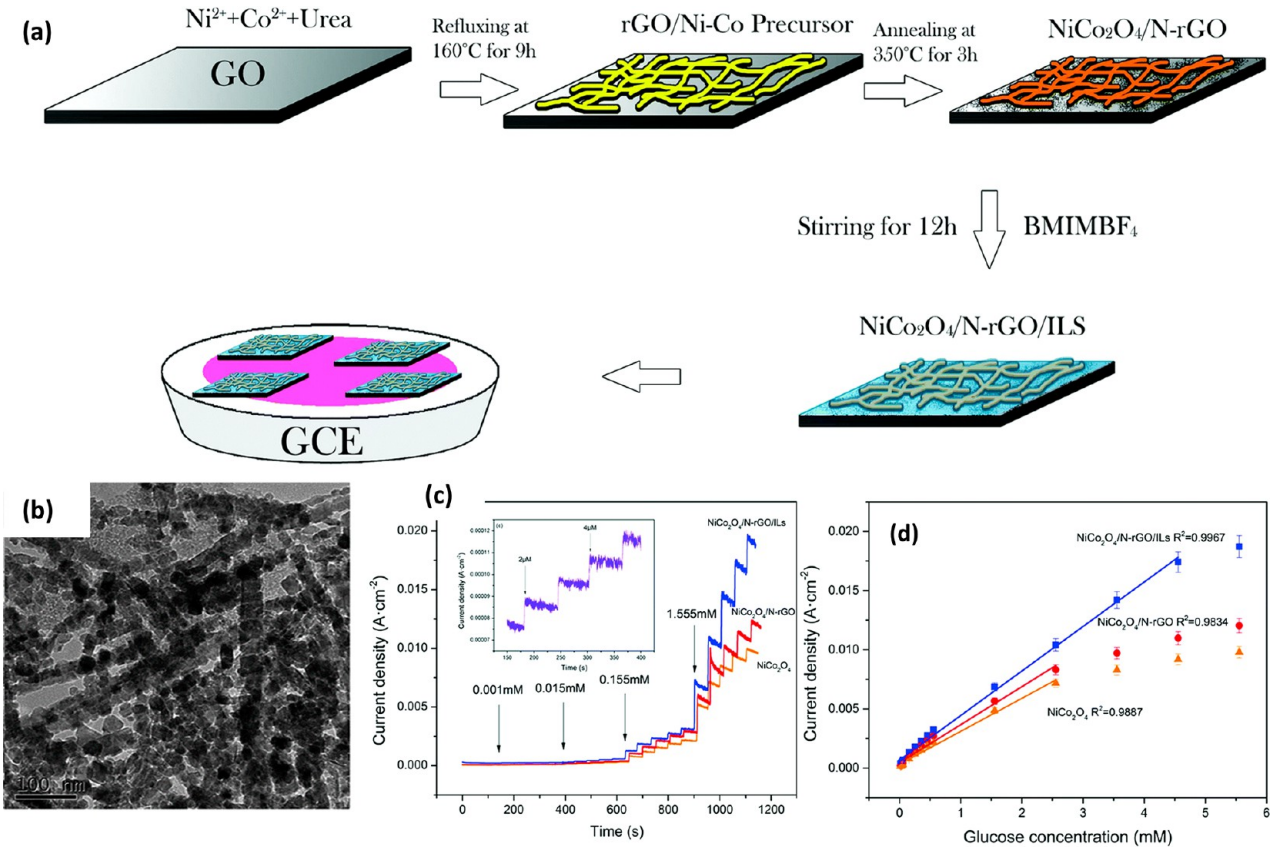

Figure 13. (a) Fabrication of $NiCo_2O_4$/N-rGO/IL/GCE. The graphene oxide (GO) was prepared; then, a mixture of $NiCl_2{\cdot}4H_2O$ (0.119 g), $CoCl_2{\cdot}6H_2O$ (0.237 g), and urea (0.09 g) was added to 10 mL of water or 10 mL of the GO dispersion (3 mg mL^{-1}) for the synthesis of the $NiCo_2O_4$/N-rGO composite. For the hydrothermal reaction, the solution was put in a 30 mL Teflon-lined stainless-steel autoclave at 160 °C for 9 h. Finally, the $NiCo_2O_4$@N-rGO composite was created by thermally treating the dried products at 350 °C for 3 h. After that, 40 mL of BMIMBF4 was applied at 1 mg mL^{-1} to a 10 mL $NiCo_2O_4$@N-rGO aqueous suspension. The mixture was ultrasonicated for 10 min before being stored in a firmly taped up glass bottle and stirred at room temperature for 12 h. The $NiCo_2O_4$@N-rGO/IL composite that resulted was then centrifuged. The $NiCo_2O_4$@N-rGO/IL composite was dispersed in ultrapure water. (b) TEM images of $NiCo_2O_4$/N-rGO/IL. (c) Amperometric responses to the consecutive accumulation of glucose and (d) corresponding concentration of glucose in 0.1 M KOH. Applied potential: +0.5 V. Reproduced with permission from ref 103. Copyright 2017 The Royal Society of Chemistry and the Centre National de la Recherche Scientifique.

compounds. The amperometric response of the sensor was unchanged for different materials interfering with glucose, but a small increase in current was reported for fructose, AA, and DA, and a large increase in current was reported for glucose. Therefore, Pt-NiO/rGO/GCE has good selectivity for glucose (Figure 14D). For practical applications, the fabricated sensor exhibits good performance for glucose detection in blood serum, and it can be directly used on concentrated blood without dilution, unlike some other sensors.[104]

Ammara et al. designed a nonenzymatic glucose sensor depending on a thin film of CNT with nickel and copper nanomaterials to form Ni/Cu/CNTs nanocomposite electrodes (Figure 15a). The CV analysis shows the oxidation peak current that increases after the addition of 0.5 mM of glucose (Figure 15b). This result is due to Cu and Ni NPs that have exceptional electrocatalytic performance for glucose oxidation and the CNT electrode that supports high conductivity to improve the electron transfer. Therefore, the Ni/Cu/CNTs sensor has outstanding electrocatalytic action aimed at glucose oxidation with extraordinary sensitivity (Figure 15c). The oxidation current of Ni/Cu/CNTs is still ~90% after 25 days, indicating good stability. The high sensitivity, good stability, and reproducibility make Ni/Cu/CNTs a promising nanocomposite candidate for glucose detection.[105]

A simple electrochemical method for fabricating AgNPs has been developed by Baghayeri et al. using metformin-functionalized MWCNTs (Ag@MH/MWCNT nanocomposite). The Ag@MH/MWCNT-based glucose biosensor was found to have a large response window for glucose concentrations ranging from 1.0 nM to 350 μM, a fast amperometric response time (4 s), a low LOD of 0.0003 μM (S/N = 3), high sensitivity, and strong selectivity. The researchers in that work assembled a low-cost glucose biosensor based on Ag@MH/MWCNT nanocomposites modified to GCEs (Figure 16A). Before each experiment, the GCE was polished in order with 1.0 and 0.3 μm alumina powder, rinsed thoroughly with distilled water between each polishing phase, ultrasonicated in ethanol and distilled water, and dried at room temperature. After that, 1.0 mg of MH/MWCNT was distributed using 2.0 mL of ethanol. After that, GCEs were treated with a 6.0 μL drop of MH/MWCNT (MH/MWCNT/GCE) or MWCNT (MWCNT/GCE) solution and dried in the air. The applied route for the formation of the Ag@MH/MWCNT nanocomposite is schematically depicted in Figure 16A. The fabricated material SEM image is illustrated in Figure 16B. The Ag@MH/MWCNT nanocomposite has great stability and excellent electrocatalytic activity in alkaline solutions for glucose oxidation. In addition, the Ag@MH/MWCNT-based

https://doi.org/10.1021/acsbiomaterials.1c00710
ACS Biomater. Sci. Eng. 2022, 8, 964−1000

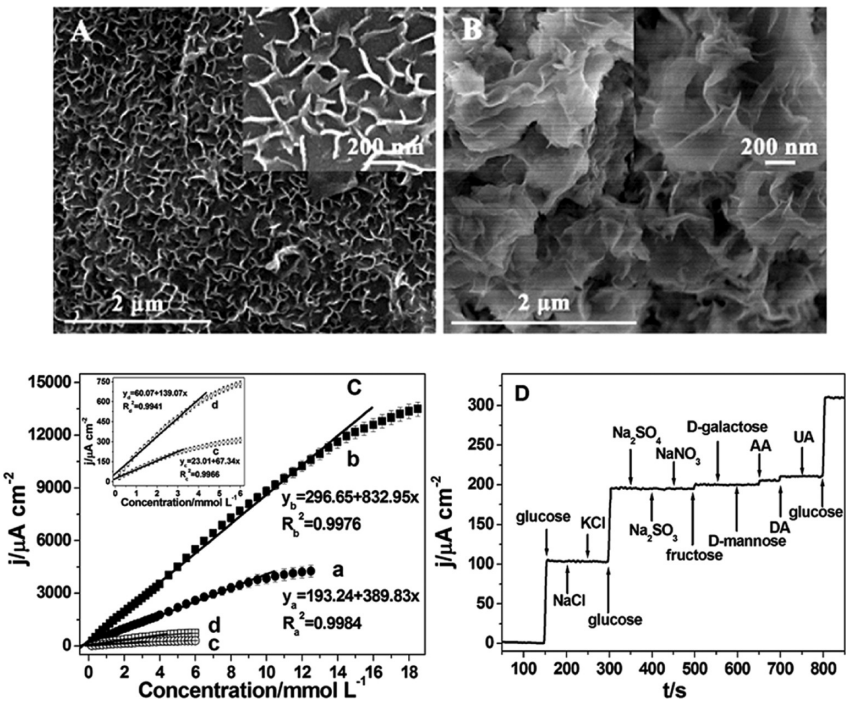

Figure 14. (A,B) SEM images of Pt-NiO/rGO and Pt-NiO, respectively. (C) Using a steady-state current versus glucose concentration as a strategy. (D) Performance of certain electroactive substances for glucose detection. 0.50 V is the applied potential. Reproduced with permission from ref 104. Copyright 2015 The Royal Society of Chemistry.

glucose biosensor displays wide linear values (1.0 nM to 350 M), a low LOD of 0.0003 M, respectable sensitivity, and low amperometric response time (4 s) (Figure 16C). The sensor was applied in glucose with interfering biomaterials. The amperometric response shows no alteration in the response current for other interfering species and increases for glucose, indicating that this sensor has high selectivity for glucose over other biological materials. The Ag@MH/MWCNT was also applied in blood serum and urine samples for glucose detection and exhibits good results compared with the spectrophotometric method. Therefore, Ag@MH/MWCNT nanocomposite materials have efficient properties to be used in practical applications.[106]

Zhang et al. prepared composites of copper ferrite ($CuFe_2O_4$) and MWCNTs as a nonenzymatic glucose sensor (Figure 17A,B). Furthermore, the $CuFe_2O_4$ material has catalytic activity for glucose oxidation, leading to an increase in the current response for $CuFe_2O_4$/GCE with respect to a bare GCE after the addition of glucose. Nonetheless, $CuFe_2O_4$/MWCNT/GCE composites show a highly increased oxidation current after the addition of glucose, as MWCNT improves the low conductivity of $CuFe_2O_4$ (Figure 17C). Therefore, $CuFe_2O_4$/MWCNT/GCE has high electroactivity for glucose oxidation, allowing its detection. This sensor exhibits a low LOD of 0.2 mM, a wide linear range of 0.5−1400 mM, and a fast amperometric response time. This sensor has high stability, reproducibility, and selectivity limited at 0.4 V. The selectivity of the $CuFe_2O_4$/MWCNTs glucose sensor is not affected by other carbohydrates, AA, DA, or UA, but it is affected by 4-acetamidophenol (AP) at >0.4 V (Figure 17D). Additionally, the $CuFe_2O_4$/MWCNT/GCE biosensor has an auspicious performance for glucose recognition in human blood serum depending on its precision and reliability.[107]

An unpretentious solvothermal method was used to create a hierarchical 3-D flower-like nickel(II)-terephthalic acid (Ni-(TPA)) metal−organic framework (MOF) structure. The MOF's optimum concentration and electrochemical interaction were increased via mixing SWCNTs with the produced Ni(TPA) MOF using an ultrasonic method. In addition, the nanocomposite has a significantly higher electrochemical response and electrocatalytic activity against glucose oxidation than the single-component Ni(TPA) and SWCNT according to the findings. The Ni(TPA)-SWCNT-modified electrode has excellent selectivity, a broad linear range (20 μM to 4.4 mM), a low LOD of 4.6 μM, and a quick response time of 5 s for glucose detection. With a deviation rate of 0−6.7% and a correlation coefficient (r) of 0.9940 (n = 20, P < 0.0001), the established sensor has good agreement with the integrated biochemical analyzer for glucose analysis in specific blood serum, which is indicative of high accuracy and a great potential for real implementation in rapid glucose analysis. Wang et al. developed a sensor based on a Ni(TPA)-SWCNT-CS dispersion added to a GCE for effective glucose oxidation (Figure 18A,B). The exceedingly electroactive and stable composite Ni(TPA)-SWCNT-CS was generated through dispersing a novel 3-D flower-like Ni(TPA) MOF in chitosan (CS) solution containing highly electroconductive carbon content of SWCNTs (Figure 18A). Merging the broad surface area and the great electronic conductivity of the SWCNT with the extraordinary electrocatalysis of Ni(TPA) for glucose oxidation, an electrochemical enzymeless glucose sensor was developed (Figure 18B). Electrocatalytic assays have found that in the present case of biological interferents, for instance, AA, DA, and UA, the identified sensor has excellent selectivity for glucose oxidation. The oxidation current of Ni(TPA)-SWCNT-CS/GCE aimed at glucose highly increases after the addition of glucose compared with the low oxidation current of Ni(TPA)-CS/GCE and the unchanging current of SWCNT-CS/GCE. This result indicates the role of Ni(TPA) in glucose oxidation and that of SWCNT, which allows the low electrical

https://doi.org/10.1021/acsbiomaterials.1c00710
ACS Biomater. Sci. Eng. 2022, 8, 964−1000

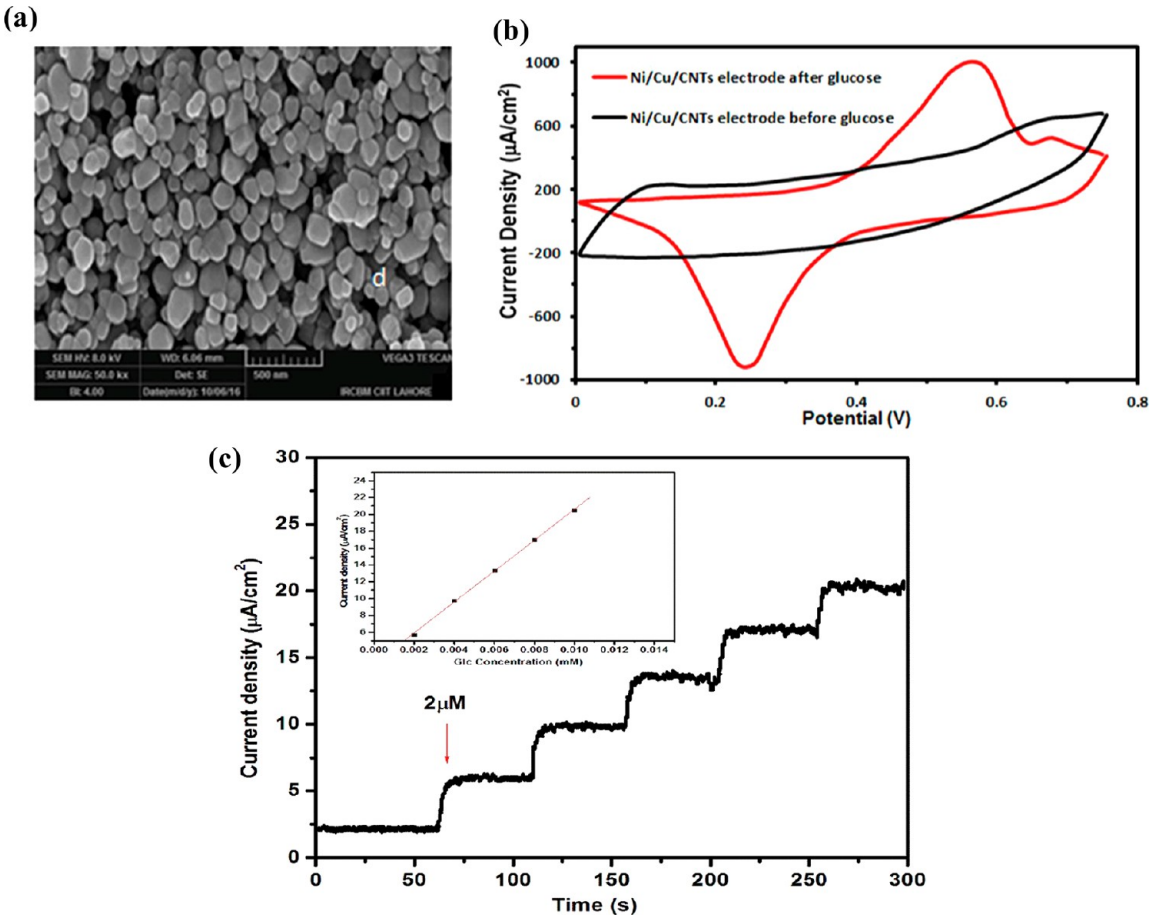

Figure 15. (a) SEM images of the Ni/Cu/CNTs electrode. (b) Cyclic voltammogram of the Ni/Cu/CNTs electrode after and before adding 0.5 mM glucose. (c) Current versus time plot of the Ni/Cu/CNTs nanocomposite for variable glucose concentrations. Inset: Plot of current and glucose concentration. Reproduced with permission from ref 105. Copyright 2018 Elsevier.

conductivity of the Ni(TPA) MOF to be improved. Therefore, the Ni(TPA)-SWCNT-CS/GCE sensor reveals excellent electrolytic ability for glucose oxidation. The Ni(TPA)-SWCNT-CS/GCE sensor shows a low LOD of 4.6 μM, a wide linear range (20 μM to 4.4 mM), and a rapid response (<5 s), indicating great potential for application in glucose detection by amperometric response (Figure 18C,D). In practical use, the Ni(TPA)-SWCNT-CS/GCE sensor was useful in human blood serum and gave similar results as the automatic biochemical analyzer. In addition, these findings suggest that a Ni(TPA)-SWCNT-based biosensor could be aimed at nonenzymatic glucose exposure in the real world. Thus the Ni(TPA)-SWCNT-CS/GCE sensor has respectable reliability and excellent selectivity for the recognition of glucose in practical applications.[108] Table 4 summarizes graphene- and carbon-based biosensors applied for diabetes detection.

Pathogenic Viruses: Zika Virus, HIV Virus, Hepatitis B Virus, and COVID-19. *Zika Virus.* The Zika virus, emerging from Uganda's Zika woodland,[109] is a *Flaviviridae* family single-stranded RNA virus.[110] This virus generates the Zika infection, which is also identified as Zika virus disease, with symptoms like rash, edema, headache joint pain, and malaise that are quite close to the symptoms of Dengue.[111] Transference is mostly attributed to the bite of the female *Aedes aegypti* mosquito.[112] In addition, the Zika disease has many transmission manners and pathways,[113−115] including blood transfusion and transplants of marrow or organs, and it can even be passed through sexual intercourse and from mother to infant.[116,117] In the scenario of horizontal transference throughout pregnancy, microcephaly in the neonate and several birth deformities can be triggered.[115,118,119]

The electrochemical adjustment of pencil carbon graphite electrodes (PCGEs) was explained by da Fonseca Alves et al. Solutions under acidic conditions have been established using materials containing 3-amino-4-hydroxybenzoic acid (3-4-AHBA). Furthermore, the substance has been used to immobilize the Zika virus's oligonucleotide ssDNA. The dip sequential of the higher electrostatic repulsion of $[Fe(CN)_6]^{3-}$, achieved by the increase in phosphates by the addition of the complementary target sequence, was used to identify the hybridization. Furthermore, using actual human serum samples loaded with Zika virus, the device demonstrated a perfect linear correlation coefficient (r^2 = 0.997), a relatively low level of diagnosis (25.4 pM), and precision (RSD) of 3.1% (Figure 19).[120]

Electrochemically synthesizing a polymer derived from 3 to 4-AHBA above the PCGE surface resulted in an innovative surrounding substance aimed at the production of biosensors. Figure 19A confirms the voltammograms acquired with the PCGE in 100 consecutive cycles. In addition, in the first potential cycle, there were two oxidation peaks (M1, at +0.75 V, and M2, at +0.85 V) but only one cathodic phase (M3, at +0.64 V) in the reverse scan. Because the electrochemical

https://doi.org/10.1021/acsbiomaterials.1c00710
ACS Biomater. Sci. Eng. 2022, 8, 964−1000

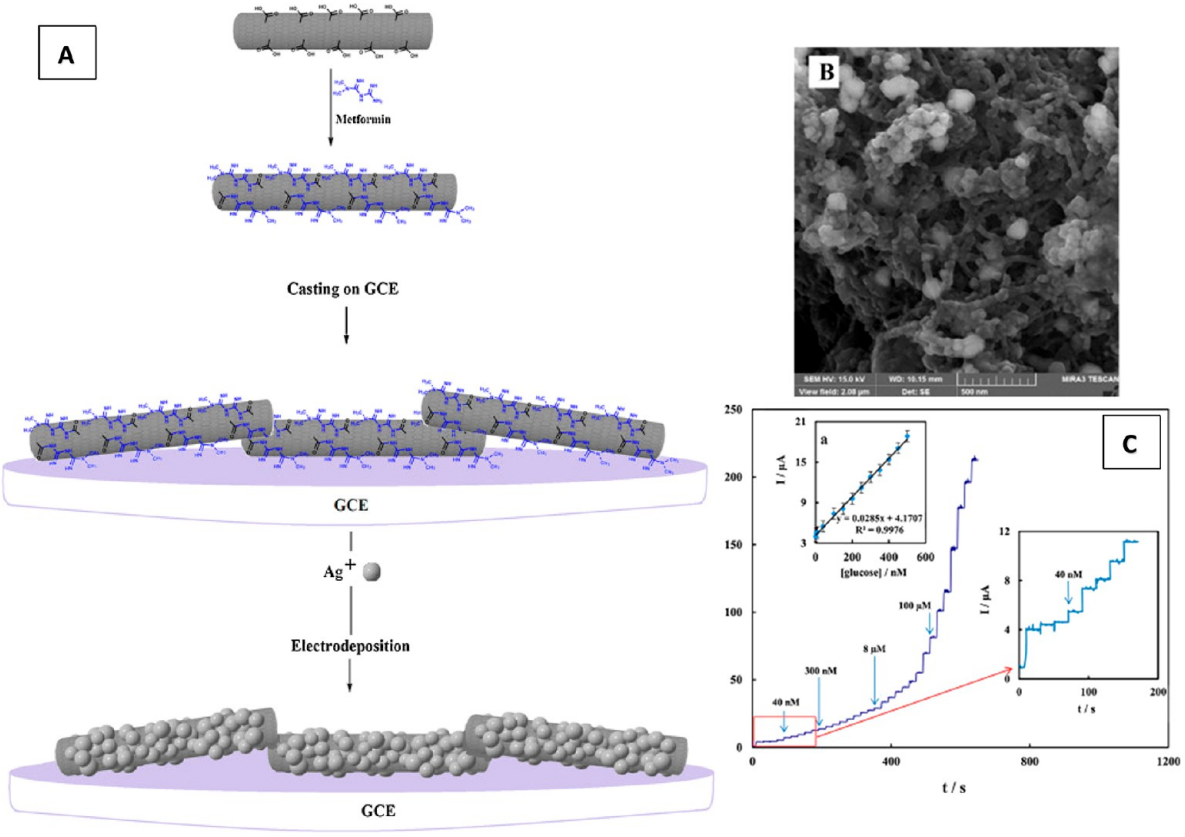

Figure 16. (A) Fabrication process of Ag@MH/MWCNT nanocomposites on the electrode surface. GCE was refined with 1.0 and 0.3 μm alumina powder in order before each experiment, bathed with distilled water between each polishing process, ultrasonicated in ethanol and distilled water, and dried at 23 °C. Next, 2.0 mL of ethanol was used to spread 1.0 mg of MH/MWCNT. After that, a 6.0 μL drop of MH/MWCNT (MH/MWCNT/GCE) or MWCNT (MWCNT/GCE) solution was added to the GCEs and dried in the air. Chronoamperometry was used to deposit Ag NPs on the electrodes in a 1.0 mM $AgNO_3$ solution, which was then deaerated via aeration with nitrogen at a 0.0 V potential (vs Ag|AgCl|KCl (3 M)) for 180 s. (B) SEM data of Ag@MH/MWCNT/GCE. (C) Sensor's amperometric response after successive additions of various concentrations of glucose in 0.1 M NaOH at a working potential of +0.70 V. Reproduced with permission from ref 106. Copyright 2015 Elsevier.

functionality of two such oxidation processes was indeed observed with 2-aminophenol (2AP), that structure's electro-oxidation pathway was explored for evaluation. The first oxidation peak (M1) in 2AP and aniline was responsible for the oxidation of the $-NH_2$ group. 2AP developed a distinct voltammetric behavior after the second oxidation process. The second oxidation peak appeared when aniline was electro-polymerized, but it was at a lower anodic potential. The current gradually decreased by improving the cycle number, which implied that the electrode's surface had been modified with a material resulting from the 3-4-AHBA. Furthermore, the monomer peak's current response decreased, implying that cation radicals were reacting and the products were put out of action above the surface, making it challenging for more monomer to enter the working electrode.[120] Throughout the first stage, there was also a contraction peak (P1, at +0.33 V). Three more oxidation peaks developed at reduced anodic potentials following the second scan, with the current expanding after each cycle. A fresh reduction wave (P5, +0.15 V) appeared after a few cycles. The presence of peaks at a lower anodic potential was clear evidence of polymer film formation. Peaks at these potentials suggested the formation of structures not formerly existent in the solution, which required less oxidizing or reducing energy (at lower anodic potential) because of the amplified mesomeric impact. Figure 19B–D demonstrates the electrochemical characterization of the polymer produced on the surface of the PCGE-utilizing solutions containing just the buffer electrolyte, potassium ferricyanide, and hexaammineruthenium(II) chloride.

As can be observed from the data, an electroactive substance was set down above the electrode surface (Figure 19B). Both the P2 and P5 pairings and the solitary oxidation peak P4 (Figure 19A) indicated that the electrode had been switched and was now coupled to the polymer's electroactivity during electropolymerization. This indicated that P1 and P3 were associated with the identical phenoxazine rings (polymer precursors) identified in 2AP and that these species were washed away during the washing process. Figure 19C shows the results obtained with the potassium ferrocyanide anionic probe in the potential range of 0.0 to 0.5 V. Figure 19D is similar to Figure 19C, but it displays the results acquired with a cationic probe that operates in the +0.1 to 0.4 V potential range. The representing electrolyte in this case had a high background current (curve d) with a reduction peak at ~0.25 V that lasted after the probe was incorporated. The polymer was connected to a 0.25 V peak, whereas the probe was connected to a 0.15 V peak. Because the polymer contributed more to the faradaic current in the electrolyte, the probe signal was obstructed. The current variation retrieved using the anionic probe, for example, was 26 A at the oxidation peak (0.1 V) but 290 A at +0.34 V, nearly 11 times higher (Figure 19C).

https://doi.org/10.1021/acsbiomaterials.1c00710
ACS Biomater. Sci. Eng. 2022, 8, 964–1000

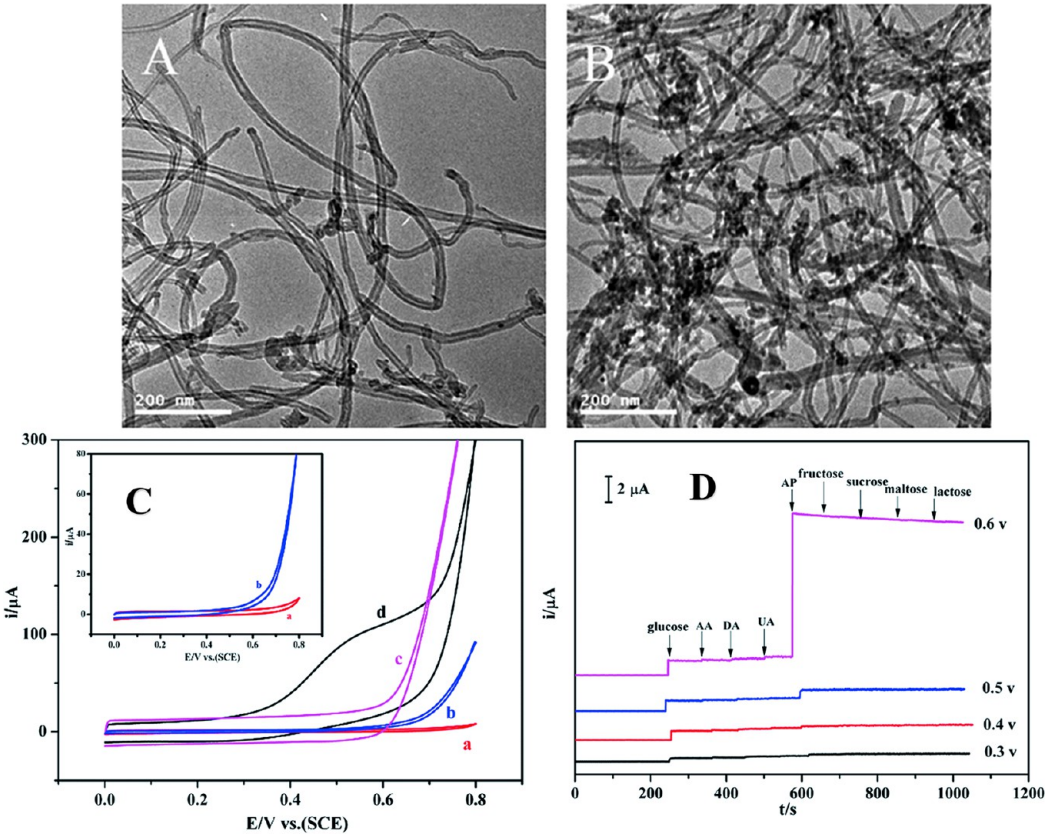

Figure 17. (A,B) TEM images of MWCNTs and $CuFe_2O_4$/MWCNTs, respectively. (C) Cyclic voltammograms of (a) GCE, (b) $CuFe_2O_4$/GCE, (c) MWCNTs/GCE, and (d) $CuFe_2O_4$/MWCNTs/GCE in 0.10 M NaOH with 1.0 mM glucose at 100 mV s^{-1}. (D) Amperometric $I-T$ curves of $CuFe_2O_4$/MWCNTs/GCE for 10 mM glucose and 0.5 mM potential interferents at different utilizing potentials. Reproduced with permission from ref 107. Copyright © 2015 The Royal Society of Chemistry.

The recorded results aimed at the left behind species result in the use of an anionic potassium ferricyanide probe.

Afsahi et al. established a cheap, compressed graphene-enabled biosensor to recognize Zika virus with a decidedly explicit immobilized monoclonal antibody. The real-time, quantitative recognition of native Zika viral (ZIKV) antigens is possible with monoclonal antibodies covalently bound to graphene using field-effect biosensing (FEB). The percentage shift in antigen response capacity (ZIKV NS1) corresponds to clinically relevant antigen detection levels in buffer concentrations as low as 450 pM. Testing Zika antigen in a simulated human serum demonstrated potential diagnostic applications. Furthermore, the graphene platform can be responsible for sophisticated quantitative data from nonclinical biophysical kinetics methods, making it suitable for both clinical and future diagnostic applications. The peculiarity of the ZIKV NS1 antigen provides the early recognition of active disease in presumptive Zika infections.[121]

When suitable biological targets are placed on the surface as the gate dielectric, the channel current and gate capacitance of a field-effect graphene transistor vary in a predictable manner (Figure 20a). The two read-out channels accessible are the I-Response (the current via the channel) and the current study concern (C-Response, capacitance of the biosensor to the liquid). As illustrated in Figure 20b, the Agile Plus program, which runs on a PC linked to the system via USB, controls the system and reads the data. Interestingly, target immobilization on the 1.0 nm thick graphene surface happens at an optimum density of 5 proteins/μm^2, verifying the C-Response transition following protein immobilization, as illustrated in the atomic force microscopy (AFM) image (Figure 20c). The graphene efficiency is indicated by means of the low D/G ratio (0.1) in the Raman spectrum (Figure 20d). Biosensors are managed during the procedure, as shown in Figure 20e. The capacitance response increased by 20% after immunoglobulin immobilization (Figure 20e). The C-Response increased by 100% between the wash phases and the calibrated baseline (Figure 20e). This shows that irreversible chemical problems existed on the surface, permitting the biosensor to be used. In that work, the C-Response channel was utilized, as Anti-Zika NS1 has a bigger effect on the graphene transistor capacity than the source-drain resistance. Figure 20e represents a complete cycle of liquid gate voltage (−100 to 100 mV) and back. Figure 20f illustrates exemplary full current versus gate-voltage curves throughout calibration, quenching, and washing. A larger I−Vg slope entails an enlarged graphene biosensor sensitivity.

MOFs have been shown to be collective fluorescence quenchers for DNA/RNA, as revealed in numerous studies. Despite this, many MOFs have a low structural stability, which restricts their practical applications. Consequently, it remains of significant interest to produce stable nanobiosensors suited for usage in complicated environments. In that work, Li et al. used as a nanobiosensor a new angle of nitrogen-doped porous carbon (NPC) derived from MOF-based precursors for the fluorescence detection of ZIKV RNA variants. A charge-coupled device (CCD)-based imaging system was applied to capture the fluorescence signal. A TAMRA-tagged ZIKV RNA probe (P-DNA) was structurally related to the NPC and

https://doi.org/10.1021/acsbiomaterials.1c00710
ACS Biomater. Sci. Eng. 2022, 8, 964−1000

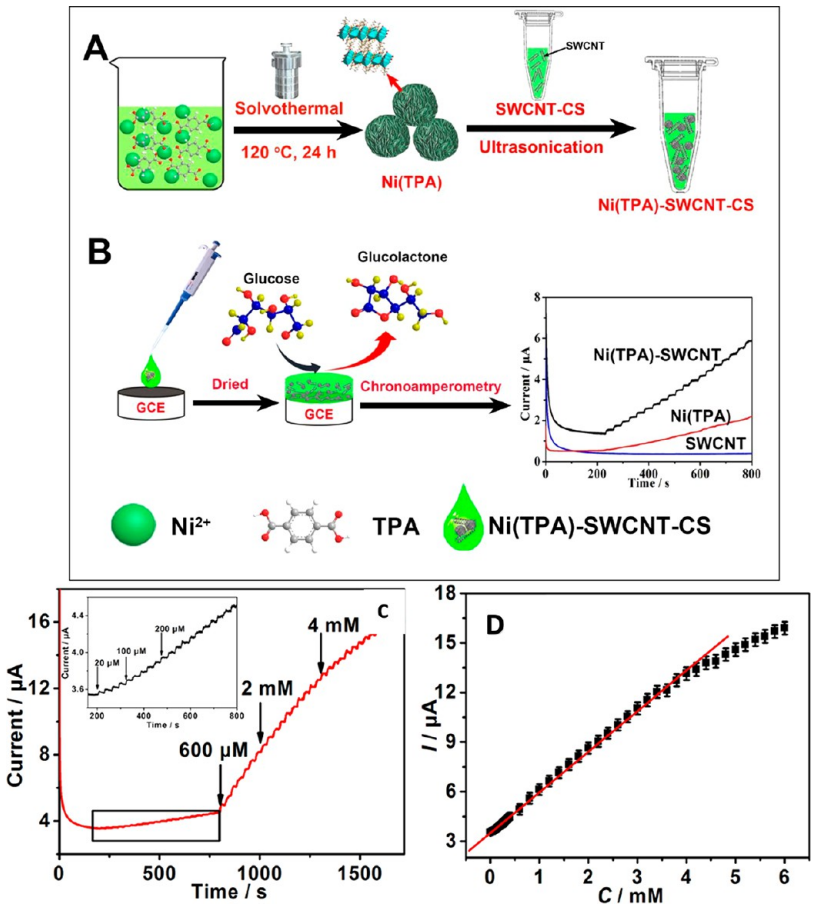

Figure 18. (A,B) Fabrication and application of the N(TPA)-SWCNT composite as a nonenzymatic electrocatalyst aimed at glucose sensing. The promising electroactive and stable composite, Ni(TPA)-SWCNT-CS MOF, was created using a solvothermal method and dispersed in chitosan (CS) solution comprising highly electroconductive carbon content of single-walled carbon nanotubes (SWCNTs) (Figure 18A). Combining the wide surface area and the extraordinary electronic conductivity of SWCNTs with the great electrocatalysis of Ni(TPA) aimed at glucose oxidation, an electrochemical enzymeless glucose sensor was developed (Figure 18B). Per the electrochemical investigations, the electrochemistry of the Ni(II)/Ni(III) pair can be clearly spotted, and its electrochemical amplitude may be substantially improved through introducing an SWCNT. Furthermore, electrocatalytic assays discovered that the identified sensor has admirable glucose oxidation selectivity with biological interferents like ascorbic acid (AA), dopamine (DA), and uric acid (UA). (C) Amperometric results of Ni(TPA)-SWCNT-CS/GCE after adding 0.02 mM glucose in 0.1 M NaOH at +0.55 V. Inset: An exaggerated amperometric curve in a low-concentration area. (D) Electrocatalytic current versus glucose concentration. Reproduced with permission from ref 108. Copyright 2018 Elsevier.

Table 4. Summary of Graphene and Carbon-based Biosensors for Diabetes Detection

glucose sensor	detection limit (μM)	sensitivity (μA mM^{-1} cm^{-2})	linear range	sample	response time (s)	ref
$CoNi_2Se_4$-rGO@NF	0.651	18890	1 μM to 4.0 mM	blood serum	4	101
rGO/CuSNFs	0.19	53.5	1−2000 μM	blood serum and urine	<6	102
$NiCo_2O_4$/N-rGO/IL	0.18	3760	0.001−4.555 mM	blood serum	<2	103
Pt-NiO/rGO	2.67	832.95	0.008−14.5 mM	blood serum	5	104
Ni/Cu/CNTs	2.0	1836.5	0.02−4.5 mM			105
Ag@MH/MWCNT	0.0003		1.0 nM to 350 μM	blood serum and urine	4	106
$CuFe_2O_4$-MWCNTs	0.2		0.0005−1.4 mM	blood serum	<5	107
Ni(TPA)-SWCNT-CS/GCE	4.6		20 μM to 4.4 mM	blood serum	<5	108

formed a P-DNA@NPC complex with substantial fluorescence quenching. When the target site's RNA (T-RNA) was introduced, the P-DNA was able to escape from NPC by producing a double-stranded hybrid and caused fluorescence recovery. With an LOD of 0.23 nM, the P-DNA@NPC complex was valid and reliable for the ZIKV RNA sequence assay, outperforming many formerly studied fluorescent DNA sensors. Furthermore, it was capable of distinguishing mismatched RNA and perceiving ZIKV RNA arrangements spiked in human saliva. This research will provide an important new perspective on the possible integration of carbon nanomaterials and a CCD-based fluorescence imaging platform aimed at the nucleic acid assay. It has been indicated that the fluorescence recovery intensity is linear, where the ZIKV T-RNA concentrations ranged from 1 to 600 nM, as shown in Figure 21. For potential practical applications, this highly sensitive and selective biosensor may be accessible.[122]

https://doi.org/10.1021/acsbiomaterials.1c00710
ACS Biomater. Sci. Eng. 2022, 8, 964−1000

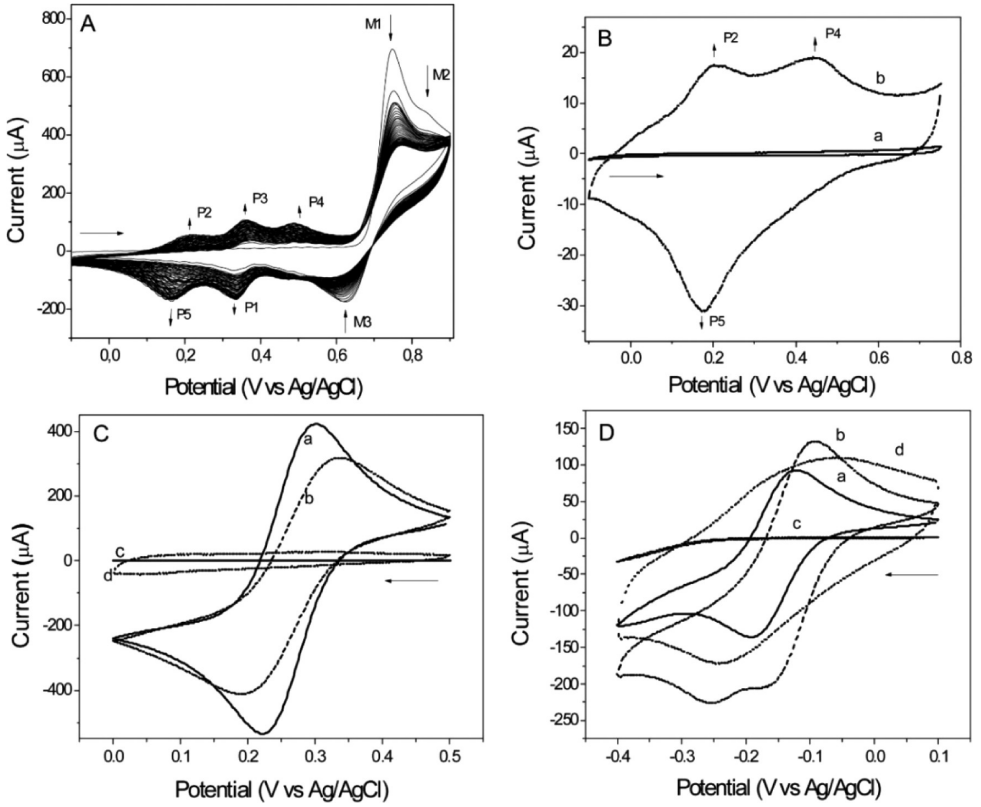

Figure 19. PCGE cyclic voltammograms: (A) In aqueous 0.5 M H_2SO_4 solution comprising 2.5 mM 3-4-AHBA, noted with 100 screenings. (The position of the current shift is indicated by the arrows.) (B) In 0.5 M H_2SO_4 solution, the pair with ν = 50.0 mV s^{-1}. (C) In 0.1 M KCl (c,d) and including 5.0 mM $K_3Fe(CN)_6$ (a,b) at the potential opening between 0.0 and 0.5 V. (D) In 0.1 M KCl (c,d) and including 5.0 mM $[Ru(NH_3)_6]C_{l2}$ (a,b) at the potential opening between −0.4 and 0.1 V. Curves a and c refer to the unmodified PCGE, whereas curves b and d refer to the poly(3-4-AHBA)-modified PCGE. Reproduced with permission from ref 120. Copyright 2019 Elsevier.

Selectivity toward certain target molecules, in addition to sensitivity, is an important metric to consider as soon as the efficiency of a sensing coordination is appraised. As can be observed in Figure 21A, the fluorescence image of T1 is slightly darker than that of T0. The picture brightness of T2 and T3 is nearly comparable to the signal of the Tris-HCl buffer solution. As shown in Figure 21B, the RE of T1 (92%) is slightly lower than the significance acquired with T0. When T2 or T3 was used to expose the P-DNA@NPC device, there was essentially no difference in the fluorescence intensity. These data reveal that the P-DNA@NPC approach is very discriminating for correct T-RNA, as indicated through the reduced fluorescence recovery even when investigating oligonucleotide patterns with only a standard discrepancy.[122]

Human Immunodeficiency Infection Virus. Since the first cases of AIDS were distinguished in 1981, almost ∼30 million deaths have been prompted by HIV.[123] Around 1.1 million individuals are ailing in the United States with HIV; of these, around 166 000 individuals have no knowledge of their condition, and 30% of new HIV diseases are passed on through people with undiscovered HIV. Whereas effective methods of HIV counteraction are valuable in controlling HIV transmission, early and precise recognizable proof of HIV disease is essential to the health of the population. The ordinary procedures for identifying HIV are carried out by methods for identifying the antibodies the body produces toward HIV.[124,125] The antibody of HIV testing has a time window of approximately 3−6 weeks after infection; antigen screening decreases the time window to ∼16 days. An intense examination is in progress to develop a fast and sensitive protease action test for HIV-1 to decrease the time window and to identify HIV toward the early phases of viral disease.[126−128]

Zhang et al. fabricated a structure for the quick, responsive, and exact recognition of HIV-1 protease focused on the GO fluorescence biosensing framework. Furthermore, for the life cycle of HIV, HIV-1 protease is essential. Fluorescence-marked peptide particles of the HIV-1 protease substrate were covalently combined with GO. Fluorescein was effectively decreased through GO without HIV-1 protease. The substrate peptide was separated into small parts, delivering fluorescence, and HIV-1 protease was detected. In addition, using this sensing procedure, HIV-1 proteases could be distinguished at 1.18 ng/mL. Furthermore, the sensor could successfully recognize HIV-1 protease in human serum.[129]

Gong et al. have set up an impedimetric HIV-1 biosensor based on graphene-Nafion composite films. The biosensor was fabricated by adsorbing the ssDNA on graphene-Nafion balanced on a layer of smooth carbon cathode through the utilization of $\pi-\pi^*$ stacking interactions. On the basis of the negative ssDNA and the steric hindrance, the electron transport of the terminals toward the $[Fe(CN)6]^{3-/4}$ redox couple was difficult. Additionally, the helix production made dsDNA release from the biosensor layer. The sensor's LOD was 2.3×10^{-14} M. This graphene-Nafion biosensor displays solid selectivity, sensibility, and reproducibility for HIV-1 recognition.[130]

https://doi.org/10.1021/acsbiomaterials.1c00710
ACS Biomater. Sci. Eng. 2022, 8, 964−1000

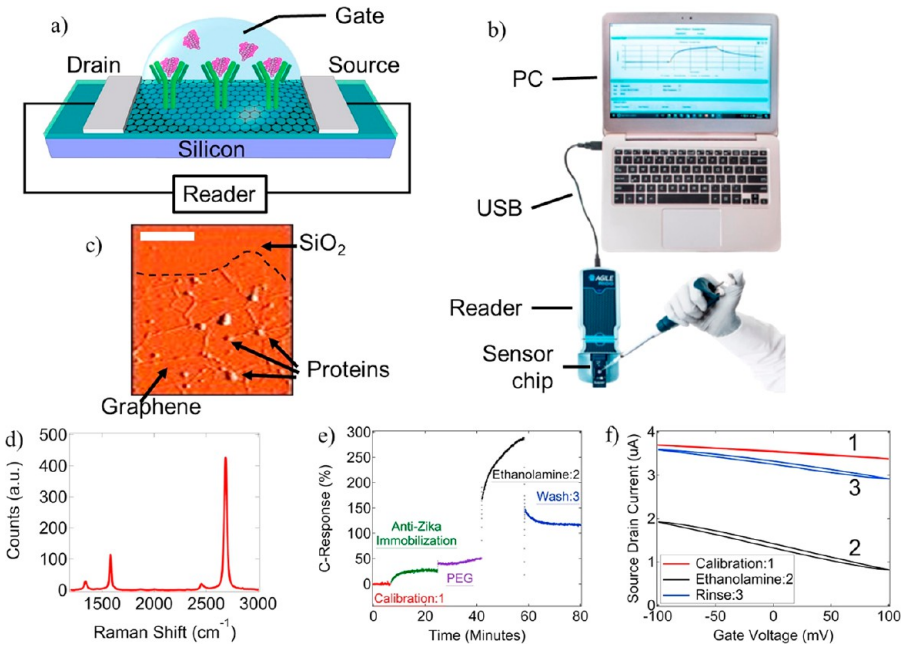

Figure 20. (a) Diagram of the graphene biosensor chip's sensor portion. A zero-length linker is used to immobilize antibodies on pristine graphene. In a graphene-channeled liquid gated transistor, these antibodies, along with the PEG block, serve as the dielectric. (b) Diagram of the complete sensor chip device along with the sensor chip, reading electronics and digital control, and PC network management display applications. (c) Graphene AFM image after active protein attachment. Scale bar: 1 μm, *Z* height: 10 nm. (d) After system fabrication, the Raman spectrum shows a low D/G ratio, indicating superior graphene. (e) Capacitance shift as a percentage above the graphene biosensor chip surface during target immobilization and quenching. (f) I−Vg curves at various stages of immobilization. The steepening of the I−Vg slope suggests a significant shift in surface chemistry and increased biosensor sensitivity. Reproduced with permission from ref 121. Copyright 2018 Elsevier.

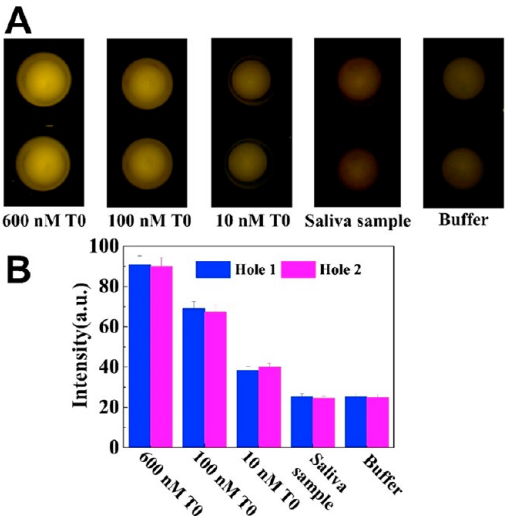

Figure 21. T-RNA recognition in complicated samples using the P-DNA@NPC device. (A) Fluorescence quenching shots after creating extra T-RNA concentrations in saliva samples plus Tris-HCl buffer solution: 600, 100, and 10 nM T-RNA. At a given concentration, compatible T-RNA (T0) and three kinds of mutation sequences, single-base mismatched T-RNA (T1), double-base mismatched T-RNA (T2), and noncomplementary T-RNA (T3), were used to study the selectivity of the NPC and the chance of distinguishing mutations (600 nM). The fluorescence image of T1 is somewhat darker than that of T0. (B) Fluorescence intensity obtained when using a different T-RNA. The picture quality of T2 and T3 is nearly comparable to the signal of the Tris-HCl buffer solution. T1's RE (92%) is slightly lower than that of T0. Reproduced with permission from ref 122. Copyright 2019 Elsevier.

Hepatitis B Virus. The hepatitis B virus (HBV) is a critical, acute, widespread viral infection. Even though the frequency of HBV infection has decreased, 2 billion individuals still have the disease, and thus >350 million persons are carriers of HBV.[131] The surface antigen of hepatitis B (HBsAg) is a virological HBV identification marker and plays a crucial role in timely identification. If the blood concentration of HBsAg is >1 ng/mL, then the individual is assumed to be diagnosed with HBV. Many researchers have found that HBV increases the risk of developing liver cirrhosis and liver cancer in men and women by as much as 40 and 15%, respectively.[132] Different conventional methods, like the ELISA,[133,134] the polymerase chain reaction,[135,136] and chemiluminescence immunoassays have been established to identify HBsAg.[137,138] Nevertheless, those techniques cannot satisfy the POC testing needs.[139,140]

Zhao et al. have built up a fluorescence immunosensor using graphene-oxide−ferrocene (GO-Fc-CS/Au)-based nanocomposites aimed at HBsAg recognition (Figure 22). The modified film demonstrated increased electrical conductivity and strong reversible redox signal, biocompatibility, and film-forming properties for fixing antibodies. For HBsAg, the immunosensor has a linear range of 0.05−150 ng/mL, with an LOD of 0.01 ng/mL. The immunosensor shows suitable characteristics for application in clinical diagnosis.[141]

For 5 min, GE was immersed in fresh piranha solution (H_2SO_4/H_2O_2 3:1), then sonicated in absolute ethanol and water. GE was then polished with alumina powder before rinsing with 100% ethanol and water twice. At 23 °C, the GO-Fc-CS solution (6 μL) was distributed evenly onto the cleaned GE surface with a syringe to generate a smooth composite sheet. The AuNPs solution (6 μL) was sprayed on the GE surface and allowed to dry at 23 °C. GE upgraded with GO-Fc-CS/AuNPs was immersed for 12 h in HBsAb (hepatitis B

https://doi.org/10.1021/acsbiomaterials.1c00710
ACS Biomater. Sci. Eng. 2022, 8, 964−1000

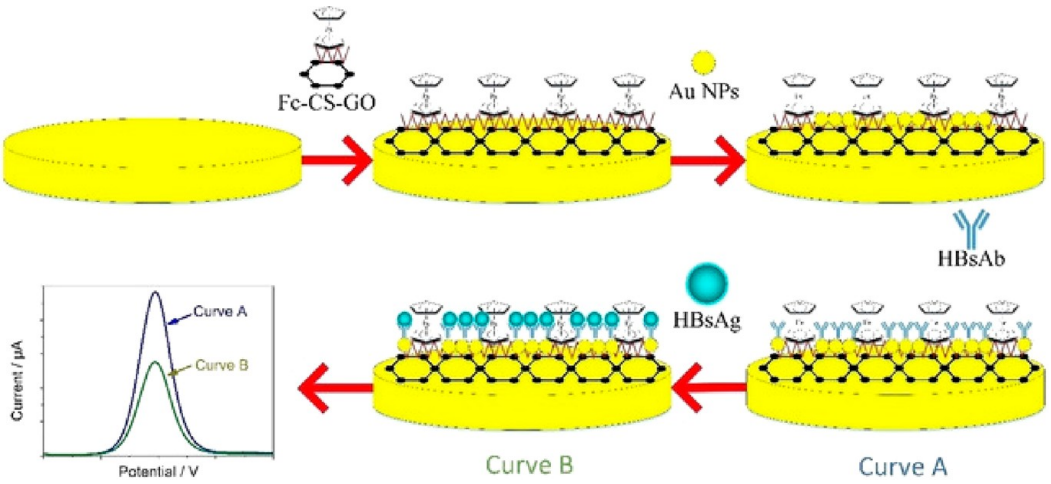

Figure 22. Graphic illustration of step-by-step immunosensor manufacturing. GE was immersed in fresh piranha solution (H_2SO_4/H_2O_2 3:1) followed by sonication in absolute ethanol and water. After that, GE was polished with alumina powder before being bathed twice with absolute ethanol and water. At 23 °C, the GO-Fc-CS solution (6 μL) was blown-out uniformly against the cleaned GE surface with a syringe to form a smooth composite film. In addition, the AuNPs solution (6 μL) was sprayed on the GE surface and allowed to dry at 23 °C. The GE modified with GO-Fc-CS/AuNPs was immersed in HBsAb solution (300 ng/mL) for 12 h. Finally, the GO-Fc-CS/AuNPs/HBsAb-modified electrode was incubated in a 0.5% BSA solution to prevent nonspecific adsorption by blocking any remaining active sites. The electrode was held in the refrigerator (4 °C) for potential use. Reproduced with permission from ref 141. Copyright 2018 John Wiley and Sons.

antibody) solution (300 ng/mL). As a final point, the GO-Fc-CS/AuNPs/HBsAb-modified electrode was incubated in a 0.5% BSA solution to prevent nonspecific adsorption by blocking any remaining active sites. For potential use, the electrode was held in the refrigerator (4 °C). Figure 22 shows a basic schematic diagram of the GO-Fc-CS/AuNPs/HBsAb immunosensor fabrication process.

Coronaviruses (COVID-19). Coronaviruses belong to the subfamily *Coronavirinae*, order *Nidovirales*, and family *Coronaviridae*. They are enveloped, spherical viruses with an ssRNA genome.[142] Currently, we are experiencing a pandemic situation linked to the coronavirus SARS-CoV-2/2019-nCoV/COVID-19 outbreak, which has lead to a serious threat to public health worldwide.[143] Together with the development of vaccines aimed at COVID-19, early and rapid diagnosis is the key to precluding the virus spread. The outstanding sensitivity and selectivity of biosensors enabled them to be applied as an effective tool for the recognition of COVID-19.[144] Biosensors have attracted attention as effective (sensitive and selective) and cost-efficient analytical diagnostic apparatuses aimed at early-stage disease diagnosis that are vital for personalized medical and lifestyle maintenance. The identification of a specific disease biomarker at the molecular level (pM level) has proven tremendously effective for monitoring disease progression during treatment. Such bioinformatics and multi-aspect analytics are required to evaluate a prescription drug's efficacy, optimize therapy, and correlate biomarker levels with disease pathogenesis. Advances in the manufacture of the sensing unit, system integration, interface, packaging, and POC sensing efficiency have enabled diagnostics to be adapted to illness management requirements and patient illness characteristics, culminating in customized testing.[145] Mujawar et al. explored tailored health-care-management-related analytical resources that can help everyone improve their health, with the overreaching aim of achieving a safe future in a responsible way.[144] Such affordable intelligent diagnostic techniques are urgently needed to manage the COVID-19 pandemic, a life-threatening infectious respiratory disease, as the quick, selective, and sensitive detection of human beta coronavirus (SARS-CoV-2) is key.[144]

Mujawar et al. described the suggested developments of the future biosensor market projection and the associated obstacles.[144] Their investigation was meant to act as a call to professionals to build improved analytical biosensing technologies for disease diagnostics that will enable personalized health care and wellbeing at individual and community levels.[146−150] Mujawar et al. recommended that scientific investigations should introduce the concept of miniaturization in biosensors to study the prerequisites for POC implementation.[144] In addition, the employment of POC biosensors using a smartphone for useful artificial intelligence (AI)- and internet of medical things (IoMT)-assisted bioinformatics analysis aimed at speedy and crucial diagnostics has also proven to be effective for prompt therapy customization and individualized disease diagnostics. More research on AI- and IoT-assisted SARS-CoV-2 recognition at small concentrations for premature COVID-19 diagnostics at the POC is needed, consistent with this study, to efficiently tackle the epidemic in a personalized way.[151−153]

Although significant developments have been made in biosensor systems, a number of hurdles remain to be dealt with, including the cost, sensitivity, mobility, longevity, bioactive chemical interoperability, and many more, with a view toward achieving home and POC disease diagnostics. The creation of innovative electric biomaterials (in particular, biopolymers such as CS, scaffolds, and other biopolymers) with total immunological compatibility and the desired interaction with human bodies will become the key consideration in sensor development. The investigation of miniaturized potentiostats (M-Ps) operated via smartphones might also be a major component for real-time diagnosis at the POC that is essential for pandemic site therapeutic interventions. Microelectromechanical system (MEMS)-based biosensing appears to be a game-changing tool for examining the nanotoxicity features of nanomaterials and the cell physiology in response to external influences including viruses,

https://doi.org/10.1021/acsbiomaterials.1c00710
ACS Biomater. Sci. Eng. 2022, 8, 964−1000

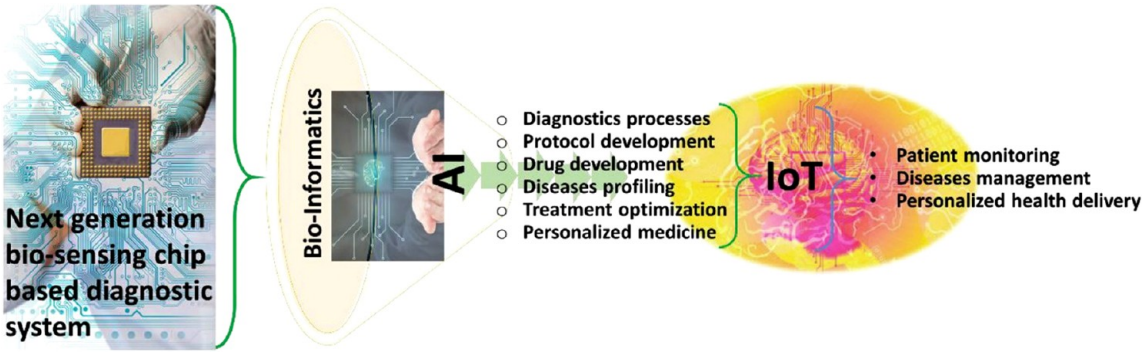

Figure 23. Diagram of the next-generation biosensor-based diagnostics system aimed at personalized health wellness through bioinformatics that manage the diagnostics processes, protocol development, disease profiling, drug improvement, treatment optimization, and personalized medicine and showing a positive effect on the patient monitoring, disease management, and personalized health delivery. Reproduced with permission from ref 144. Copyright 2020 Elsevier.

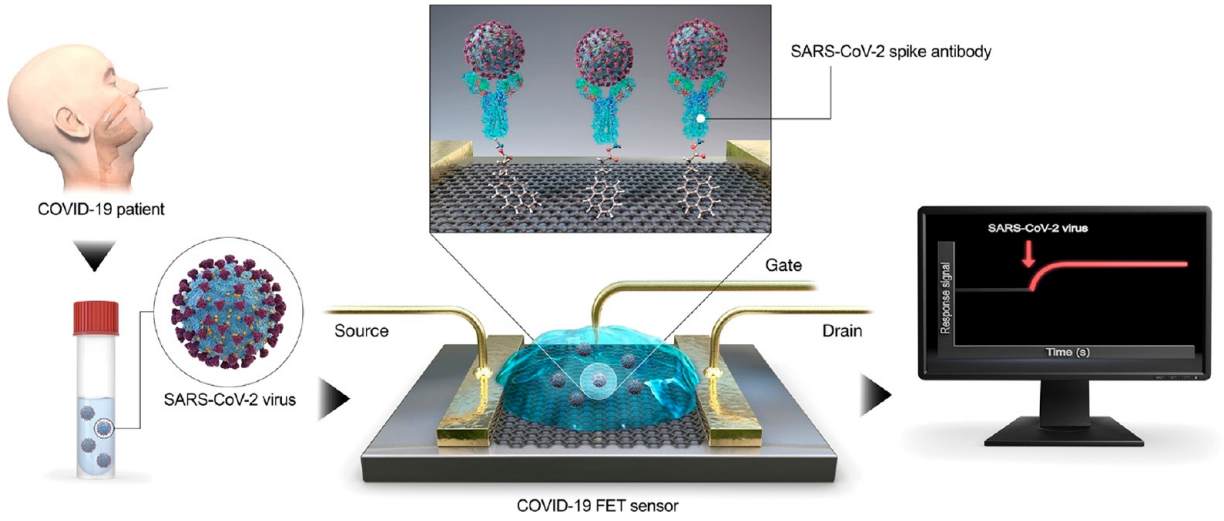

Figure 24. Operation of the COVID-19 FET sensor. The SARS-CoV-2 spike antibody is attached to the graphene sheet using a probe linker called 1-pyrenebutyric acid *N*-hydroxysuccinimide ester (PBASE). Reproduced with permission from ref 154. Copyright 2020 American Chemical Society.

transmitted diseases, and the inhalation of pollution particles. The use of sophisticated chip-based sensors would be extremely beneficial for managing the concentration of various NPs aimed at biomedical applications, the evaluation of drug efficacy, and the evaluation of therapeutic potential.[145−153] The results of such a sensing technology, as illustrated in Figure 23, can provide the required informatics for the development of a product for daily use and for drug/vaccine therapy to provide better treatment.

Seo et al. fabricated a graphene-based FET biosensor aimed at revealing SARS-CoV-2 in clinical samples using immunoassays.[154] Graphene sheets of the FET were covered with a specific SARS-CoV-2 antibody through 1-pyrenebutyric acid *N*-hydroxysuccinimide ester (PBASE) (an interfacing molecule used as a probe linker). They possibly identified the SARS-CoV-2 spike protein in phosphate-buffered saline (PBS) and clinical transport medium, showing an LOD of 1 and 100 fg/mL, respectively. Furthermore, the FET sensor could detect SARS-CoV-2 in culture medium with an LOD of 1.6×10^1 pfu/mL. In addition, nasopharyngeal swab samples of COVID-19 patients were used to test the detection efficiency of the biosensor. With an LOD of 2.42×10^2 copies/mL, the COVID-19 FET sensor may possibly differentiate among infected and noninfected persons. This FET biosensor shows high performance with good sensitivity at low concentrations without any sample pretreatment or labeling.[154−158]

Seo et al. developed a graphene-based biosensing technology that was functionalized with the SARS-CoV-2 spike antibody to utilize as a SARS-CoV-2 viral recognition tool (COVID-19 FET sensor).[154] The SARS-CoV-2 spike antibody was immobilized onto the manufactured device using PBASE, an excellent interface binding agent employed as a probe linker (Figure 24). In addition, that sensor was also capable of telling the difference between SARS-CoV-2 and MERS-CoV antigen proteins. These results demonstrate that a COVID-19 FET sensor based on the combination of a SARS-CoV-2 spike antibody with graphene can recognize the SARS-CoV-2 virus in clinical specimens with great sensitivity.[159−162]

Clinical samples can be used to test the COVID-19 FET sensor's detection performance aimed at the SARS-CoV-2 pathogen in patient cases. Seo et al. gathered and stored nasopharyngeal swab swabs from COVID-19 patients and healthy volunteers in universal transport medium (UTM) to achieve this goal. Before adding patient samples to the device, they tested nasopharyngeal swab samples from normal subjects to establish the basal signal. In addition, the FET sensor also

https://doi.org/10.1021/acsbiomaterials.1c00710
ACS Biomater. Sci. Eng. 2022, 8, 964−1000

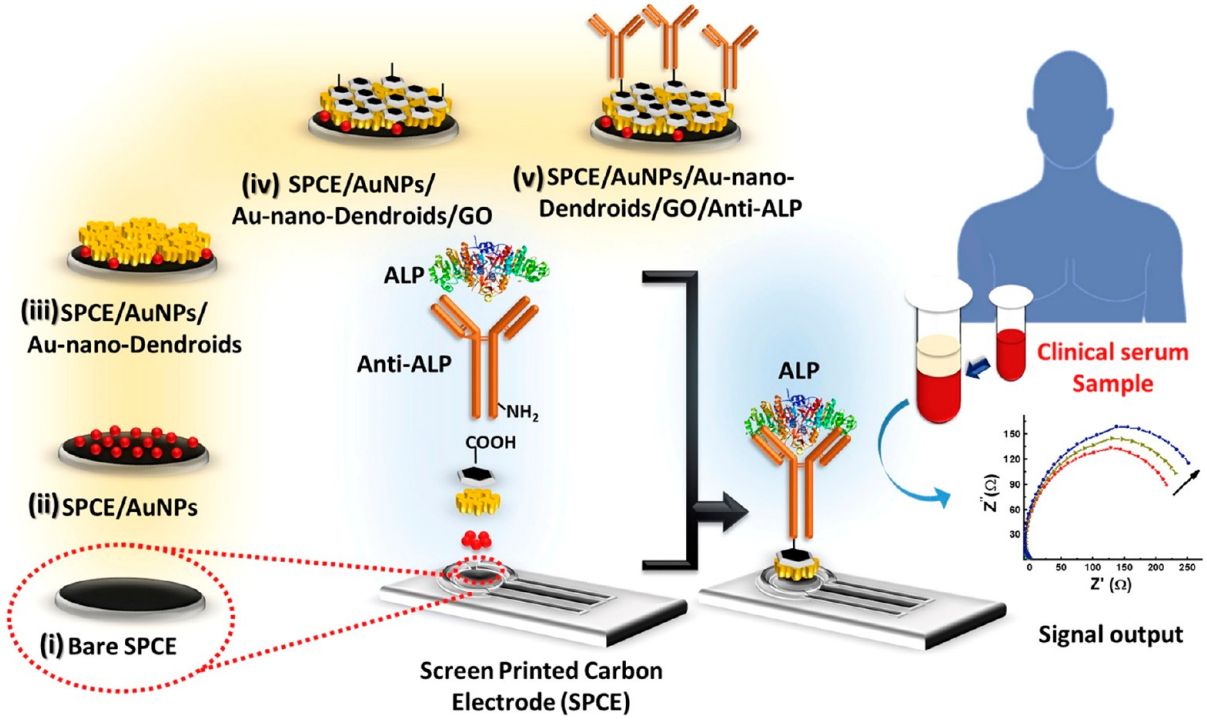

Figure 25. Conceptual diagram of the SPCE/NPs/nano-Dendroids/GO/Ab probe production for POC identification of COVID-19 infection. In the initial step, SPCE was modified using electrochemically deposited AuNPs. In addition, the AuNPs were electrochemically deposited with an acid solution of $HAuCl_4$ in the bare SPCE as an electrolyte in a three-electrode device. Next, the Au-nano-Dendroids on the amended surface of the SPCE/AuNP were electrochemically produced. In the next stage, the synthesized GO was subsequently coated with the SPCE/AuNP/Au-nano-Dendroids. The anti-ALP immobilization then took place on the dried surface of the SPCE/AuNP/Au-nano-Dendroids/GO electrode. The sensor surface was carefully rinsed with distilled water after incubation to extract unreacted anti-ALP, then blocked with 0.1% bovine serum albumin to remove nonspecific contact sites. The name supplied to the final revised sensor was SPCE/AuNPs/Au-nano-Dendroids/GO/anti-ALP. Reproduced with permission from ref 167. Copyright 2020 Elsevier.

responded to patient samples diluted up to 1:1 × 10^5 (242 copies/mL), and the normalized response curve of the FET sensor was linear. Given that UTM contains various reagents and generates noise signals, they believed that the COVID-19 FET sensor's LOD was low enough for practical application. Nonetheless, novel FET sensor materials for UTM should be developed to improve the detection accuracy by reducing noise signals. For comparison, the existing COVID-19 molecular diagnostic tests have an LOD of 50−100 copies.[163−166]

Mahato et al. demonstrated a label-free EIS-based biomarker localization method by sequentially depositing metallic NPs, electrochemically tailored nanodendroids, and GO nanocomposites over an SPCE. In addition, the antibodies againstthe particular biomarker were restrained by utilizing a bioconjugation method.[167,168] Because of its power and high explanatory execution, the improvement of this detection device for COVID-19 location was proposed by incorporating the recognition stage with newfound markers explicit to COVID-19 as RNA-subordinate RNA polymerase (RdRp)/helicase (H) genes of SARS-CoV-2. Subsequently, the SPCE/NPs/nano-Dendroids/GO/anti-RdRp helicase (Figure 25) may be another approach for effectively analyzing the contamination of COVID-19.[168,169]

The sensor probe was constructed by performing sequential surface changes over the bare SPCE. The AuNPs were deposited electrochemically on the bare SPCE within that procedure, utilizing an acidic solution of $HAuCl_4$ (0.005% in 0.5 M H_2SO_4) as the electrolyte in a three-electrode device capable of five successive linear sweep voltammetry (LSV) scans inside a conceivable frame of 1.5 to 0.4 V at a scan rate of 100 mV/s. The voltage and time given were −0.6 V and 60 s, respectively. The electrochemical installation of Au-nano-Dendroids was proficient via a chrono-amperometric method, which was carried out at −0.3 V for 600 s using a three-electrode device containing $HAuCl_4$ solution (5% in KCl 0.1 M) as an electrolyte. In the following stage, the synthesized GO was coated onto the modified electrode surface of SPCE/AuNPs/Au-nano-Dendroids. In a nutshell, a GO solution (1 mg/mL) was created by dissolving GO in ethanol and spin coating 2 μL of the solution followed by 30 min of drying. The anti-ALP immobilization was then performed on the withered SPCE/AuNPs/Au-nano-Dendroids/GO electrode surface. In addition, 50 mL of EDC/NHS (100/100 mM) solution was preserved and protected for 30 min. The final upgraded sensor probe was assigned the name SPCE/AuNPs/Au-nano-Dendroids/GO/anti-ALP. Figure 25 depicts the step-by-step fabrication of the sensor probe and the detection theory.

In an ongoing report based on a nonenzymatic electrochemical nanoprobe for chemical analyte assurance in blood samples,[170] Chandra used a gold-sputtered, nanohierarchical 3D dendritic structure, MWCNT-coordinated, dendrite-modified electrode, leading to high conductivity and electrocatalysis. Subsequently, these nanoprobes are valuable as a stage to get and break down the different COVID-19 infection biomarkers, such as the spike protein (S), envelope protein (E), nucleocapsid protein (N), membrane protein (M), and open reading frame 1b (ORF1b) of the viral RNA.[168,171−173]

https://doi.org/10.1021/acsbiomaterials.1c00710
ACS Biomater. Sci. Eng. 2022, 8, 964−1000

Table 5. Summary of Electrochemical Approaches in Virus Detection

electrochemical approaches	type of electrodes	targeted virus	limit of detection (LOD)	ref
conductometry	Ag nanofiber array electrode	bovine viral diarrhea virus (BVDV)	103 CCID/mL	174
cyclic voltammetry	graphene microelectrode	rotavirus	10^3 PFU/mL	175
EIS	Au electrode	human influenza A virus H3N2	8 ng/mL	176
DPV	nanostructured alumina on Pt wire electrode	Dengue type 2 virus (DENV-2)	1 PFU/mL	177
EIS ferrocene methanol	nanostructured alumina on Pt wire electrode	DENV-2	1 PFU/mL	178
amperometry	polypyrrole nanoribbons on Au microelectrode array	cucumber mosaic virus (CMV)	10 ng/mL	179
SSWV, fluorescence	AuNPs on carbon electrode	murine norovirus (MNV)	180 viruses	180
DPV	graphene/AuNP composite on carbon electrode	norovirus	100 pM	181
EIS	gold electrode	avian influenza virus	8 ng/mL	176
chrono-amperometric, DPV	carbon SPE	H5N1 and H1N1 virus protein	8.3 pM (H5N1) and 9.4 pM (H1N1)	182
electrochemical LFIA	gold electrode	SARS-CoV-2	5 ng/mL	183
luciferase immunosorbent assay	gold electrode	SARS-CoV-2	0.4 ng/mL	184
LFIA based on superparamagnetic nanoparticles	gold electrode	SARS-CoV-2	5 ng/mL	185
paper-based ELISA	nanostructured alumina on Pt wire electrode	SARS-CoV-2	9 mg/mL	186
disposable ELISA	nanostructured alumina on Pt wire electrode	SARS-CoV-2	2.8 ng/mL	187
vertical-flow paper-based assay	Au electrode	SARS-CoV-2	750 ng/mL	188
DPV	GCE	influenza virus A	0.43 pg/mL	189
chrono-amperometry	carbon electrode	human influenza A virus H9N2	16 HAU	190
SWV	AuNPs on carbon electrode	Middle East respiratory syndrome	400 fg/mL	191
EIS	Au interdigitated microelectrode array	avian influenza virus (AIV) H5N1	10^3 EDI50/mL	192

These sensors are being evaluated for coupling the electronic signal to cell phones for improved diagnostic systems.[168]

Because the quest to produce a COVID-19 vaccine is the main focus right now, it is important to comprehend the epidemiological physiognomies with the purpose of combating the outbreak. Furthermore, it is recommended that the disease's potent intermediate hosts be identified to avoid and eliminate the disease in the near future. These measures necessitate a convincing disease detection strategy. As a result, POC-based, label-free recognition procedures incorporated into smartphones can not only monitor the disease's spread around the world but also enable the development of a library of data and the facts necessary for potential pandemic preparedness. When early warning is delivered in affected areas, clinicians can rapidly identify the proper care for each new patient, and public health officials can control the disease spread. The efficient integration of label-free technology can be used to develop a tailor-made analysis framework for COVID-19 and other infectious disorders. Table 5 summarizes and compares electrochemical methods in virus detection, especially new detection methods in SARS-CoV-2.

FINAL REMARKS

Nanomaterial-based biosensors provide excellent sensing capability, high sensitivity, and high selectivity, even at lower concentrations. In this Review, we have described the recent advancement of graphene and carbon nanomaterials modifying the electrode of biosensors. Biosensors based on graphene or carbon nanomaterials incorporated with other nanomaterials have promising performance in the detection of biomarkers, for instance, DNA, proteins, and hormones, for the early diagnosis of diseases, for instance, cancer, AD, and diabetes. They are also useful for pathogenic viruses that cause diseases such as the Zika virus, HIV, HBV, and, finally, the recent virus COVID-19. Important efforts have been carried out to detect these diseases early to develop and overcome the problems of conventional methods. The use of biosensors is attractive and of interest because they allow an effective, sensitive, selective, rapid, and low-cost diagnosis. The biosensor is an analytical device that is based on receptors for the process of detection and transducers for getting the measuring response. Biosensors can be of different types, such as electrochemical, piezoelectric, thermal, and optical biosensors that depend on the process of transduction. Biosensor-based graphene and CNTs have shown sensitivity and selectivity for analyte detection, a wide linear range, a low LOD, a fast response time, long stability, and respectable reproducibility. All of these features are ascribed to their enormous surface area and good electrochemical and mechanical activities.

In recent years, many biosensors have been made that match the sensitivity and selectivity criteria for practical applications, but they have been insufficient for industrial manufacturing and marketing. Some challenges to mass production are the sophisticated sensor assembly operations, expensive elements, potential undesirable nanoscale characteristics, and lack of storage stability. The integration of biosensors into automated and miniaturized systems and even some strategies to create the same sensor sets and to expand to industrial customization remain to be accomplished. In addition, many of the available biosensors have not been authenticated by means of a significant number of patient samples. While still in its early phases, research on carbon-based biosensors aimed at cancer and disease recognition has shown promise and a vision for future illness diagnosis and health monitoring. Biomarker sensors aimed at routine clinical directions are expected to be developed as this area progresses. As a result, on the basis of

https://doi.org/10.1021/acsbiomaterials.1c00710
ACS Biomater. Sci. Eng. 2022, 8, 964−1000

the current progress, carbon-nanomaterial-based biosensors have a promising future, and their growth, and the inclusion of new biomarkers, will continue. This Review describes the state of the art of the development of biosensors based on graphene and CNTs and the techniques for the detection and early diagnoses of the most common diseases, including different types of cancer, and also presents the ability of graphene and carbon aimed at the exposure of pathogenic viruses and proteins.

FUTURE PERSPECTIVES

Because optical and electrochemical approaches are both very sensitive and selective, they are excellent for on-site, real-time, easy-to-use, and low-cost virus recognition. The sustainability of electrode materials can be a constraint for electrochemical approaches; however, handled professionally, electrodes (e.g., in the configuration of microchips) could give acceptable sustainabilty. Cyan graphene and graphene acid, two graphene derivatives that are both conductive and have a distinct chemical nature, provide innovative avenues for a graphene-based raised area that can be utilized to accurately design biosensors. For larger and more reliable directions of graphene derivatives in (bio)sensorics, high batch-to-batch reproducibility and standardization are required. Additionally, the increased use of these kinds of materials may motivate additional investigations. The dispensability of graphene-based nanocomposites allows them to be utilized as an ink for ink-printed electrodes and paper-based biosensors, broadening their biosensor applications and enabling downsizing. Atomically precise manufacturing, standardization, and multi-readout biosensors should all be taken into consideration because they can assist in reducing the number of false-positive and -negative results. Miniaturization, integration with fluid systems, and multichip systems are all key difficulties aimed at the next generation of graphene-based biosensors. Additionally, these features, in response to the elevated sensitivity, selectivity, and large-scale processing, make graphene sensors ideal for detecting a wide spectrum of viral species. With the purpose of offering a low-cost, effective, and adaptable platform for (bio)sensing that can be utilized on site, for example, as POC devices, an amalgamation of graphene-based biosensors with smartphones has much potential. Graphene and its derivatives are without a doubt ideal materials for constructing efficient virus detection biosensors that can be readily applied to novel viruses. Graphene-based biosensors are in the early stages of development, but they have much commercial potential.

AUTHOR INFORMATION

Corresponding Authors

Heba Mohamed Fahmy − *Biophysics Department, Faculty of Science, Cairo University, 12613 Giza, Egypt*; Email: hfahmy@sci.cu.edu.eg

Esraa Samy Abu Serea − *Chemistry and Biochemistry Department, Faculty of Science, Cairo University, 12613 Giza, Egypt; BCMaterials-Basque Center for Materials, Applications and Nanostructures, Leioa 48940, Spain*; Email: esraasamy03@gmail.com

◆**Ahmed Esmail Shalan** − *BCMaterials-Basque Center for Materials, Applications and Nanostructures, Leioa 48940, Spain; Central Metallurgical Research and Development Institute, 11422 Cairo, Egypt*; orcid.org/0000-0002-3424-1609; Email: a.shalan133@gmail.com, ahmed.shalan@bcmaterials.net

Senentxu Lanceros-Méndez − *BCMaterials-Basque Center for Materials, Applications and Nanostructures, Leioa 48940, Spain; IKERBASQUE, Basque Foundation for Science, 48009 Bilbao, Spain*; orcid.org/0000-0001-6791-7620; Email: senentxu.lanceros@bcmaterials.net

Authors

Reem Essam Salah-Eldin − *Chemistry and Zoology Department, Faculty of Science, Cairo University, 12613 Giza, Egypt*

Sara Ayman Al-Hafiry − *Biophysics Department, Faculty of Science, Cairo University, 12613 Giza, Egypt*

Miar Khaled Ali − *Biotechnology/Biomolecular Chemistry Program, Faculty of Science, Cairo University, 12613 Giza, Egypt*

Complete contact information is available at: https://pubs.acs.org/10.1021/acsbiomaterials.1c00710

Author Contributions

○H.M.F. and E.S.A.S. contributed equally.

Notes

The authors declare no competing financial interest.

◆A.E.S.: Currently on leave from CMRDI.

ACKNOWLEDGMENTS

We recognize Cairo University for supporting the completion of the current project. H.M.F. extends gratitude for the continued support and encouragement given to the Student Research Team (SRT), Cairo University by Prof. Dr. Abdel Hameed Wagdi Elmanawi, Dean of the Faculty of Science, Cairo University and Prof. Dr Hesham Ahmad Yousef, Vice-Dean for Education and Student Affairs, Faculty of Science, Cairo University. A.E.S. acknowledges the National Research grants from MINECO, Spain, "Juan de la Cierva" [FJCI-2018-037717]. Financial support from the Spanish State Research Agency (AEI) and the European Regional Development Fund (ERFD) through the project PID2019-106099RB-C43/AEI/10.13039/501100011033 and from the Basque Government Industry and Education Departments under the ELKARTEK and PIBA (PIBA-2018-06) programs, respectively, is also acknowledged.

REFERENCES

(1) Chen, C.; Xie, Q.; Yang, D.; Xiao, H.; Fu, Y.; Tan, Y.; Yao, S. Recent Advances in Electrochemical Glucose Biosensors: A Review. *RSC Adv.* **2013**, *3* (14), 4473.

(2) Veiseh, O.; Tang, B. C.; Whitehead, K. A.; Anderson, D. G.; Langer, R. Managing Diabetes with Nanomedicine: Challenges and Opportunities. *Nat. Rev. Drug Discov* **2015**, *14* (1), 45−57.

(3) Malhotra, B. D.; Kumar, S.; Pandey, C. M. Nanomaterials Based Biosensors for Cancer Biomarker Detection. *J. Phys.: Conf. Ser.* **2016**, *704*, 012011.

(4) Coroş, M.; Pruneanu, S.; Stefan-van Staden, R.-I. Review—Recent Progress in the Graphene-Based Electrochemical Sensors and Biosensors. *J. Electrochem. Soc.* **2020**, *167* (3), 037528.

(5) Stefan-van Staden, R.-I.; Popa-Tudor, I.; Badulescu, M.; Anghel, A. Fast Screening Method for Molecular Recognition of Islet Amyloid Polypeptide from Whole Blood Samples Collected from Diabetic Patients with Disposable Stochastic Sensors Obtained by Nanolayer, and Nanolayer by Nanolayer Deposition Using Cold Plasma. *Anal. Bioanal. Chem.* **2020**, *412* (17), 4135−4141.

(6) Stefan-van Staden, R.-I.; Ilie-Mihai, R.-M.; Pogacean, F.; Pruneanu, S. M. Needle Stochastic Sensors for On-Site Fast Recognition and Quantification of Biomarkers for Gastric Cancer in Biological Samples. *New J. Chem.* **2020**, *44* (46), 20203−20211.
(7) Stefan-van Staden, R.-I.; Balahura, L.-R.; Cioates-Negut, C.; Aboul-Enein, H. Y. Stochastic Microsensors for the Assessment of DNA Damage in Cancer. *Anal. Biochem.* **2020**, *605* (113839), 113839.
(8) Ilie-Mihai, R. M.; Gheorghe, S. S.; Stefan-van Staden, R.; Bratei, A. Electroanalysis of Interleukins 1β, 6, and 12 in Biological Samples Using a Needle Stochastic Sensor Based on Nanodiamond Paste. *Electroanalysis* **2021**, *33* (1), 6−10.
(9) Stefan-van Staden, R.-I.; Moscalu-Lungu, A.; Badulescu, M. Disposable Stochastic Sensors Based on Nanolayer Deposition(s) of Silver and AgC Composite on Plastic for the Assay of α-Amylase in Whole Blood and Saliva. *Nanomaterials (Basel)* **2020**, *10* (8), 1528.
(10) Stefan-van Staden, R.-I.; Ilie-Mihai, R.-M.; Magerusan, L.; Coros, M.; Pruneanu, S. Enantioanalysis of Glutamine-a Key Factor in Establishing the Metabolomics Process in Gastric Cancer. *Anal. Bioanal. Chem.* **2020**, *412* (13), 3199−3207.
(11) Baldea, I.; Olteanu, D.; Filip, G. A.; Pogacean, F.; Coros, M.; Suciu, M.; Tripon, S. C.; Cenariu, M.; Magerusan, L.; Stefan-van Staden, R.-I.; Pruneanu, S. Cytotoxicity Mechanisms of Nitrogen-Doped Graphene Obtained by Electrochemical Exfoliation of Graphite Rods, on Human Endothelial and Colon Cancer Cells. *Carbon N. Y.* **2020**, *158*, 267−281.
(12) Stefan-van Staden, R.-I.; Gheorghe, D.-C.; Ilie-Mihai, R.-M.; Tudoran, L.-B.; Pruneanu, S. M. Stochastic Biosensors Based on N- and S-Doped Graphene for the Enantioanalysis of Aspartic Acid in Biological Samples. *RSC Adv.* **2021**, *11* (38), 23301−23309.
(13) Morales-Narváez, E.; Merkoçi, A. Graphene Oxide as an Optical Biosensing Platform. *Adv. Mater.* **2012**, *24* (25), 3298−3308.
(14) Singh, P.; Campidelli, S.; Giordani, S.; Bonifazi, D.; Bianco, A.; Prato, M. Organic Functionalisation and Characterisation of Single-Walled Carbon Nanotubes. *Chem. Soc. Rev.* **2009**, *38* (8), 2214−2230.
(15) Guo, X. Single-Molecule Electrical Biosensors Based on Single-Walled Carbon Nanotubes. *Adv. Mater.* **2013**, *25* (25), 3397−3408.
(16) Zhang, X.; Li, C.-R.; Wang, W.-C.; Xue, J.; Huang, Y.-L.; Yang, X.-X.; Tan, B.; Zhou, X.-P.; Shao, C.; Ding, S.-J.; Qiu, J.-F. A Novel Electrochemical Immunosensor for Highly Sensitive Detection of Aflatoxin B1 in Corn Using Single-Walled Carbon Nanotubes/Chitosan. *Food Chem.* **2016**, *192*, 197−202.
(17) Ahammad, A. J. S.; Lee, J.-J.; Rahman, M. A. Electrochemical Sensors Based on Carbon Nanotubes. *Sensors (Basel)* **2009**, *9* (4), 2289−2319.
(18) Pan, J.; Li, F.; Choi, J. H. Single-Walled Carbon Nanotubes as Optical Probes for Bio-Sensing and Imaging. *J. Mater. Chem. B Mater. Biol. Med.* **2017**, *5* (32), 6511−6522.
(19) Chen, J.; Liu, B.; Gao, X.; Xu, D. A Review of the Interfacial Characteristics of Polymer Nanocomposites Containing Carbon Nanotubes. *RSC Adv.* **2018**, *8* (49), 28048−28085.
(20) Holzinger, M.; Baur, J.; Haddad, R.; Wang, X.; Cosnier, S. Multiple Functionalization of Single-Walled Carbon Nanotubes by Dip Coating. *Chem. Commun. (Camb.)* **2011**, *47* (8), 2450−2452.
(21) Wu, Z.; Zhen, Z.; Jiang, J.-H.; Shen, G.-L.; Yu, R.-Q. Terminal Protection of Small-Molecule-Linked DNA for Sensitive Electrochemical Detection of Protein Binding via Selective Carbon Nanotube Assembly. *J. Am. Chem. Soc.* **2009**, *131* (34), 12325−12332.
(22) Cho, I.-H.; Lee, J.; Kim, J.; Kang, M.-S.; Paik, J.; Ku, S.; Cho, H.-M.; Irudayaraj, J.; Kim, D.-H. Current Technologies of Electrochemical Immunosensors: Perspective on Signal Amplification. *Sensors (Basel)* **2018**, *18* (2), 207.
(23) Knyazev, A.; Louise, L.; Veber, M.; Langevin, D.; Filoramo, A.; Prina-Mello, A.; Campidelli, S. Selective Adsorption of Proteins on Single-Wall Carbon Nanotubes by Using a Protective Surfactant. *Chemistry* **2011**, *17* (51), 14663−14671.
(24) Zhou, Y.; Fang, Y.; Ramasamy, R. P. Non-Covalent Functionalization of Carbon Nanotubes for Electrochemical Biosensor Development. *Sensors (Basel)* **2019**, *19* (2), 392.
(25) Agüí, L.; Yáñez-Sedeño, P.; Pingarrón, J. M. Role of Carbon Nanotubes in Electroanalytical Chemistry: A Review. *Anal. Chim. Acta* **2008**, *622* (1−2), 11−47.
(26) Gayathri, C. H.; Mayuri, P.; Sankaran, K.; Kumar, A. S. An Electrochemical Immunosensor for Efficient Detection of Uropathogenic E. Coli Based on Thionine Dye Immobilized Chitosan/Functionalized-MWCNT Modified Electrode. *Biosens. Bioelectron.* **2016**, *82*, 71−77.
(27) Zheng, W.; Zheng, Y. F. Gelatin-Functionalized Carbon Nanotubes for the Bioelectrochemistry of Hemoglobin. *Electrochem. commun.* **2007**, *9* (7), 1619−1623.
(28) Li, H.; Wang, D. Q.; Chen, H. L.; Liu, B. L.; Gao, L. Z. A Novel Gelatin-Carbon Nanotubes Hybrid Hydrogel. *Macromol. Biosci.* **2003**, *3* (12), 720−724.
(29) Haider, S.; Park, S.-Y.; Saeed, K.; Farmer, B. L. Swelling and Electroresponsive Characteristics of Gelatin Immobilized onto Multi-Walled Carbon Nanotubes. *Sens. Actuators B Chem.* **2007**, *124* (2), 517−528.
(30) Li, M.; Wang, P.; Li, F.; Chu, Q.; Li, Y.; Dong, Y. An Ultrasensitive Sandwich-Type Electrochemical Immunosensor Based on the Signal Amplification Strategy of Mesoporous Core-Shell Pd@Pt Nanoparticles/Amino Group Functionalized Graphene Nanocomposite. *Biosens. Bioelectron.* **2017**, *87*, 752−759.
(31) Xu, L.; Zhu, Y.; Tang, L.; Yang, X.; Li, C. Biosensor Based on Self-Assembling Glucose Oxidase and Dendrimer-Encapsulated Pt Nanoparticles on Carbon Nanotubes for Glucose Detection. *Electroanalysis* **2007**, *19* (6), 717−722.
(32) Kavosi, B.; Salimi, A.; Hallaj, R.; Amani, K. A Highly Sensitive Prostate-Specific Antigen Immunosensor Based on Gold Nanoparticles/PAMAM Dendrimer Loaded on MWCNTS/Chitosan/Ionic Liquid Nanocomposite. *Biosens. Bioelectron.* **2014**, *52*, 20−28.
(33) Wei, Y.; Ling, X.; Zou, L.; Lai, D.; Lu, H.; Xu, Y. A Facile Approach toward Preparation of Sulfonated Multi-Walled Carbon Nanotubes and Their Dispersibility in Various Solvents. *Colloids Surf. A Physicochem. Eng. Asp.* **2015**, *482*, 507−513.
(34) Jiang, Z.; Chen, D.; Yu, Y.; Miao, J.; Liu, Y.; Zhang, L. Composite Fibers Prepared from Multi-Walled Carbon Nanotubes/Cellulose Dispersed/Dissolved in Ammonium/Dimethyl Sulfoxide Mixed Solvent. *RSC Adv.* **2017**, *7* (4), 2186−2192.
(35) Singh, C.; Srivastava, S.; Ali, M. A.; Gupta, T. K.; Sumana, G.; Srivastava, A.; Mathur, R. B.; Malhotra, B. D. Carboxylated Multiwalled Carbon Nanotubes Based Biosensor for Aflatoxin Detection. *Sens. Actuators B Chem.* **2013**, *185*, 258−264.
(36) Cao, S.-H.; Li, L.-H.; Wei, W.-Y.; Feng, Y.; Jiang, W.-L.; Wang, J.-L.; Zhang, X.-P.; Cai, S.-H.; Chen, Z. A Label-Free and Ultrasensitive DNA Impedimetric Sensor with Enzymatic and Electrical Dual-Amplification. *Analyst* **2019**, *144* (14), 4175−4179.
(37) Li, B.; Pan, G.; Avent, N. D.; Lowry, R. B.; Madgett, T. E.; Waines, P. L. Graphene Electrode Modified with Electrochemically Reduced Graphene Oxide for Label-Free DNA Detection. *Biosens. Bioelectron.* **2015**, *72*, 313−319.
(38) Cai, B.; Wang, S.; Huang, L.; Ning, Y.; Zhang, Z.; Zhang, G.-J. Ultrasensitive Label-Free Detection of PNA-DNA Hybridization by Reduced Graphene Oxide Field-Effect Transistor Biosensor. *ACS Nano* **2014**, *8* (3), 2632−2638.
(39) Dong, H.; Zhu, Z.; Ju, H.; Yan, F. Triplex Signal Amplification for Electrochemical DNA Biosensing by Coupling Probe-Gold Nanoparticles-Graphene Modified Electrode with Enzyme Functionalized Carbon Sphere as Tracer. *Biosens. Bioelectron.* **2012**, *33* (1), 228−232.
(40) Moreira, F. T. C.; Sale, M. G. F.; Di Lorenzo, M. Towards Timely Alzheimer Diagnosis: A Self-Powered Amperometric Biosensor for the Neurotransmitter Acetylcholine. *Biosens. Bioelectron.* **2017**, *87*, 607−614.
(41) Laurent, S.; Ejtehadi, M. R.; Rezaei, M.; Kehoe, P. G.; Mahmoudi, M. Interdisciplinary Challenges and Promising Theranostic Effects of Nanoscience in Alzheimer's Disease. *RSC Adv.* **2012**, *2* (12), 5008.

(42) Azimzadeh, M.; Nasirizadeh, N.; Rahaie, M.; Naderi-Manesh, H. Early Detection of Alzheimer's Disease Using a Biosensor Based on Electrochemically-Reduced Graphene Oxide and Gold Nanowires for the Quantification of Serum MicroRNA-137. *RSC Adv.* **2017**, *7* (88), 55709−55719.
(43) Cao, H.; Liu, S.; Tu, W.; Bao, J.; Dai, Z. A Carbon Nanotube/Quantum Dot Based Photoelectrochemical Biosensing Platform for the Direct Detection of MicroRNAs. *Chem. Commun. (Camb.)* **2014**, *50* (87), 13315−13318.
(44) Viswambharan, V.; Thanseem, I.; Vasu, M. M.; Poovathinal, S. A.; Anitha, A. MiRNAs as Biomarkers of Neurodegenerative Disorders. *Biomark. Med.* **2017**, *11* (2), 151−167.
(45) Baluta, S.; Lesiak, A.; Cabaj, J. Graphene Quantum Dots-Based Electrochemical Biosensor for Catecholamine Neurotransmitters Detection. *Electroanalysis* **2018**, *30*, 1781.
(46) Sun, D.; Li, H.; Li, M.; Li, C.; Dai, H.; Sun, D.; Yang, B. Electrodeposition Synthesis of a NiO/CNT/PEDOT Composite for Simultaneous Detection of Dopamine, Serotonin, and Tryptophan. *Sens. Actuators B Chem.* **2018**, *259*, 433−442.
(47) Apetrei, I. M.; Popa, C. V.; Apetrei, C.; Tutunaru, D. Biosensors Based on Graphene Modified Screen-Printed Electrodes for The Detection of Catecholamines Rom. *Biotechnol. Lett.* **2014**, *19*, 9801−9809.
(48) Kim, Y.-H.; Lee, K.; Jung, H.; Kang, H. K.; Jo, J.; Park, I.-K.; Lee, H. H. Direct Immune-Detection of Cortisol by Chemiresistor Graphene Oxide Sensor. *Biosens. Bioelectron.* **2017**, *98*, 473−477.
(49) Raymundo-Pereira, P. A.; Campos, A. M.; Vicentini, F. C.; Janegitz, B. C.; Mendonça, C. D.; Furini, L. N.; Boas, N. V.; Calegaro, M. L.; Constantino, C. J. L.; Machado, S. A. S.; Oliveira, O. N., Jr. Sensitive Detection of Estriol Hormone in Creek Water Using a Sensor Platform Based on Carbon Black and Silver Nanoparticles. *Talanta* **2017**, *174*, 652−659.
(50) Cincotto, F. H.; Canevari, T. C.; Machado, S. A. S.; Sánchez, A.; Barrio, M. A. R.; Villalonga, R.; Pingarrón, J. M. Reduced Graphene Oxide-Sb_2O_5 Hybrid Nanomaterial for the Design of a Laccase-Based Amperometric Biosensor for Estriol. *Electrochim. Acta* **2015**, *174*, 332−339.
(51) Eissa, S.; Tlili, C.; L'Hocine, L.; Zourob, M. Electrochemical Immunosensor for the Milk Allergen β-Lactoglobulin Based on Electrografting of Organic Film on Graphene Modified Screen-Printed Carbon Electrodes. *Biosens. Bioelectron.* **2012**, *38* (1), 308−313.
(52) Feng, L.; Wu, L.; Wang, J.; Ren, J.; Miyoshi, D.; Sugimoto, N.; Qu, X. Detection of a Prognostic Indicator in Early-Stage Cancer Using Functionalized Graphene-Based Peptide Sensors. *Adv. Mater.* **2012**, *24* (1), 125−131.
(53) Yagati, A. K.; Pyun, J.-C.; Min, J.; Cho, S. Label-Free and Direct Detection of C-Reactive Protein Using Reduced Graphene Oxide-Nanoparticle Hybrid Impedimetric Sensor. *Bioelectrochemistry* **2016**, *107*, 37−44.
(54) Zhong, Z.; Wu, W.; Wang, D.; Wang, D.; Shan, J.; Qing, Y.; Zhang, Z. Nanogold-Enwrapped Graphene Nanocomposites as Trace Labels for Sensitivity Enhancement of Electrochemical Immunosensors in Clinical Immunoassays: Carcinoembryonic Antigen as a Model. *Biosens. Bioelectron.* **2010**, *25* (10), 2379−2383.
(55) Krishna, G.; Srileka, V.; Singara Charya, M. A.; Abu Serea, E. S.; Shalan, A. E. Biogenic Synthesis and Cytotoxic Effects of Silver Nanoparticles Mediated by White Rot Fungi. *Heliyon* **2021**, *7* (3), No. e06470.
(56) Bohunicky, B.; Mousa, S. A. Biosensors: The New Wave in Cancer Diagnosis. *Nanotechnol. Sci. Appl.* **2010**, *4*, 1−10.
(57) Huang, K.-J.; Niu, D.-J.; Xie, W.-Z.; Wang, W. A Disposable Electrochemical Immunosensor for Carcinoembryonic Antigen Based on Nano-Au/Multi-Walled Carbon Nanotubes-Chitosans Nanocomposite Film Modified Glassy Carbon Electrode. *Anal. Chim. Acta* **2010**, *659* (1−2), 102−108.
(58) Jiang, W.; Yuan, R.; Chai, Y.-Q.; Yin, B. Amperometric Immunosensor Based on Multiwalled Carbon Nanotubes/Prussian Blue/Nanogold-Modified Electrode for Determination of α-Fetoprotein. *Anal. Biochem.* **2010**, *407* (1), 65−71.
(59) Hassanpour, S.; Hasanzadeh, M.; Saadati, A.; Shadjou, N.; Soleymani, J.; Jouyban, A. A Novel Paper Based Immunoassay of Breast Cancer Specific Carbohydrate (CA 15.3) Using Silver Nanoparticles-Reduced Graphene Oxide Nano-Ink Technology: A New Platform to Construction of Microfluidic Paper-Based Analytical Devices (MPADs) towards Biomedical Analysis. *Microchem. J.* **2019**, *146*, 345−358.
(60) Bahavarnia, F.; Saadati, A.; Hassanpour, S.; Hasanzadeh, M.; Shadjou, N.; Hassanzadeh, A. Paper Based Immunosensing of Ovarian Cancer Tumor Protein CA 125 Using Novel Nano-Ink: A New Platform for Efficient Diagnosis of Cancer and Biomedical Analysis Using Microfluidic Paper-Based Analytical Devices (MPAD). *Int. J. Biol. Macromol.* **2019**, *138*, 744−754.
(61) Panini, N. V.; Messina, G. A.; Salinas, E.; Fernández, H.; Raba, J. Integrated Microfluidic Systems with an Immunosensor Modified with Carbon Nanotubes for Detection of Prostate Specific Antigen (PSA) in Human Serum Samples. *Biosens. Bioelectron.* **2008**, *23* (7), 1145−1151.
(62) Jayanthi, V. S. P. K. S. A.; Das, A. B.; Saxena, U. Recent Advances in Biosensor Development for the Detection of Cancer Biomarkers. *Biosens. Bioelectron.* **2017**, *91*, 15−23.
(63) Singh, V. K.; Kumar, S.; Pandey, S. K.; Srivastava, S.; Mishra, M.; Gupta, G.; Malhotra, B. D.; Tiwari, R. S.; Srivastava, A. Fabrication of Sensitive Bioelectrode Based on Atomically Thin CVD Grown Graphene for Cancer Biomarker Detection. *Biosens. Bioelectron.* **2018**, *105*, 173−181.
(64) Yang, T.; Jia, H.; Liu, Z.; Qiu, X.; Gao, Y.; Xu, J.; Lu, L.; Yu, Y. Label-Free Electrochemical Immunoassay for α-Fetoprotein Based on a Redox Matrix of Prussian Blue-Reduced Graphene Oxide/Gold Nanoparticles-Poly(3,4-Ethylenedioxythiophene) Composite. *J. Electroanal. Chem. (Lausanne Switz)* **2017**, *799*, 625−633.
(65) Jia, X.; Liu, Z.; Liu, N.; Ma, Z. A Label-Free Immunosensor Based on Graphene Nanocomposites for Simultaneous Multiplexed Electrochemical Determination of Tumor Markers. *Biosens. Bioelectron.* **2014**, *53*, 160−166.
(66) Chen, X.; Jia, X.; Han, J.; Ma, J.; Ma, Z. Electrochemical Immunosensor for Simultaneous Detection of Multiplex Cancer Biomarkers Based on Graphene Nanocomposites. *Biosens. Bioelectron.* **2013**, *50*, 356−361.
(67) Khoshroo, A.; Mazloum-Ardakani, M.; Forat-Yazdi, M. Enhanced Performance of Label-Free Electrochemical Immunosensor for Carbohydrate Antigen 15-3 Based on Catalytic Activity of Cobalt Sulfide/Graphene Nanocomposite. *Sens. Actuators B Chem.* **2018**, *255*, 580−587.
(68) Fan, Y.; Shi, S.; Ma, J.; Guo, Y. A Paper-Based Electrochemical Immunosensor with Reduced Graphene Oxide/Thionine/Gold Nanoparticles Nanocomposites Modification for the Detection of Cancer Antigen 125. *Biosens. Bioelectron.* **2019**, *135*, 1−7.
(69) Salimi, A.; Kavosi, B.; Fathi, F.; Hallaj, R. Highly Sensitive Immunosensing of Prostate-Specific Antigen Based on Ionic Liquid-Carbon Nanotubes Modified Electrode: Application as Cancer Biomarker for Prostate Biopsies. *Biosens. Bioelectron.* **2013**, *42*, 439−446.
(70) Mandal, D.; Nunna, B. B.; Zhuang, S.; Rakshit, S.; Lee, E. S. Carbon Nanotubes Based Biosensor for Detection of Cancer Antigens (CA-125) under Shear Flow Condition. *Nano-struct. nano-objects* **2018**, *15*, 180−185.
(71) Yang, F.; Han, J.; Zhuo, Y.; Yang, Z.; Chai, Y.; Yuan, R. Highly Sensitive Impedimetric Immunosensor Based on Single-Walled Carbon Nanohorns as Labels and Bienzyme Biocatalyzed Precipitation as Enhancer for Cancer Biomarker Detection. *Biosens. Bioelectron.* **2014**, *55*, 360−365.
(72) Xu, T.; Liu, N.; Yuan, J.; Ma, Z. Triple Tumor Markers Assay Based on Carbon-Gold Nanocomposite. *Biosens. Bioelectron.* **2015**, *70*, 161−166.
(73) Bray, F.; Ferlay, J.; Soerjomataram, I.; Siegel, R. L.; Torre, L. A.; Jemal, A. Global Cancer Statistics 2018: GLOBOCAN Estimates of

Incidence and Mortality Worldwide for 36 Cancers in 185 Countries. *CA Cancer J. Clin.* **2018**, *68* (6), 394−424.
(74) Yang, G.; Xiao, Z.; Tang, C.; Deng, Y.; Huang, H.; He, Z. Recent Advances in Biosensor for Detection of Lung Cancer Biomarkers. *Biosens. Bioelectron.* **2019**, *141* (111416), 111416.
(75) Chiu, N.-F.; Lin, T.-L.; Kuo, C.-T. Highly Sensitive Carboxyl-Graphene Oxide-Based Surface Plasmon Resonance Immunosensor for the Detection of Lung Cancer for Cytokeratin 19 Biomarker in Human Plasma. *Sens. Actuators B Chem.* **2018**, *265*, 264−272.
(76) Yoshimura, A.; Uchino, J.; Hasegawa, K.; Tsuji, T.; Shiotsu, S.; Yuba, T.; Takumi, C.; Yamada, T.; Takayama, K.; Hiraoka, N. Carcinoembryonic Antigen and CYFRA 21−1 Responses as Prognostic Factors in Advanced Non-Small Cell Lung Cancer. *Transl. Lung Cancer Res.* **2019**, *8* (3), 227−234.
(77) Xu, X.-W.; Weng, X.-H.; Wang, C.-L.; Lin, W.-W.; Liu, A.-L.; Chen, W.; Lin, X.-H. Detection EGFR Exon 19 Status of Lung Cancer Patients by DNA Electrochemical Biosensor. *Biosens. Bioelectron.* **2016**, *80*, 411−417.
(78) Wu, T.; Chen, W.; Kong, D.; Li, X.; Lu, H.; Liu, S.; Wang, J.; Du, L.; Kong, Q.; Huang, X.; Lu, Z. MiR-25 Targets the Modulator of Apoptosis 1 Gene in Lung Cancer. *Carcinogenesis* **2015**, *36* (8), 925−935.
(79) Han, J.; Zhuo, Y.; Chai, Y.-Q.; Yuan, Y.-L.; Yuan, R. Novel Electrochemical Catalysis as Signal Amplified Strategy for Label-Free Detection of Neuron-Specific Enolase. *Biosens. Bioelectron.* **2012**, *31* (1), 399−405.
(80) Altintas, Z.; Tothill, I. Biomarkers and Biosensors for the Early Diagnosis of Lung Cancer. *Sens. Actuators B Chem.* **2013**, *188*, 988−998.
(81) Wei, Y.; Ma, H.; Ren, X.; Ding, C.; Wang, H.; Sun, X.; Du, B.; Zhang, Y.; Wei, Q. A Dual-Signaling Electrochemical Ratiometric Method for Sensitive Detection of Carcinoembryonic Antigen Based on Au-Cu_2S-CuS/Graphene and Au-CeO_2 Supported Toluidine Blue Complex. *Sens. Actuators B Chem.* **2018**, *256*, 504−511.
(82) Zhu, L.; Xu, L.; Jia, N.; Huang, B.; Tan, L.; Yang, S.; Yao, S. Electrochemical Immunoassay for Carcinoembryonic Antigen Using Gold Nanoparticle-Graphene Composite Modified Glassy Carbon Electrode. *Talanta* **2013**, *116*, 809−815.
(83) Zhang, Q.; Li, X.; Qian, C.; Dou, L.; Cui, F.; Chen, X. Label-Free Electrochemical Immunoassay for Neuron Specific Enolase Based on 3D Macroporous Reduced Graphene Oxide/Polyaniline Film. *Anal. Biochem.* **2018**, *540*−*541*, 1−8.
(84) Chen, M.; Wang, Y.; Su, H.; Mao, L.; Jiang, X.; Zhang, T.; Dai, X. Three-Dimensional Electrochemical DNA Biosensor Based on 3D Graphene-Ag Nanoparticles for Sensitive Detection of CYFRA21−1 in Non-Small Cell Lung Cancer. *Sens. Actuators B Chem.* **2018**, *255*, 2910−2918.
(85) Shoja, Y.; Kermanpur, A.; Karimzadeh, F. Diagnosis of EGFR Exon21 L858R Point Mutation as Lung Cancer Biomarker by Electrochemical DNA Biosensor Based on Reduced Graphene Oxide /Functionalized Ordered Mesoporous Carbon/Ni-Oxytetracycline Metallopolymer Nanoparticles Modified Pencil Graphite Electrode. *Biosens. Bioelectron.* **2018**, *113*, 108−115.
(86) Jia, X.; Song, T.; Liu, Y.; Meng, L.; Mao, X. An Immunochromatographic Assay for Carcinoembryonic Antigen on Cotton Thread Using a Composite of Carbon Nanotubes and Gold Nanoparticles as Reporters. *Anal. Chim. Acta* **2017**, *969*, 57−62.
(87) Gao, X.; Zhang, Y.; Chen, H.; Chen, Z.; Lin, X. Amperometric Immunosensor for Carcinoembryonic Antigen Detection with Carbon Nanotube-Based Film Decorated with Gold Nanoclusters. *Anal. Biochem.* **2011**, *414* (1), 70−76.
(88) Asadzadeh-Firouzabadi, A.; Zare, H. R. Preparation and Application of AgNPs/SWCNTs Nanohybrid as an Electroactive Label for Sensitive Detection of MiRNA Related to Lung Cancer. *Sens. Actuators B Chem.* **2018**, *260*, 824−831.
(89) Nolan, C. J.; Damm, P.; Prentki, M. Type 2 Diabetes across Generations: From Pathophysiology to Prevention and Management. *Lancet* **2011**, *378* (9786), 169−181.
(90) Cho, N. H.; Shaw, J. E.; Karuranga, S.; Huang, Y.; da Rocha Fernandes, J. D.; Ohlrogge, A. W.; Malanda, B. IDF Diabetes Atlas: Global Estimates of Diabetes Prevalence for 2017 and Projections for 2045. *Diabetes Res. Clin. Pract.* **2018**, *138*, 271−281.
(91) Zaidi, S. A.; Shin, J. H. Recent Developments in Nanostructure Based Electrochemical Glucose Sensors. *Talanta* **2016**, *149*, 30−42.
(92) American Diabetes Association. 2. Classification and Diagnosis of Diabetes: Standards of Medical Care in Diabetes-2021. *Diabetes Care* **2021**, *44* (Suppl 1), S15−S33.
(93) Shackery, I.; Patil, U.; Song, M.-J.; Sohn, J. S.; Kulkarni, S.; Some, S.; Lee, S. C.; Nam, M. S.; Lee, W.; Jun, S. C. Sensitivity Enhancement in Nickel Hydroxide/3D-Graphene as Enzymeless Glucose Detection. *Electroanalysis* **2015**, *27* (10), 2363−2370.
(94) Yang, J.; Cho, M.; Pang, C.; Lee, Y. Highly Sensitive Non-Enzymatic Glucose Sensor Based on over-Oxidized Polypyrrole Nanowires Modified with $Ni(OH)_2$ Nanoflakes. *Sens. Actuators B Chem.* **2015**, *211*, 93−101.
(95) Zheng, B.; Liu, G.; Yao, A.; Xiao, Y.; Du, J.; Guo, Y.; Xiao, D.; Hu, Q.; Choi, M. M. F. A Sensitive AgNPs/CuO Nanofibers Non-Enzymatic Glucose Sensor Based on Electrospinning Technology. *Sens. Actuators B Chem.* **2014**, *195*, 431−438.
(96) Jiang, L.-C.; Zhang, W.-D. A Highly Sensitive Nonenzymatic Glucose Sensor Based on CuO Nanoparticles-Modified Carbon Nanotube Electrode. *Biosens. Bioelectron.* **2010**, *25* (6), 1402−1407.
(97) Lu, X.; Ye, Y.; Xie, Y.; Song, Y.; Chen, S.; Li, P.; Chen, L.; Wang, L. Copper Coralloid Granule/Polyaniline/Reduced Graphene Oxide Nanocomposites for Nonenzymatic Glucose Detection. *Anal. Methods* **2014**, *6* (13), 4643.
(98) Hui, J.; Cui, J.; Xu, G.; Adeloju, S. B.; Wu, Y. Direct Electrochemistry of Glucose Oxidase Based on Nafion-Graphene-GOD Modified Gold Electrode and Application to Glucose Detection. *Mater. Lett.* **2013**, *108*, 88−91.
(99) Cella, L. N.; Chen, W.; Myung, N. V.; Mulchandani, A. Single-Walled Carbon Nanotube-Based Chemiresistive Affinity Biosensors for Small Molecules: Ultrasensitive Glucose Detection. *J. Am. Chem. Soc.* **2010**, *132* (14), 5024−5026.
(100) Ensafi, A. A.; Zandi-Atashbar, N.; Rezaei, B.; Ghiaci, M.; Chermahini, M. E.; Moshiri, P. Non-Enzymatic Glucose Electrochemical Sensor Based on Silver Nanoparticle Decorated Organic Functionalized Multiwall Carbon Nanotubes. *RSC Adv.* **2016**, *6* (65), 60926−60932.
(101) Amin, B. G.; Masud, J.; Nath, M. A Non-Enzymatic Glucose Sensor Based on a $CoNi_2Se_4$/RGO Nanocomposite with Ultrahigh Sensitivity at Low Working Potential. *J. Mater. Chem. B Mater. Biol. Med.* **2019**, *7* (14), 2338−2348.
(102) Yan, X.; Gu, Y.; Li, C.; Zheng, B.; Li, Y.; Zhang, T.; Zhang, Z.; Yang, M. A Non-Enzymatic Glucose Sensor Based on the CuS Nanoflakes-Reduced Graphene Oxide Nanocomposite. *Anal. Methods* **2018**, *10* (3), 381−388.
(103) Rao, H.; Zhang, Z.; Ge, H.; Liu, X.; Zou, P.; Wang, X.; Wang, Y. Enhanced Amperometric Sensing Using a $NiCo_2O_4$/Nitrogen-Doped Reduced Graphene Oxide/Ionic Liquid Ternary Composite for Enzyme-Free Detection of Glucose. *New J. Chem.* **2017**, *41* (9), 3667−3676.
(104) Wang, L.; Lu, X.; Wen, C.; Xie, Y.; Miao, L.; Chen, S.; Li, H.; Li, P.; Song, Y. One-Step Synthesis of Pt-NiO Nanoplate Array/Reduced Graphene Oxide Nanocomposites for Nonenzymatic Glucose Sensing. *J. Mater. Chem. A Mater. Energy Sustain.* **2015**, *3* (2), 608−616.
(105) Ammara, S.; Shamaila, S.; Zafar, N.; Bokhari, A.; Sabah, A. Nonenzymatic Glucose Sensor with High Performance Electrodeposited Nickel/Copper/Carbon Nanotubes Nanocomposite Electrode. *J. Phys. Chem. Solids* **2018**, *120*, 12−19.
(106) Baghayeri, M.; Amiri, A.; Farhadi, S. Development of Non-Enzymatic Glucose Sensor Based on Efficient Loading Ag Nanoparticles on Functionalized Carbon Nanotubes. *Sens. Actuators B Chem.* **2016**, *225*, 354−362.
(107) Zhang, Y.; Zhou, E.; Li, Y.; He, X. A Novel Nonenzymatic Glucose Sensor Based on Magnetic Copper Ferrite Immobilized on

https://doi.org/10.1021/acsbiomaterials.1c00710
ACS Biomater. Sci. Eng. 2022, 8, 964−1000

Multiwalled Carbon Nanotubes. *Anal. Methods* **2015**, *7* (6), 2360−2366.
(108) Wang, F.; Chen, X.; Chen, L.; Yang, J.; Wang, Q. High-Performance Non-Enzymatic Glucose Sensor by Hierarchical Flower-like Nickel(II)-Based MOF/Carbon Nanotubes Composite. *Mater. Sci. Eng. C Mater. Biol. Appl.* **2019**, *96*, 41−50.
(109) Etymologia: Zika Virus, *Emerg. Infect. Dis.* **2014**, *20* (6), 1090.
(110) Mota, M. T. d. O.; Terzian, A. C.; Silva, M. L. C. R.; Estofolete, C.; Nogueira, M. L. Mosquito-Transmitted Viruses -the Great Brazilian Challenge. *Braz. J. Microbiol.* **2016**, *47 Suppl 1*, 38−50.
(111) Saxena, S. K.; Elahi, A.; Gadugu, S.; Prasad, A. K. Zika Virus Outbreak: An Overview of the Experimental Therapeutics and Treatment. *Virusdisease* **2016**, *27* (2), 111−115.
(112) Camacho, E.; Paternina-Gomez, M.; Blanco, P. J.; Osorio, J. E.; Aliota, M. T. Detection of Autochthonous Zika Virus Transmission in Sincelejo, Colombia. *Emerg. Infect. Dis.* **2016**, *22* (5), 927−929.
(113) Faria, N. R.; Azevedo, R. d. S. d. S.; Kraemer, M. U. G.; Souza, R.; Cunha, M. S.; Hill, S. C.; Theze, J.; Bonsall, M. B.; Bowden, T. A.; Rissanen, I.; Rocco, I. M.; Nogueira, J. S.; Maeda, A. Y.; Vasami, F. G. d. S.; Macedo, F. L. d. L.; Suzuki, A.; Rodrigues, S. G.; Cruz, A. C. R.; Nunes, B. T.; Medeiros, D. B. d. A.; Rodrigues, D. S. G.; Nunes Queiroz, A. L.; Silva, E. V. P. d.; Henriques, D. F.; Travassos da Rosa, E. S.; de Oliveira, C. S.; Martins, L. C.; Vasconcelos, H. B.; Casseb, L. M. N.; Simith, D. d. B.; Messina, J. P.; Abade, L.; Lourenco, J.; Alcantara, L. C. J.; Lima, M. M. d.; Giovanetti, M.; Hay, S. I.; de Oliveira, R. S.; Lemos, P. d. S.; Oliveira, L. F. d.; de Lima, C. P. S.; da Silva, S. P.; Vasconcelos, J. M. d.; Franco, L.; Cardoso, J. F.; Vianez-Junior, J. L. d. S. G.; Mir, D.; Bello, G.; Delatorre, E.; Khan, K.; Creatore, M.; Coelho, G. E.; de Oliveira, W. K.; Tesh, R.; Pybus, O. G.; Nunes, M. R. T.; Vasconcelos, P. F. C. Zika Virus in the Americas: Early Epidemiological and Genetic Findings. *Science* **2016**, *352* (6283), 345−349.
(114) Fauci, A. S.; Morens, D. M. Zika Virus in the Americas — yet Another Arbovirus Threat. *N. Engl. J. Med.* **2016**, *374* (7), 601−604.
(115) Cugola, F. R.; Fernandes, I. R.; Russo, F. B.; Freitas, B. C.; Dias, J. L. M.; Guimarães, K. P.; Benazzato, C.; Almeida, N.; Pignatari, G. C.; Romero, S.; Polonio, C. M.; Cunha, I.; Freitas, C. L.; Brandão, W. N.; Rossato, C.; Andrade, D. G.; Faria, D. d. P.; Garcez, A. T.; Buchpigel, C. A.; Braconi, C. T.; Mendes, E.; Sall, A. A.; Zanotto, P. M. de A.; Peron, J. P. S.; Muotri, A. R.; Beltrão-Braga, P. C. B. The Brazilian Zika Virus Strain Causes Birth Defects in Experimental Models. *Nature* **2016**, *534* (7606), 267−271.
(116) Hofer, U. Viral Pathogenesis: Tracing the Steps of Zika Virus. *Nat. Rev. Microbiol.* **2016**, *14* (7), 401.
(117) Musso, D.; Roche, C.; Robin, E.; Nhan, T.; Teissier, A.; Cao-Lormeau, V.-M. Potential Sexual Transmission of Zika Virus. *Emerg. Infect. Dis.* **2015**, *21* (2), 359−361.
(118) Li, C.; Xu, D.; Ye, Q.; Hong, S.; Jiang, Y.; Liu, X.; Zhang, N.; Shi, L.; Qin, C.-F.; Xu, Z. Zika Virus Disrupts Neural Progenitor Development and Leads to Microcephaly in Mice. *Cell Stem Cell* **2016**, *19* (1), 120−126.
(119) Mlakar, J.; Korva, M.; Tul, N.; Popović, M.; Poljšak-Prijatelj, M.; Mraz, J.; Kolenc, M.; Resman Rus, K.; Vesnaver Vipotnik, T.; Fabjan Vodušek, V.; Vizjak, A.; Pižem, J.; Petrovec, M.; Avšič Županc, T. Zika Virus Associated with Microcephaly. *N. Engl. J. Med.* **2016**, *374* (10), 951−958.
(120) da Fonseca Alves, R.; Franco, D. L.; Cordeiro, M. T.; de Oliveira, E. M.; Fireman Dutra, R. A.; Del Pilar Taboada Sotomayor, M. Novel Electrochemical Genosensor for Zika Virus Based on a Poly-(3-Amino-4-Hydroxybenzoic Acid)-Modified Pencil Carbon Graphite Electrode. *Sens. Actuators B Chem.* **2019**, *296* (126681), 126681.
(121) Afsahi, S.; Lerner, M. B.; Goldstein, J. M.; Lee, J.; Tang, X.; Bagarozzi, D. A., Jr.; Pan, D.; Locascio, L.; Walker, A.; Barron, F.; Goldsmith, B. R. Novel Graphene-Based Biosensor for Early Detection of Zika Virus Infection. *Biosens. Bioelectron.* **2018**, *100*, 85−88.
(122) Li, J.; Yang, K.; Wu, Z.; Li, X.; Duan, Q. Nitrogen-Doped Porous Carbon-Based Fluorescence Sensor for the Detection of ZIKV RNA Sequences: Fluorescence Image Analysis. *Talanta* **2019**, *205*, 120091.
(123) De Cock, K. M.; Jaffe, H. W.; Curran, J. W. Reflections on 30 Years of AIDS. *Emerg. Infect. Dis.* **2011**, *17* (6), 1044−1048.
(124) Laird, G. M.; Eisele, E. E.; Rabi, S. A.; Lai, J.; Chioma, S.; Blankson, J. N.; Siliciano, J. D.; Siliciano, R. F. Rapid Quantification of the Latent Reservoir for HIV-1 Using a Viral Outgrowth Assay. *PLoS Pathog.* **2013**, *9* (5), No. e1003398.
(125) Bhimji, A.; Zaragoza, A. A.; Live, L. S.; Kelley, S. O. Electrochemical Enzyme-Linked Immunosorbent Assay Featuring Proximal Reagent Generation: Detection of Human Immunodeficiency Virus Antibodies in Clinical Samples. *Anal. Chem.* **2013**, *85* (14), 6813−6819.
(126) Davis, D. A.; Tebbs, I. R.; Daniels, S. I.; Stahl, S. J.; Kaufman, J. D.; Wingfield, P.; Bowman, M. J.; Chmielewski, J.; Yarchoan, R. Analysis and Characterization of Dimerization Inhibition of a Multi-Drug-Resistant Human Immunodeficiency Virus Type 1 Protease Using a Novel Size-Exclusion Chromatographic Approach. *Biochem. J.* **2009**, *419* (2), 497−506.
(127) Esseghaier, C.; Ng, A.; Zourob, M. A Novel and Rapid Assay for HIV-1 Protease Detection Using Magnetic Bead Mediation. *Biosens. Bioelectron.* **2013**, *41*, 335−341.
(128) Biswas, P.; Cella, L. N.; Kang, S. H.; Mulchandani, A.; Yates, M. V.; Chen, W. A Quantum-Dot Based Protein Module for in Vivo Monitoring of Protease Activity through Fluorescence Resonance Energy Transfer. *Chem. Commun. (Camb.)* **2011**, *47* (18), 5259−5261.
(129) Zhang, Y.; Chen, X.; Roozbahani, G. M.; Guan, X. Graphene Oxide-Based Biosensing Platform for Rapid and Sensitive Detection of HIV-1 Protease. *Anal. Bioanal. Chem.* **2018**, *410* (24), 6177−6185.
(130) Gong, Q.; Wang, Y.; Yang, H. A Sensitive Impedimetric DNA Biosensor for the Determination of the HIV Gene Based on Graphene-Nafion Composite Film. *Biosens. Bioelectron.* **2017**, *89*, 565−569.
(131) Polaris Observatory Collaborators. Global Prevalence, Treatment, and Prevention of Hepatitis B Virus Infection in 2016: A Modelling Study. *Lancet Gastroenterol. Hepatol.* **2018**, *3* (6), 383−403.
(132) Zhou, Y.; Wan, Y.; Ye, Z.-W.; He, Z.; Liu, Q.; Shi, Y. How Hepatitis B Virus Causes Cirrhosis and Liver Cancer. *Med. Hypotheses* **2017**, *108*, 52−53.
(133) Hou, J.; Ren, J.; Song, L.; Zhao, F.; Liang, P. Analytical Performance of Three Diagnostic Reagents for HBsAg on an Automatic ELISA Analyzer. *J. Clin. Lab. Anal.* **2018**, *32* (1), e22159.
(134) Costa, C. I.; Delgado, I. F.; da Costa, J. A. C.; de Carvalho, R. F.; Mouta e Junior, S. d. S.; Vianna, C. O. A.; de Moraes, M. T. B. Establishment and Validation of an ELISA for the Quantitation of HBsAg in Recombinant Hepatitis B Vaccines. *J. Virol. Methods* **2011**, *172* (1−2), 32−37.
(135) Amaya-González, S.; de-los-Santos-Álvarez, N.; Lobo-Castañón, M. J.; Miranda-Ordieres, A. J.; Tuñón-Blanco, P. Amperometric Quantification of Gluten in Food Samples Using an ELISA Competitive Assay and Flow Injection Analysis. *Electroanalysis* **2011**, *23* (1), 108−114.
(136) Paryan, M.; Khodayar, M.; Kia, V.; Mohammadi-Yeganeh, S.; Kaghazian, H. Development of an In-House TaqMan Real-Time PCR-Based Method to Detect Residual Host Cell DNA in HBV Vaccine. *Appl. Biochem. Biotechnol.* **2016**, *179* (3), 375−382.
(137) Izmirli, S.; Celik, D. G.; Yuksel, P.; Saribas, S.; Aslan, M.; Ergin, S.; Bahar, H.; Sen, S.; Cakal, B.; Oner, A.; Kocazeybek, B. The Detection of Occult HBV Infection in Patients with HBsAg Negative Pattern by Real-Time PCR Method. *Transfus. Apher. Sci.* **2012**, *47* (3), 283−287.
(138) Xu, J.; Li, W.; Liu, R.; Yang, Y.; Lin, Q.; Xu, J.; Shen, P.; Zheng, Q.; Zhang, Y.; Han, Z.; Li, J.; Zheng, T. Ultrasensitive Low-Background Multiplex Mycotoxin Chemiluminescence Immunoassay by Silica-Hydrogel Photonic Crystal Microsphere Suspension Arrays in Cereal Samples. *Sens. Actuators B Chem.* **2016**, *232*, 577−584.

(139) Zhang, K.; Lv, S.; Lin, Z.; Li, M.; Tang, D. Bio-Bar-Code-Based Photoelectrochemical Immunoassay for Sensitive Detection of Prostate-Specific Antigen Using Rolling Circle Amplification and Enzymatic Biocatalytic Precipitation. *Biosens. Bioelectron.* **2018**, *101*, 159−166.
(140) Taylor, A. J.; Dexter, A.; Bunch, J. Exploring Ion Suppression in Mass Spectrometry Imaging of a Heterogeneous Tissue. *Anal. Chem.* **2018**, *90* (9), 5637−5645.
(141) Zhao, F.; Bai, Y.; Zeng, R.; Cao, L.; Zhu, J.; Han, G.; Chen, Z. An Electrochemical Immunosensor with Graphene-Oxide-Ferrocene-Based Nanocomposites for Hepatitis B Surface Antigen Detection. *Electroanalysis* **2018**, *30* (11), 2774−2780.
(142) Lara, P.; Palma-Florez, S.; Salas-Huenuleo, E.; Polakovicova, I.; Guerrero, S.; Lobos-Gonzalez, L.; Campos, A.; Muñoz, L.; Jorquera-Cordero, C.; Varas-Godoy, M.; Cancino, J.; Arias, E.; Villegas, J.; Cruz, L. J.; Albericio, F.; Araya, E.; Corvalan, A. H.; Quest, A. F. G.; Kogan, M. J. Gold Nanoparticle Based Double-Labeling of Melanoma Extracellular Vesicles to Determine the Specificity of Uptake by Cells and Preferential Accumulation in Small Metastatic Lung Tumors. *J. Nanobiotechnology* **2020**, *18* (1), 20.
(143) Ji, T.; Liu, Z.; Wang, G.; Guo, X.; Akbar Khan, S.; Lai, C.; Chen, H.; Huang, S.; Xia, S.; Chen, B.; Jia, H.; Chen, Y.; Zhou, Q. Detection of COVID-19: A Review of the Current Literature and Future Perspectives. *Biosens. Bioelectron.* **2020**, *166*, 112455.
(144) Mujawar, M. A.; Gohel, H.; Bhardwaj, S. K.; Srinivasan, S.; Hickman, N.; Kaushik, A. Nano-Enabled Biosensing Systems for Intelligent Healthcare: Towards COVID-19 Management. *Mater. Today Chem.* **2020**, *17*, 100306.
(145) Kumar, S.; Nehra, M.; Mehta, J.; Dilbaghi, N.; Marrazza, G.; Kaushik, A. Point-of-Care Strategies for Detection of Waterborne Pathogens. *Sensors (Basel)* **2019**, *19* (20), 4476.
(146) Tolga, A. C. Real Options Valuation of an IoT Based Healthcare Device with Interval Type-2 Fuzzy Numbers. *Socioecon. Plann. Sci.* **2020**, *69*, 100693.
(147) Ali, M. A.; Dong, L.; Dhau, J.; Khosla, A.; Kaushik, A. Perspective—Electrochemical Sensors for Soil Quality Assessment. *J. Electrochem. Soc.* **2020**, *167* (3), 037550.
(148) Shinde, R. B.; Veerapandian, M.; Kaushik, A.; Manickam, P. State-of-Art Bio-Assay Systems and Electrochemical Approaches for Nanotoxicity Assessment. *Front. Bioeng. Biotechnol.* **2020**, *8*, 325.
(149) Park, S.-W.; Park, J.; Bong, K.; Shin, D.; Lee, J.; Choi, S.; Yoo, H.-J. An Energy-Efficient and Scalable Deep Learning/Inference Processor with Tetra-Parallel MIMD Architecture for Big Data Applications. *IEEE Trans. Biomed. Circuits Syst.* **2016**, *9* (6), 838−848.
(150) Ali, F.; Islam, S. M. R.; Kwak, D.; Khan, P.; Ullah, N.; Yoo, S.-J.; Kwak, K. S. Type-2 Fuzzy Ontology-Aided Recommendation Systems for IoT-Based Healthcare. *Comput. Commun.* **2018**, *119*, 138−155.
(151) Prather, K. A.; Wang, C. C.; Schooley, R. T. Reducing Transmission of SARS-CoV-2. *Science* **2020**, *368* (6498), 1422−1424.
(152) Morales-Narváez, E.; Dincer, C. The Impact of Biosensing in a Pandemic Outbreak: COVID-19. *Biosens. Bioelectron.* **2020**, *163*, 112274.
(153) Rothan, H. A.; Byrareddy, S. N. The Epidemiology and Pathogenesis of Coronavirus Disease (COVID-19) Outbreak. *J. Autoimmun.* **2020**, *109*, 102433.
(154) Seo, G.; Lee, G.; Kim, M. J.; Baek, S.-H.; Choi, M.; Ku, K. B.; Lee, C.-S.; Jun, S.; Park, D.; Kim, H. G.; Kim, S.-J.; Lee, J.-O.; Kim, B. T.; Park, E. C.; Kim, S. I. Rapid Detection of COVID-19 Causative Virus (SARS-CoV-2) in Human Nasopharyngeal Swab Specimens Using Field-Effect Transistor-Based Biosensor. *ACS Nano* **2020**, *14* (4), 5135−5142.
(155) Zou, L.; Ruan, F.; Huang, M.; Liang, L.; Huang, H.; Hong, Z.; Yu, J.; Kang, M.; Song, Y.; Xia, J.; Guo, Q.; Song, T.; He, J.; Yen, H. L.; Peiris, M.; Wu, J. SARS-CoV-2 Viral Load in Upper Respiratory Specimens of Infected Patients. *N. Engl. J. Med.* **2020**, *382*, 1177−1179.
(156) Janissen, R.; Sahoo, P. K.; Santos, C. A.; da Silva, A. M.; von Zuben, A. A. G.; Souto, D. E. P.; Costa, A. D. T.; Celedon, P.; Zanchin, N. I. T.; Almeida, D. B.; Oliveira, D. S.; Kubota, L. T.; Cesar, C. L.; Souza, A. P.; Cotta, M. A. InP Nanowire Biosensor with Tailored Biofunctionalization: Ultrasensitive and Highly Selective Disease Biomarker Detection. *Nano Lett.* **2017**, *17*, 5938−5949.
(157) Liu, J.; Chen, X.; Wang, Q.; Xiao, M.; Zhong, D.; Sun, W.; Zhang, G.; Zhang, Z. Ultrasensitive Monolayer MoS_2 Field-Effect Transistor Based DNA Sensors for Screening of Down Syndrome. *Nano Lett.* **2019**, *19*, 1437−1444.
(158) Cooper, D. R.; D'Anjou, B.; Ghattamaneni, N.; Harack, B.; Hilke, M.; Horth, A.; Majlis, N.; Massicotte, M.; Vandsburger, L.; Whiteway, E.; Yu, V. Experimental Review of Graphene. *ISRN Condens. Matter Phys.* **2012**, *2012*, 501686.
(159) Geim, A. K.; Novoselov, K. S. The Rise of Graphene. *Nat. Mater.* **2007**, *6*, 183−191.
(160) Lei, Y. M.; Xiao, M. M.; Li, Y. T.; Xu, L.; Zhang, H.; Zhang, Z. Y.; Zhang, G. J. Detection of Heart Failure-Related Biomarker in Whole Blood with Graphene Field Effect Transistor Biosensor. *Biosens. Bioelectron.* **2017**, *91*, 1−7.
(161) Zhou, L.; Mao, H.; Wu, C.; Tang, L.; Wu, Z.; Sun, H.; Zhang, H.; Zhou, H.; Jia, C.; Jin, Q.; Chen, X.; Zhao, J. Label-Free Graphene Biosensor Targeting Cancer Molecules Based on Non-Covalent Modification. *Biosens. Bioelectron.* **2017**, *87*, 701−707.
(162) Wu, G.; Tang, X.; Meyyappan, M.; Lai, K. W. C. Doping Effects of Surface Functionalization on Graphene with Aromatic Molecule and Organic Solvents. *Appl. Surf. Sci.* **2017**, *425*, 713−721.
(163) Liu, Y.; Yuan, L.; Yang, M.; Zheng, Y.; Li, L.; Gao, L.; Nerngchamnong, N.; Nai, C. T.; Sangeeth, C. S.; Feng, Y. P.; Nijhuis, C. A.; Loh, K. P. Giant Enhancement in Vertical Conductivity of Stacked CVD Graphene Sheets by Self-Assembled Molecular Layers. *Nat. Commun.* **2014**, *5*, 5461.
(164) Liu, J.-Y.; Chang, H.-Y.; Truong, Q. D.; Ling, Y.-C. Synthesis of nitrogen-doped graphene by pyrolysis of ionic-liquid-functionalized graphene. *J. Mater. Chem. C* **2013**, *1*, 1713−1716.
(165) Choi, Y.; Kang, J.; Jariwala, D.; Kang, M. S.; Marks, T. J.; Hersam, M. C.; Cho, J. H. Low-Voltage Complementary Electronics from Ion-Gel-Gated Vertical van der Waals Heterostructures. *Adv. Mater.* **2016**, *28*, 3742−3748.
(166) Teng, F.; Hu, K.; Ouyang, W.; Fang, X. Photoelectric Detectors Based on Inorganic p-Type Semiconductor Materials. *Adv. Mater.* **2018**, *30*, 1706262.
(167) Mahato, K.; Purohit, B.; Kumar, A.; Chandra, P. Clinically Comparable Impedimetric Immunosensor for Serum Alkaline Phosphatase Detection Based on Electrochemically Engineered Au-Nano-Dendroids and Graphene Oxide Nanocomposite. *Biosens. Bioelectron.* **2020**, *148*, 111815.
(168) Chandra, P. Miniaturized Label-Free Smartphone Assisted Electrochemical Sensing Approach for Personalized COVID-19 Diagnosis. *Sensors International* **2020**, *1*, 100019.
(169) Chu, H.; Chan, J. F.-W.; Wang, Y.; Yuen, T. T.-T.; Chai, Y.; Shuai, H.; Yang, D.; Hu, B.; Huang, X.; Zhang, X.; Hou, Y.; Cai, J.-P.; Zhang, A. J.; Zhou, J.; Yuan, S.; To, K. K.-W.; Hung, I. F.-N.; Cheung, T. T.; Ng, A. T.-L.; Hau-Yee Chan, I.; Wong, I. Y.-H.; Law, S. Y.-K.; Foo, D. C.-C.; Leung, W.-K.; Yuen, K.-Y. SARS-CoV-2 Induces a More Robust Innate Immune Response and Replicates Less Efficiently than SARS-CoV in the Human Intestines: An Ex Vivo Study with Implications on Pathogenesis of COVID-19. *Cell. Mol. Gastroenterol. Hepatol.* **2021**, *11* (3), 771−781.
(170) Purohit, B.; Mahato, K.; Kumar, A.; Chandra, P. Sputtering Enhanced Peroxidase like Activity of a Dendritic Nanochip for Amperometric Determination of Hydrogen Peroxide in Blood Samples. *Mikrochim. Acta* **2019**, *186* (9), 658.
(171) Naveen, M. H.; Gurudatt, N. G.; Noh, H.-B.; Shim, Y.-B. Dealloyed AuNi Dendrite Anchored on a Functionalized Conducting Polymer for Improved Catalytic Oxygen Reduction and Hydrogen Peroxide Sensing in Living Cells. *Adv. Funct. Mater.* **2016**, *26* (10), 1590−1601.
(172) Valera, A. E.; Nesbitt, N. T.; Archibald, M. M.; Naughton, M. J.; Chiles, T. C. On-Chip Electrochemical Detection of Cholera Using

a Polypyrrole-Functionalized Dendritic Gold Sensor. *ACS Sens.* **2019**, *4* (3), 654−659.
(173) Chu, D. K. W.; Pan, Y.; Cheng, S. M. S.; Hui, K. P. Y.; Krishnan, P.; Liu, Y.; Ng, D. Y. M.; Wan, C. K. C.; Yang, P.; Wang, Q.; Peiris, M.; Poon, L. L. M. Molecular Diagnosis of a Novel Coronavirus (2019-NCoV) Causing an Outbreak of Pneumonia. *Clin. Chem.* **2020**, *66* (4), 549−555.
(174) Luna, D. M. N.; Avelino, K. Y. P. S.; Cordeiro, M. T.; Andrade, C. A. S.; Oliveira, M. D. L. Electrochemical Immunosensor for Dengue Virus Serotypes Based on 4-Mercaptobenzoic Acid Modified Gold Nanoparticles on Self-Assembled Cysteine Monolayers. *Sens. Actuators B Chem.* **2015**, *220*, 565−572.
(175) Liu, F.; Choi, K. S.; Park, T. J.; Lee, S. Y.; Seo, T. S. Graphene-Based Electrochemical Biosensor for Pathogenic Virus Detection. *Biochip J.* **2011**, *5* (2), 123−128.
(176) Hassen, W. M.; Duplan, V.; Frost, E.; Dubowski, J. J. Quantitation of Influenza A Virus in the Presence of Extraneous Protein Using Electrochemical Impedance Spectroscopy. *Electrochim. Acta* **2011**, *56* (24), 8325−8328.
(177) Cheng, M. S.; Ho, J. S.; Tan, C. H.; Wong, J. P. S.; Ng, L. C.; Toh, C.-S. Development of an Electrochemical Membrane-Based Nanobiosensor for Ultrasensitive Detection of Dengue Virus. *Anal. Chim. Acta* **2012**, *725*, 74−80.
(178) Nguyen, B. T. T.; Peh, A. E. K.; Chee, C. Y. L.; Fink, K.; Chow, V. T. K.; Ng, M. M. L.; Toh, C.-S. Electrochemical Impedance Spectroscopy Characterization of Nanoporous Alumina Dengue Virus Biosensor. *Bioelectrochemistry* **2012**, *88*, 15−21.
(179) Chartuprayoon, N.; Rheem, Y.; Ng, J. C. K.; Nam, J.; Chen, W.; Myung, N. V. Polypyrrole nanoribbon based chemiresistive immunosensors for viral plant pathogen detection. *Anal. Methods* **2013**, *5*, 3497−3502.
(180) Giamberardino, A.; Labib, M.; Hassan, E. M.; Tetro, J. A.; Springthorpe, S.; Sattar, S. A.; Berezovski, M. V.; DeRosa, M. C. Ultrasensitive Norovirus Detection Using DNA Aptasensor Technology. *PLoS One* **2013**, *8* (11), No. e79087.
(181) Chand, R.; Neethirajan, S. Microfluidic Platform Integrated with Graphene-Gold Nano-Composite Aptasensor for One-Step Detection of Norovirus. *Biosens. Bioelectron.* **2017**, *98*, 47−53.
(182) Veerapandian, M.; Hunter, R.; Neethirajan, S. Dual Immunosensor Based on Methylene Blue-Electroadsorbed Graphene Oxide for Rapid Detection of the Influenza A Virus Antigen. *Talanta* **2016**, *155*, 250−257.
(183) Samper, I. C.; Sánchez-Cano, A.; Khamcharoen, W.; Jang, I.; Siangproh, W.; Baldrich, E.; Geiss, B. J.; Dandy, D. S.; Henry, C. S. Electrochemical Capillary-Flow Immunoassay for Detecting Anti-SARS-CoV-2 Nucleocapsid Protein Antibodies at the Point of Care. *ACS Sens.* **2021**, *6*, 4067.
(184) Liang, Y.; Yan, H.; Huang, L.; Zhao, J.; Wang, H.; Kang, M.; Wan, Z.; Shui, J.; Tang, S. A Luciferase Immunosorbent Assay for Quantitative Detection of IgG Antibodies against SARS-CoV-2 Nucleoprotein. *J. Virol Methods* **2021**, *292*, 114141.
(185) Bayin, Q.; Huang, L.; Ren, C.; Fu, Y.; Ma, X.; Guo, J. Anti-SARS-CoV-2 IgG and IgM Detection with a GMR Based LFIA System. *Talanta* **2021**, *227*, 122207.
(186) Kasetsirikul, S.; Umer, M.; Soda, N.; Sreejith, K. R.; Shiddiky, M. J. A.; Nguyen, N.-T. Detection of the SARS-CoV-2 Humanized Antibody with Paper-Based ELISA. *Analyst* **2020**, *145* (23), 7680−7686.
(187) Carrell, C.; Link, J.; Jang, I.; Terry, J.; Scherman, M.; Call, Z.; Panraksa, Y.; Dandy, D. S.; Geiss, B. J.; Henry, C. Point-of-Need Disposable ELISA System for COVID-19 Serology Testing. *ChemRxiv* **2020**, DOI: 10.26434/chemrxiv.13050539.v2.
(188) Kim, S.; Hao, Y.; Miller, E. A.; Tay, D. M. Y.; Yee, E.; Kongsuphol, P.; Jia, H.; McBee, M.; Preiser, P. R.; Sikes, H. D. Vertical Flow Cellulose-Based Assays for SARS-CoV-2 Antibody Detection in Human Serum. *ACS Sens.* **2021**, *6* (5), 1891−1898.
(189) Yang, Z.-H.; Zhuo, Y.; Yuan, R.; Chai, Y.-Q. An Amplified Electrochemical Immunosensor Based on in Situ-Produced 1-Naphthol as Electroactive Substance and Graphene Oxide and Pt Nanoparticles Functionalized CeO_2 Nanocomposites as Signal Enhancer. *Biosens. Bioelectron.* **2015**, *69*, 321−327.
(190) Sayhi, M.; Ouerghi, O.; Belgacem, K.; Arbi, M.; Tepeli, Y.; Ghram, A.; Anik, Ü.; Österlund, L.; Laouini, D.; Diouani, M. F. Electrochemical Detection of Influenza Virus H9N2 Based on Both Immunomagnetic Extraction and Gold Catalysis Using an Immobilization-Free Screen Printed Carbon Microelectrode. *Biosens. Bioelectron.* **2018**, *107*, 170−177.
(191) Layqah, L. A.; Eissa, S. An Electrochemical Immunosensor for the Corona Virus Associated with the Middle East Respiratory Syndrome Using an Array of Gold Nanoparticle-Modified Carbon Electrodes. *Mikrochim. Acta* **2019**, *186* (4), 224.
(192) Lum, J.; Wang, R.; Lassiter, K.; Srinivasan, B.; Abi-Ghanem, D.; Berghman, L.; Hargis, B.; Tung, S.; Lu, H.; Li, Y. Rapid Detection of Avian Influenza H5N1 Virus Using Impedance Measurement of Immuno-Reaction Coupled with RBC Amplification. *Biosens. Bioelectron.* **2012**, *38* (1), 67−73.